

AD-A097 741

SYRACUSE RESEARCH CORP NY

F/6 1/3

ELECTROMAGNETIC SYSTEM TRADE--OFFS AND DATA BASE MANAGEMENT FOR--ETC(U)

FEB 81 D AUCKLAND, R WALLENBERG

N00014-78-C-0673

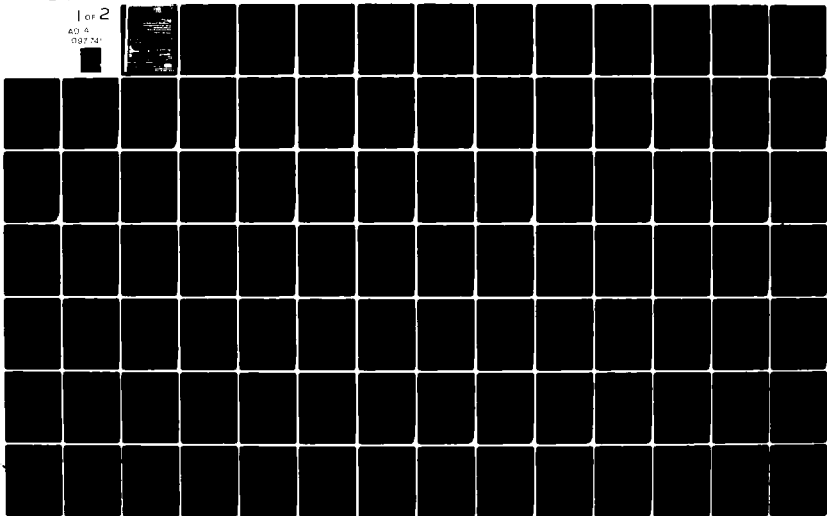
UNCLASSIFIED

SRC-TR-81-1084

NL

1 of 2

AO A
087 741



LEVEL II

AD A 097 741

9 Final Report.

1 Aug 78 - 31 Dec 80.

6 Electromagnetic System Trade - Offs and Data Base Management for Advanced Composite Aircraft Study. Composite Coupling Analysis.

10 D. / Auckland
R. / Wallenberg

DTIC ELECTRONIC
APR 15 1981
A

DTIC FILE COPY

15 N00014-78-C-0673

14 SRC-TR-81-1084

11 Feb 1981

This document has been approved for public release and sale; the distribution is unlimited.

12 159

410 003



SYRACUSE RESEARCH CORPORATION

81 3 20 012

UNCLASSIFIED

SECURITY CLASSIFICATION OF THIS PAGE (When Data Entered)

REPORT DOCUMENTATION PAGE		READ INSTRUCTIONS BEFORE COMPLETING FORM
1. REPORT NUMBER SRC TR 81-1084	2. GOVT ACCESSION NO. AD A097741	3. RECIPIENT'S CATALOG NUMBER
4. TITLE (and Subtitle) ELECTROMAGNETIC SYSTEM TRADE-OFFS AND DATA BASE MANAGEMENT FOR ADVANCED COMPOSITE AIRCRAFT STUDY -- Composite Coupling Analysis	5. TYPE OF REPORT & PERIOD COVERED Final Report 08/01/78 - 12/31/80	6. PERFORMING ORG. REPORT NUMBER SRC TR 81-1084
7. AUTHOR(s) Dr. D. Auckland Dr. R. Wallenberg	8. CONTRACT OR GRANT NUMBER(s) N00014-78-C-0673	
9. PERFORMING ORGANIZATION NAME AND ADDRESS Syracuse Research Corporation Merrill Lane Syracuse, New York 13210	10. PROGRAM ELEMENT, PROJECT, TASK AREA & WORK UNIT NUMBERS	
11. CONTROLLING OFFICE NAME AND ADDRESS Office of Naval Research 800 N. Quincy St., Arlington, VA 22217 Attn: Code 221 (R.A. Nichols, CDR, USN)	12. REPORT DATE February 1981	13. NUMBER OF PAGES 168
14. MONITORING AGENCY NAME & ADDRESS (if different from Controlling Office) Naval Air Systems Command Washington, D.C. 20361 Attn: Code AIR-5181 (Dr. J. Birken)	15. SECURITY CLASS. (of this report) Unclassified	15a. DECLASSIFICATION/DOWNGRADING SCHEDULE
16. DISTRIBUTION STATEMENT (of this Report) for pub dist		
17. DISTRIBUTION STATEMENT (of the abstract entered in Block 20, if different from Report) MAR 10 1981		
18. SUPPLEMENTARY NOTES A		
19. KEY WORDS (Continue on reverse side if necessary and identify by block number) electromagnetic coupling composite materials		
20. ABSTRACT (Continue on reverse side if necessary and identify by block number) The problem of electromagnetic interference which couples to the interior of composite material shell enclosures is studied. Interference sources considered are a distant nuclear electromagnetic pulse, near-strike lightning, and direct-strike lightning. The electromagnetic properties of the composite material shell wall are simplified by assuming a constant bulk conductivity σ . Several models for the		

DD FORM 1473
1 JAN 73

EDITION OF 1 NOV 65 IS OBSOLETE

UNCLASSIFIED

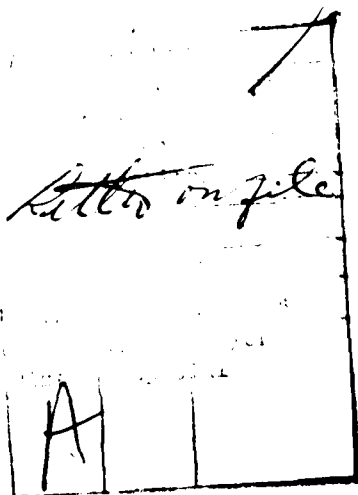
SECURITY CLASSIFICATION OF THIS PAGE (When Data Entered)

UNCLASSIFIED

SECURITY CLASSIFICATION OF THIS PAGE/When Data Entered

20. ABSTRACT (Continued)

coupling mechanism are analyzed including integral equation formulations, exact series solutions, and a diffusion coupling model. Several computer programs are presented to determine the interior fields over a large range of frequencies when the shell is modeled as an infinitely long two-dimensional cylinder of arbitrary cross section. A user-oriented interactive computer program is also described which is used to determine the response of circuits situated inside the shell.



UNCLASSIFIED

SECURITY CLASSIFICATION OF THIS PAGE/When Data Entered

TABLE OF CONTENTS

<u>Section</u>		<u>Page</u>
1	INTRODUCTION	1-1
2	PERFECTLY CONDUCTING CYLINDERS OF ARBITRARY CROSS SECTIONAL SHAPE	2-1
	2.1 Introduction	2-1
	2.2 E-Field Formulation	2-8
	2.3 H-Field Formulation	2-13
	2.4 Combined Field Formulation	2-16
	2.5 Formulas for Scattering Cross Section	2-18
	2.6 Exact Series Solution	2-20
	2.7 Oblique Incidence	2-22
	2.8 Current Distribution on Conductor Due to Impressed Longitudinal Current	2-27
	2.9 References	2-32
3	THIN SHELLS OF ARBITRARY CROSS SECTION AND FINITE CONDUCTIVITY	3-1
	3.1 Introduction	3-1
	3.2 Impedance Sheet Approximation	3-4
	3.3 Traveling Wave Approximation	3-7
	3.4 Computation of Fields Due to Two-Dimensional Current Distributions	3-13
	3.5 References	3-21
4	SHELLS OF CIRCULAR CROSS SECTION AND FINITE CONDUCTIVITY	4-1
	4.1 Introduction	4-1
	4.2 General Solution	4-1
	4.3 Low Frequency Approximation	4-7
	4.4 TM Line Source Excitation	4-12
	4.5 References	4-17
5	DIFFUSION COUPLING MODELS FOR LIGHTNING AND NUCLEAR ELECTROMAGNETIC PULSE	5-1
	5.1 Introduction	5-1
	5.2 Near-Strike Lightning	5-2
	5.3 Nuclear Pulse Excitation	5-9
	5.4 Direct-Strike Lightning Attachment	5-12
	5.5 References	5-19

TABLE OF CONTENTS (Continued)

<u>Section</u>	<u>Page</u>	
6	INTERIOR FIELD RESULTS AND APPLICATION OF LOW FREQUENCY COUPLING MODELS	6-1
6.1	Results and Application of Models	6-1
6.2	References	6-19
 <u>Appendix</u>		
A	PROGRAMS FOR PERFECTLY CONDUCTING CYLINDERS OF ARBITRARY CROSS SECTION	A-1
A.1	E-Field Program	A-6
A.2	Combined-Field Program	A-11
A.3	Exact Series Program	A-17
A.4	Program to Compute Current Distribution Due to Impressed Longitudinal Current	A-22
B	PROGRAMS FOR THIN SHELLS OF ARBITRARY CROSS SECTION AND FINITE CONDUCTIVITY	B-1
B.1	Impedance Sheet Approximation Program	B-1
B.2	Exact-Series Program	B-9
C	CAD HOMOGENEOUS SHELL COUPLING ANALYSIS PROGRAM	C-1

LIST OF ILLUSTRATIONS

<u>Figure</u>		<u>Page</u>
2-1	Original Problem: Arbitrary Polarized Plane Wave Normally Incident Upon Infinite Cylinder	2-4
2-2	The Contour C Approximated by NC Straight Line Segments . .	2-6
2-3	Contour C Carrying Total z-Directed Current I_z	2-28
3-1	Original Problem: Plane Wave Illuminating a Shell of Uniform Thickness d	3-2
3-2	Approximation of Shell by Contour C	3-3
3-3	Incident Field Causing Normal Component of Polarization Current	3-6
3-4	Infinite Slab Representation of Shell Subsection	3-8
3-5	Geometry Relating to the Computation of \vec{Q} and \vec{P}	3-16
4-1	Plane Wave Incident Upon a Circular Shell	4-2
4-2	Interior Fields	4-8
4-3	Thin Shell in the Presence of a Line Source	4-13
5-1	Near-Strike Lightning Situation	5-2
5-2	Normalized Spectrum of Double Exponential Lightning Waveform	5-4
5-3	NEMP Excitation	5-10
5-4	Normalized Amplitude Spectrum of the NEMP Double Exponential Waveform	5-11
5-5	Direct-Strike Lightning Attachment to Aircraft Shell Section	5-13
5-6	Contour in Complex z Plane for Computation of Integral in Equation (29)	5-15
5-7	Contour in the Complex z Plane Used to Compute the Integral in Equation (35)	5-16

LIST OF ILLUSTRATIONS (Continued)

<u>Figure</u>		<u>Page</u>
6-1	Free Space Longitudinal Current Distribution on Conducting Cylinder Contour, $I_{total} = 20 \text{ kA}$	6-5
6-2	Electric Shielding Effectiveness (TM Case) at Center of Lossy Circular Shell, Radius = 0.5m, Thickness = 1mm	6-6
6-3	Magnetic Shielding Effectiveness (TE Case) At Center of Lossy Circular Shell, Radius = 0.5m, Thickness = 1mm	6-7
6-4	External and Internal NSL Magnetic Field for Circular Shell	6-8
6-5	Time Derivatives of Internal and External NSL Magnetic Fields for Cylindrical Shell A of Figure 6-4	6-9
6-6	Open-Circuit Voltage and Short-Circuit Current Induced on Transmission Line Inside Shell of Figure 6-5	6-10
6-7	Upper Bound on Induced Power Available in Transmission Line of Figure 6-6	6-11
6-8	Log of V_{oc} and I_{sc} Versus Transmission Line Length for Shell A of Figure 6-4	6-12
6-9	Log of P_{max} and Wunsch Constant Versus Transmission Line Length for Shell A of Figure 6-4	6-13
6-10	Log of V_{oc} and I_{sc} Versus Normalized Load Impedance for Shell A of Figure 6-4	6-14
6-11	Log of P_{max} and Wunsch Constant Versus Normalized Load Impedance for Shell A of Figure 6-4	6-15
6-12	External and Internal NEMP Magnetic Field for Circular Shell	6-16
6-13	Open-Circuit Voltage and Short-Circuit Current Induced on Transmission Lines Inside Circular Shells of Figure 6-12	6-17
6-14	Upper Bounds on Induced Power Available in Transmission Line Cases of Figure 6-13	6-18

LIST OF ILLUSTRATIONS (Continued)

<u>Figure</u>		<u>Page</u>
C-1	Cutaway View of Infinitely Long Homogeneous Cylindrical Shell with Loaded Transmission Line Circuit Inside	C-2
C-2	CAD Block Diagram	C-3

LIST OF TABLES

<u>Table</u>		<u>Page</u>
A-1	Input Data Card Sequence	A-3
A-2	Subroutines Corresponding to Computation	A-4
A-3	Common Block Variables	A-5

SECTION 1

INTRODUCTION

A major concern with the increasing use of composite materials and low voltage electronics is the amount of electromagnetic (EM) coupling to the interior of an aircraft and to the cables and electronic devices within it. The introduction of boron/epoxy, graphite/epoxy, and Kevlar/epoxy composite materials as structural elements in modern airframes will result in a substantial reduction in airframe weight, due to the high strength-to-weight ratios of these materials. The use of these new composite materials has raised questions relative to the aircraft vulnerability resulting from the effects of lightning, high power radar, nuclear electromagnetic pulse (EMP), and precipitation static. The problems are further compounded by the fact that these materials are relatively easy to construct, and have resulted in a proliferation of available composite materials.

This final report on Office of Naval Research Contract N00014-78-C-0673 describes methods for determining the shielding provided by an aircraft's exterior surface and the coupling of the interior fields to cables and transmission lines within aircraft cavities. This data is used to determine whether devices commonly found on aircraft will be subject to upset or burnout.

The penetration of an external electromagnetic field into the interior of a homogeneous shell enclosure has been widely studied and various formulations can be found in the open literature. Analytical solutions are available for the canonical geometries of twin parallel plates, a spherical shell, and an infinitely long circular shell. The utility of these solutions is manifested in a transfer function relating the interior field at a point to the field that would exist there in the absence of the shell. This result is usually presented in the frequency domain and, for low frequencies, obviates a relatively simple relationship between the interior field and the excitation field. For canonical shell geometries, this low frequency transfer function is written in terms of shell wall conductivity and thickness and shell enclosure volume-to-surface ratio. Application to noncanonical geometries can be

made as long as volume-to-surface ratios are known. As the frequency content of the excitation spectrum becomes large enough so that the electrical size of the shell cross section becomes resonant (on the order of a free-space wavelength), then the low frequency transfer function is no longer adequate to describe the penetrability of the shell. In this case it is necessary to resort to approximate numerical techniques.

In this report, several models of the shell coupling mechanism are analyzed with frequency regions of validity from dc to several gigahertz depending on shell cross section dimensions. Two-dimensional shell enclosures of infinite extent in one dimension are considered in order to facilitate the computer program solutions. Results from these theoretical enclosures are applicable to physically realizable three-dimensional enclosures which are long compared to their cross section dimension (i.e., some airplane fuselage and wing sections).

In Section 2, various integral equation formulations are outlined for determining the induced current density on perfectly conducting two-dimensional cylindrical shells having an arbitrary cross section. Though no penetration occurs if the shell wall is a perfect conductor ($\sigma = \infty$), the current density on the exterior surface caused by an incident field is much the same as that on a highly conducting (but finite σ) shell. The various integral equations are solved by the method of moments, and specific matrix operators are defined for later use. A user-oriented computer program is given in Appendix A with sample input/output data.

In Section 3, two approximate shell coupling formulations are presented for two-dimensional shells having an arbitrary cross section. The matrix operators defined in Section 2 are used in the moment method solution of the resulting integral equations. Comparison with the exact series solution for the circular cross section is used as a check. A user-oriented computer program is given in Appendix B with sample input/output data.

The exact series solution for a normally incident plane wave exciting a shell of circular cross section is summarized in Section 4. Simple low-frequency formulas are derived for the interior fields. The case of axial electric current line source excitation is also analyzed for later application to the case of near-strike lightning.

The preceding analysis is presented only in the frequency domain. However, if the excitation spectrum is sufficiently band limited and the transfer functions for the canonical geometries are valid over that frequency range, then analytical expressions for the interior field may be derived in the time domain. This is done in Section 5 for near-strike lightning, direct-strike lightning, and a nuclear electromagnetic pulse.

These techniques may be integrated to provide an accurate description of the penetration fields inside a homogeneous two-dimensional enclosure. The effect of this interior field on circuits situated inside the enclosure is of primary importance and an interactive computer program was written for this purpose which utilizes the results of Section 5. This program is described in Appendix C.

SECTION 2

PERFECTLY CONDUCTING CYLINDERS OF ARBITRARY CROSS SECTIONAL SHAPE

Although no field penetrates an enclosure with perfectly conducting walls, the electric current density induced on the wall exterior due to an external field will not differ greatly from that in the case of walls having a finite conductivity of $\sigma \approx 1000$. In fact some shell coupling formulations require a "short-circuit current" which is used to excite an equivalent problem for the shell. This is simply the current flowing on the outside surface of the shell when the walls are perfectly conducting ($\sigma = \infty$).

The purpose of this section is to present the E-field, H-field, and combined-field integral equation formulations for perfectly conducting cylinders of infinite length and arbitrary cross section illuminated by a normally incident plane wave. The E-field equation is obtained by requiring that the total tangential electric field be zero on the contour C defining the cylinder cross section. The H-field equation is obtained by requiring that the total tangential component of magnetic field equal zero just inside C. The combined-field equation is obtained by taking a linear combination of the E-field and H-field equations. These integral equations are written in matrix form by using a method of moments Galerkin procedure. The unknown electric current on C is then solved for by standard matrix methods. The exact series solution is also presented for comparison purposes when C is a circle. Generalization to oblique incidence is also outlined but not programmed. Computer programs are documented in Appendix A for the E-field, combined-field, and exact series solutions.

2.1 INTRODUCTION

The E-field and H-field formulations for this problem are well known [1,2] and some E-field computer programs have been documented [3,4]. The cross section of the cylinder is defined by the contour C, which will be approximated by straight line segments. For each formulation, an integral equation is written involving an equivalent electric current which replaces the conducting contour C.

The integral equation is then solved for the electric current by a method of moments Galerkin procedure [2,5]. Once this electric current is determined, quantities such as the scattered far field pattern and radar cross section may be easily computed.

For a normally incident plane wave, as discussed in the next subsection, the total field may be expressed as the superposition of a TE (transverse electric to z) part and a TM (transverse magnetic to z) part. Since it is not the purpose of this section to rigorously derive the different formulations, they are presented with brevity in Subsections 2.2 through 2.4 where explicit formulas are given as an aid in understanding the programs. Formulas for the scattered field pattern are given in Subsection 2.5. For comparison purposes, one may check the programs against the exact series solution presented in Subsection 2.6. A generalization to oblique incidence is given in Subsection 2.7 for the E-field integral equation. The special problem of a longitudinal impressed current excitation is considered in Subsection 2.8. Finally, detailed instructions for using the computer programs are included in Appendix A.

2.1.1 Excitation

The cylinder is assumed infinite in the z direction and is defined by the two-dimensional contour C lying in the x - y plane. The shape of C is independent of z . For simplicity, the cylinder is illuminated by a normally incident ($k_z = 0$) uniform plane wave. A time dependence of $e^{j\omega t}$ is implicit throughout. This excitation gives rise to a scattered field which is also independent of z . Thus the TE case (magnetic field parallel to z) and the TM case (electric field parallel to z) may be treated separately. The source of the scattered field is postulated to be an electric current \underline{J}_C which takes the place of the perfect conductor and which is defined on C . It is separated into a z component (TM case) and a transverse component (TE case) directed along C . For the more general excitation, where $\theta \neq \pi/2$, the two components of electric current are coupled and thus both polarizations must be treated together as indicated in Subsection 2.7.

In terms of its TE and TM parts, the incident field may be expressed as

$$\underline{E}^i = \underline{E}^{ie} + \underline{E}^{ih} \quad (1)$$

and

$$\underline{H}^i = \underline{H}^{ie} + \underline{H}^{ih} \quad (2)$$

The superscripts e and h denote TM and TE, respectively. These parts are written explicitly as

$$\underline{E}^{ie} = \underline{\hat{z}} \eta a e^{j\alpha} e^{-jk(\underline{\hat{k}} \cdot \underline{r})} \quad (3)$$

$$\underline{E}^{ih} = -(\underline{\hat{k}} \times \underline{\hat{z}}) \eta b e^{j\beta} e^{-jk(\underline{\hat{k}} \cdot \underline{r})} \quad (4)$$

$$\underline{H}^{ie} = (\underline{\hat{k}} \times \underline{\hat{z}}) a e^{j\alpha} e^{-jk(\underline{\hat{k}} \cdot \underline{r})} \quad (5)$$

$$\underline{H}^{ih} = \underline{\hat{z}} b e^{j\beta} e^{-jk(\underline{\hat{k}} \cdot \underline{r})} \quad (6)$$

in terms of the coordinate system of Fig. 2-1.

In the above, k and η are the wave number and impedance, respectively, of the space surrounding the cylinder. The unit vector $\underline{\hat{k}}$ is defined by

$$\underline{\hat{k}} = \underline{\hat{x}} \cos \phi^i + \underline{\hat{y}} \sin \phi^i \quad (7)$$

where ϕ^i is the angle of incidence measured counterclockwise from the x axis. The vector \underline{r} is from the origin to a point on the x-y plane. The real numbers a and b are chosen so that $a^2 + b^2 = 1$ and choices of $ae^{j\alpha}$ and $be^{j\beta}$ determine the polarization of the incident field, which is elliptical in general. For example, a choice of $ae^{j\alpha} = 1$ and $be^{j\beta} = 0$ gives the linearly polarized TM case. A choice of $ae^{j\alpha} = 1/\sqrt{2}$ and $be^{j\beta} = j/\sqrt{2}$ gives a left-hand circular polarization. For simplicity, $ae^{j\alpha}$ and $be^{j\beta}$ are taken to be equal to unity here.

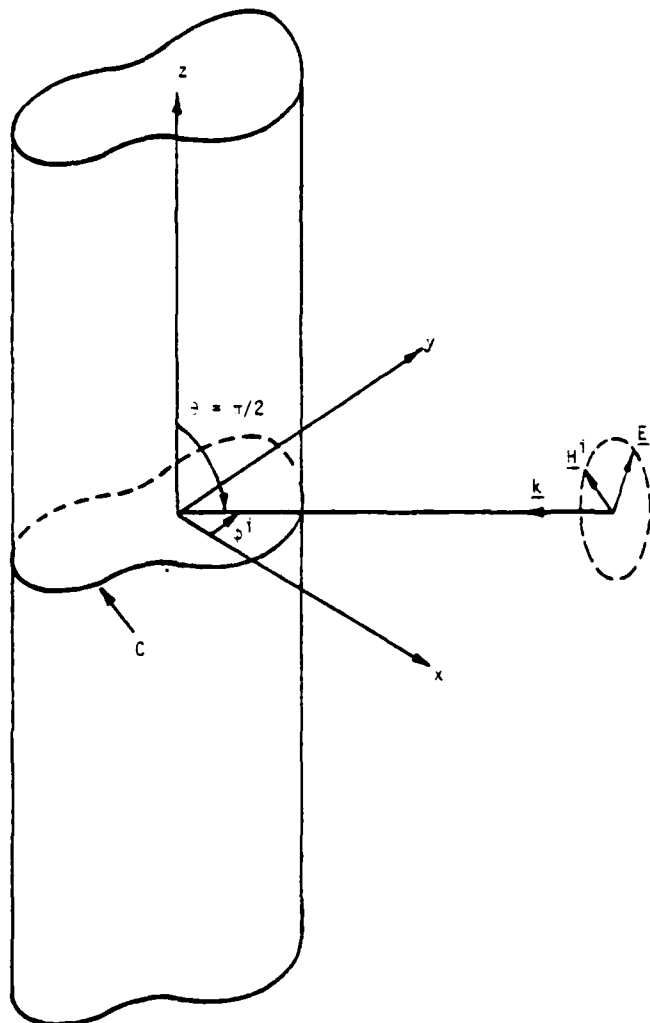


Figure 2-1. Original Problem: Arbitrary Polarized Plane Wave Normally Incident Upon Infinite Cylinder

The total field inside C is zero and the total field outside C is written as $(\underline{E}^i + \underline{E}^S, \underline{H}^i + \underline{H}^S)$ where $(\underline{E}^i, \underline{H}^i)$ is the field which exists everywhere without the cylinder present. The scattered field $(\underline{E}^S, \underline{H}^S)$ is written in terms of an electric current \underline{J}_C as [6]:

$$\underline{E}^S = \hat{\underline{E}}^S(\underline{J}_C) = -j \eta \left[k \underline{A} + \frac{1}{k} \underline{\nabla} \underline{\nabla} \cdot \underline{A} \right] \quad (8)$$

$$\underline{H}^S = \hat{\underline{H}}^S(\underline{J}_C) = \underline{\nabla} \times \underline{A} \quad (9)$$

where the magnetic vector potential \underline{A} is given by

$$\underline{A} = \frac{1}{4j} \int_C \underline{J}_C(t') H_0^{(2)}(k |\underline{r} - \underline{r}'(t')|) dt' \quad (10)$$

The symbols $\hat{\underline{E}}$ and $\hat{\underline{H}}$ denote electric and magnetic field operators, respectively. The domain of integration in Equation (10) is restricted to C, where \underline{J}_C is defined in terms of t' , the arc length variable along C. The vectors \underline{r} and \underline{r}' denote field and source points, respectively, in the x-y plane and $H_0^{(2)}$ denotes the Hankel function of the second kind, order zero.

2.1.2 Specification of Contour C

To proceed with a numerical solution, the contour C is approximated by a finite number (NC) of straight line segments as shown in Fig. 2-2. This is done by specifying the x-y coordinates of the end points of each segment starting with (x_1, y_1) and proceeding clockwise to (x_{NC+1}, y_{NC+1}) . In the E-field formulation, it is not necessary for the contour to be closed. A closed contour is one for which $(x_1, y_1) = (x_{NC+1}, y_{NC+1})$. This requirement must be met, however for the H-field formulation and hence for the combined-field formulation. Each straight line segment ΔC_n has length Δ_n , a normal unit vector $\hat{\underline{n}}_n$, and a tangent unit vector $\hat{\underline{t}}_n$ for integers $n = 1, 2, \dots, NC$. These unit vectors are related by

$$\hat{\underline{t}}_n \times \hat{\underline{n}}_n = \hat{\underline{z}} \quad (11)$$

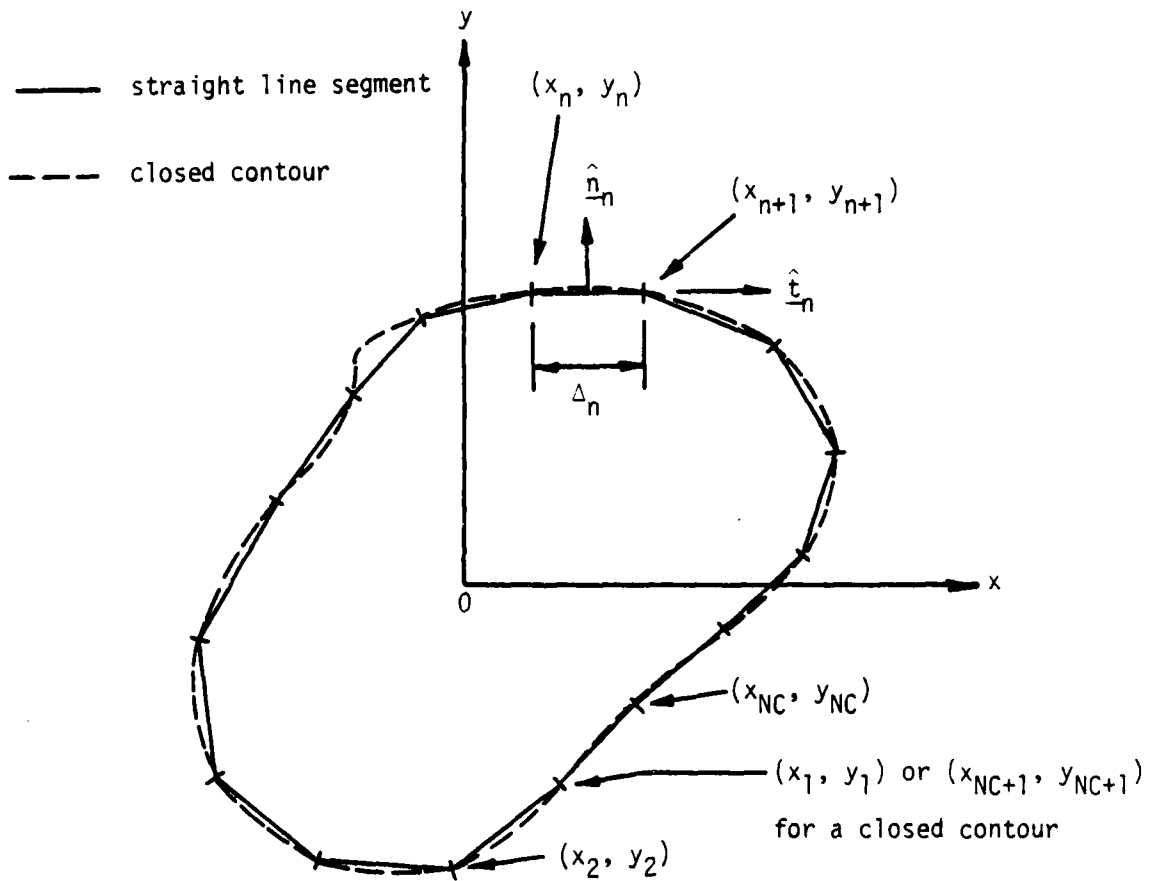


Figure 2-2. The Contour C Approximated by NC Straight Line Segments

The parameter t is introduced to represent the arc length along C measured from the point (x_1, y_1) to any point on C . Subscripted values of t are given by the formula

$$t_n = \sum_{i=1}^{n-1} \Delta_i \quad (12)$$

for $n = 2, 3, \dots, NC$ and with $t_1 \equiv 0$.

2.1.3 Definition of Expansion Functions and Symmetric Product

As mentioned earlier, \underline{J}_c may be separated into z -directed and transverse-directed components. This is written as

$$\underline{J}_c = \underline{J}_t + \underline{J}_z \quad (13)$$

Since there is a charge associated with \underline{J}_t , it is desirable that its representation in terms of a set of expansion functions be differentiable. There is no charge associated with \underline{J}_z , however, but \underline{J}_z does become unbounded near sharp edges of perfect conductors. With this in mind, we define a set of triangle functions as

$$\underline{t}_m(t) = \begin{cases} \frac{t - t_{m-1}}{t_m - t_{m-1}} \hat{t}_{m-1} & \text{for } t_{m-1} \leq t \leq t_m \\ \frac{t - t_{m+1}}{t_m - t_{m+1}} \hat{t}_m & \text{for } t_m \leq t \leq t_{m+1} \\ 0 & \text{for } t \text{ elsewhere} \end{cases} \quad (14)$$

and a set of pulse functions as

$$P_m(t) = \begin{cases} 1 & \text{for } t_m \leq t \leq t_{m+1} \\ 0 & \text{for } t \text{ elsewhere} \end{cases} \quad (15)$$

for integers $m = 1, 2, \dots, NC$ and with $t_0 \equiv -\Delta_{NC}$ and $\hat{t}_0 \equiv \hat{t}_{NC}$.

The electric current \underline{J}_c is then expanded as

$$\underline{J}_c(t) = \sum_{n=1}^{NC} I_n^h \underline{T}_n(t) + I_n^e P_n(t) \quad (16)$$

where I_n^h and I_n^e are complex coefficients to be determined for the TE and TM cases, respectively. For the TM case, $\underline{J}_t = 0$ and for the TE case, $\underline{J}_z = 0$.

In the Galerkin procedure, the testing functions are chosen to be identical to the expansion functions. Hence, to carry out this procedure, a symmetric product is defined by

$$\langle \underline{A}, \underline{B} \rangle = \int_C \underline{A} \cdot \underline{B} dt \quad (17)$$

with \underline{A} and \underline{B} defined on C .

2.2 E-FIELD FORMULATION

The E-field integral equation is obtained by setting the tangential component of the total electric field equal to zero on C . This is written as

$$-\frac{k}{\eta} \hat{E}_t^S(\underline{J}_c) = \frac{k}{\eta} \underline{E}_t^i \quad \text{on } C \quad (18)$$

where the extra factor of k/η was multiplied through for later convenience. The operator \hat{E}_t^S is defined by Equations (8) and (10) and the subscript t denotes tangential component found by the usual $-\hat{n} \times \hat{n} \times$ operation. After expanding \underline{J}_c in terms of Equations (14) or (15), depending on the polarization considered, and testing Equation (18) with the same functions used for expansion, one obtains the following sets of matrix equations:

$$[Z^e] \vec{I}^e = \vec{V}^e \quad (19)$$

for the TM case, and

$$[Z^h] \vec{I}^h = \vec{V}^h \quad (20)$$

for the TE case. The vectors \vec{I}^e and \vec{I}^h contain the coefficients of expansion in Equation (16).

2.2.1 Formulas for [Z]

The elements of the matrices $[Z^e]$ and $[Z^h]$ are given by the following formulas, where $1 \leq m \leq NC$ and $1 \leq n \leq NC$. For the TM case, we have

$$\begin{aligned} Z_{mn}^e &= -\frac{k}{\eta} \langle \underline{P}_m, \hat{E}_t^S(\underline{P}_n) \rangle \\ &= -\frac{k^2}{4} \int_{t_m}^{t_{m+1}} \underline{P}_m(t) \cdot \hat{n}_m \times \hat{n}_m \\ &\quad \times \int_{t_n}^{t_{n+1}} \underline{P}_n(t') H_0^{(2)}(k|\underline{r}(t) - \underline{r}'(t')|) dt' dt \end{aligned} \quad (21)$$

After transforming both source and field intervals to the interval $[-1,1]$ and letting $\gamma_i = k\Delta_i$, we obtain

$$z_{mn}^e = \begin{cases} \frac{\gamma_m \gamma_n}{16} \int_{-1}^1 \int_{-1}^1 H_0^{(2)} \left(\left| \frac{\gamma_m}{2} u \hat{t}_m - \frac{\gamma_n}{2} u' \hat{t}_n + \underline{R}'_{m,n} \right| \right) du' du & \text{if } m \neq n \\ \frac{\gamma_m}{8} \int_{-1}^1 \left[\alpha \left(\frac{\gamma_m}{2} (1+u) \right) + \alpha \left(\frac{\gamma_m}{2} (1-u) \right) \right] du & \text{if } m = n \end{cases} \quad (22)$$

where $\underline{R}'_{m,n}$ is k times the vector from the midpoint of ΔC_n to the midpoint of ΔC_m . The function α is defined by

$$\alpha(z) = \int_0^z H_0^{(2)}(u) du \quad (23)$$

which is computed using Struve functions [7]. The integrals in Equation (22) are readily approximated by a Gaussian quadrature integration rule [8,9]. For the TE case we have

$$\begin{aligned} z_{mn}^h &= -\frac{k}{n} \langle \underline{t}_m, \hat{E}_t^S(\underline{t}_n) \rangle \\ &= -k^2 \int_{t_{m-1}}^{t_{m+1}} \underline{t}_m(t) \cdot \hat{n} \times \hat{n} \times \left(1 + \frac{1}{k^2} \underline{\nabla} \cdot \underline{\nabla} \right) \\ &\quad \cdot \int_{t_{n-1}}^{t_{n+1}} \underline{t}_n(t') H_0^{(2)}(k|\underline{r}(t) - \underline{r}'(t')|) dt' dt \end{aligned} \quad (24)$$

where the unit vector \hat{n} resides on the field interval $\Delta C_{m-1} \cup \Delta C_m$. It is convenient to break the above integral up into four parts. Considering the contribution from each part separately, Equation (24) is rewritten as

$$z_{mn}^h = SZ^h(m-1, n-1, 1, 1) + SZ^h(m-1, n, 1, -1) + SZ^h(m, n-1, -1, 1) + SZ^h(m, n, -1, -1) \quad (25)$$

where the function SZ^h is defined by

$$SZ^h(m, n, p, q) = \left\{ \begin{array}{l} \frac{\gamma_m \gamma_n}{16} \int_{-1}^1 \int_{-1}^1 \left[\left(\frac{pu}{2} + \frac{1}{2} \right) \left(\frac{qu'}{2} + \frac{1}{2} \right) \hat{t}_m \cdot \hat{t}_n - \frac{p}{\gamma_m} \frac{q}{\gamma_n} \right] \\ \cdot H_0^{(2)} \left(\left| \frac{\gamma_m}{2} u \hat{t}_m - \frac{\gamma_n}{2} u' \hat{t}_n + \underline{R}_{m,n}' \right| \right) du' du \\ \text{if } m \neq n \\ \\ \frac{\gamma_m}{8} \int_{-1}^1 \left\{ \left[\left(\frac{pu}{2} + \frac{1}{2} \right) \left(\frac{qu}{2} + \frac{1}{2} \right) - \frac{pq}{\gamma_m} \right] \left[\alpha \left(\frac{\gamma_m}{2} (1+u) \right) \right. \right. \\ \left. \left. + \alpha \left(\frac{\gamma_m}{2} (1-u) \right) \right] + q \left(\frac{pu}{2} + \frac{1}{2} \right) \left[\left(\frac{1}{2} - \frac{u}{2} \right) \right. \right. \\ \left. \left. \cdot H_1^{(2)} \left(\frac{\gamma_m}{2} (1-u) \right) - \left(\frac{1}{2} + \frac{u}{2} \right) \right. \right. \\ \left. \left. \cdot H_1^{(2)} \left(\frac{\gamma_m}{2} (1+u) \right) \right] \right\} du \text{ if } m = n \end{array} \right. \quad (26)$$

where $H_1^{(2)}$ denotes the Hankel function of second kind, order one. Note that $[Z^e]$ and $[Z^h]$ are both symmetric matrices so that one need only compute the upper right triangle portion of each.

2.2.2 Formulas for \vec{V}^i

The elements of the excitation vectors \vec{V}^{ie} and \vec{V}^{ih} are given by the following formulas where $1 \leq m \leq NC$. For the TM case we have

$$\begin{aligned} V_m^{ie} &= \frac{k}{\eta} \langle \underline{p}_m, \underline{E}_t^{ie} \rangle \\ &= \gamma_m e^{j\hat{k} \cdot \underline{R}'_m} \frac{\sin \frac{\gamma_m}{2} (\hat{k} \cdot \underline{t}_m)}{\frac{\gamma_m}{2} (\hat{k} \cdot \underline{t}_m)} \end{aligned} \quad (27)$$

where \underline{R}'_m is k times the vector from the origin to the midpoint of ΔC_m and \hat{k} is defined by Equation (7). For the TE case we have

$$\begin{aligned} V_m^{ih} &= \frac{k}{\eta} \langle \underline{r}_m, \underline{E}_t^{ih} \rangle \\ &= \frac{\gamma_{m-1}}{2} \frac{a_{m-1}}{j b_{m-1}} e^{j\hat{k} \cdot \underline{R}'_{m-1}} \left[e^{j b_{m-1}} - \frac{\sin b_{m-1}}{b_{m-1}} \right] \\ &\quad + \frac{\gamma_m}{2} \frac{a_m}{j b_m} e^{j\hat{k} \cdot \underline{R}'_m} \left[\frac{\sin b_m}{b_m} - e^{-j b_m} \right] \end{aligned} \quad (28)$$

where $a_m = -\hat{n}_m \cdot \hat{k}$ and $b_m = (\gamma_m/2) \hat{k} \cdot \underline{t}_m$.

2.3 H-FIELD FORMULATION

The H-field integral equation is obtained by setting the tangential component of the total magnetic field equal to zero just inside C. This is written as

$$-k \hat{n} \times \hat{H}^S(\underline{J}_C) = k \hat{n} \times \hat{H}^i \quad \text{on } C^- \quad (29)$$

where C^- denotes a contour just on the $-\hat{n}$ side of C. The factor of k has been multiplied through for later convenience. The magnetic field operator, \hat{H}^S , is defined by Equations (9) and (10). After expanding \underline{J}_C in terms of Equations (13) or (14), depending on the polarization considered, and testing Equation (29) with the same functions used for expansion, one obtains the following sets of matrix equations:

$$[T^e] \vec{I}^e = \vec{I}^{ie} \quad (30)$$

for the TM case, and

$$[T^h] \vec{I}^h = \vec{I}^{ih} \quad (31)$$

for the TE case. The vectors \vec{I}^e and \vec{I}^h again contain the coefficients of expansion in Equation (16).

2.3.1 Formulas for [T]

The elements of the matrices $[T^e]$ and $[T^h]$ are given by the following formulas, where $1 \leq m \leq NC$ and $1 \leq n \leq NC$. For the TM case we have

$$\begin{aligned}
 T_{mn}^e &= -k \langle \underline{P}_m, \hat{n} \times \hat{H}^S(\underline{P}_n) \rangle \\
 &= k \int_{t_m}^{t_{m+1}} \frac{1}{2} \underline{P}_m(t) \cdot \underline{P}_n(t) dt - \frac{k^2}{4j} \int_{t_m}^{t_{m+1}} \underline{P}_m(t) \\
 &\quad \cdot \int_{t_n}^{t_{n+1}} \hat{n}_m \times \underline{P}_n(t') \times \frac{(\underline{r} - \underline{r}')}{|\underline{r} - \underline{r}'|} H_1^{(2)}(k|\underline{r} - \underline{r}'|) dt' dt
 \end{aligned} \tag{32}$$

The first term is simply the Ampere's law contribution to the integral when the field point is on C^- . Again, after some algebra, one may obtain

$$T_{mn}^e = \begin{cases} \frac{\gamma_m}{2} & \text{if } m = n \\ -\frac{\gamma_m \gamma_n}{16j} \int_{-1}^1 \int_{-1}^1 \frac{\hat{n}_m \cdot \hat{R}'_{m,n}}{|\hat{R}'_{m,n}|} H_1^{(2)}(|\hat{R}'_{m,n}|) du' du & \text{if } m \neq n \end{cases} \tag{33}$$

In the above, $\hat{R}'_{m,n}$ is given by

$$\hat{R}'_{m,n} = \frac{R'_{m,n}}{R_{m,n}} + \frac{\gamma_m}{2} u \hat{t}_m - \frac{\gamma_n}{2} u' \hat{t}_n \tag{34}$$

where $\underline{R}'_{m,n}$ is k times the vector from the midpoint of ΔC_n to the midpoint of ΔC_m . For the TE case we have

$$\begin{aligned}
 T_{mn}^h &= -k \langle \underline{r}_m, \hat{n} \times \underline{H}^S(\underline{r}_n) \rangle \\
 &= \frac{k}{2} \int_{t_{m-1}}^{t_{m+1}} \underline{r}_m(t) \cdot \underline{r}_n(t) dt - \frac{k^2}{4j} \int_{t_{m-1}}^{t_{m+1}} \underline{r}_m(t) \\
 &\quad \cdot \int_{t_{n-1}}^{t_{n+1}} \hat{n} \times \underline{r}_n(t') \times \frac{(\underline{r} - \underline{r}')}{|\underline{r} - \underline{r}'|} H_1^{(2)}(k|\underline{r} - \underline{r}'|) dt' dt
 \end{aligned} \tag{35}$$

The first term is again the Ampere's law contribution when the field and source interval coincide. It is also convenient to break the whole integral in Equation (35) into four parts. Considering the contribution from each part separately, Equation (35) is rewritten as

$$\begin{aligned}
 T_{mn}^h &= ST^h(m-1, n-1, 1, 1) + ST^h(m-1, n, 1, -1) \\
 &\quad + ST^h(m, n-1, -1, 1) + ST^h(m, n, -1, -1)
 \end{aligned} \tag{36}$$

where the function ST^h is defined by

$$ST^h(m,n,p,q) = \begin{cases} -\frac{\gamma_m \gamma_n}{16j} \int_{-1}^1 \int_{-1}^1 \left(p \frac{u}{2} + \frac{1}{2}\right) \left(q \frac{u'}{2} + \frac{1}{2}\right) \epsilon(m,n) du' du & \text{if } m \neq n \\ \frac{\gamma_m}{4} \left(\frac{1}{2} + \frac{pq}{6}\right) & \text{if } m = n \end{cases} \tag{37}$$

where

$$p(m,n) = \frac{\hat{n} \cdot \hat{R}'_{m,n}}{|\hat{R}'_{m,n}|} H_1^{(2)}(|\hat{R}'_{m,n}|) \quad (38)$$

2.3.2 Formulas for \vec{I}^i

The elements of the excitation vectors, \vec{I}^{ih} and \vec{I}^{ie} , are given by the following formulas where $1 \leq m \leq NC$. In the TM case we have

$$\begin{aligned} I_m^{ie} &= k \langle \hat{p}_m, \hat{n} \times \underline{H}^i \rangle \\ &= (\hat{n}_m \cdot \hat{k}) \gamma_m e^{jk \cdot \underline{R}'_m} \frac{\sin \frac{\gamma_m}{2} (\hat{k}_m \cdot \hat{t}_m)}{\frac{\gamma_m}{2} (\hat{k}_m \cdot \hat{t}_m)} \end{aligned} \quad (39)$$

For the TE case we have

$$\begin{aligned} I_m^{ih} &= k \langle \hat{t}_m, \hat{n} \times \underline{H}^i \rangle \\ &= \frac{\gamma_{m-1}}{2} \frac{e^{jk \cdot \underline{R}'_{m-1}}}{jb_{m-1}} \left[e^{jb_{m-1}} - \frac{\sin b_{m-1}}{b_{m-1}} \right] \\ &\quad + \frac{\gamma_m}{2} \frac{e^{jk \cdot \underline{R}'_m}}{jb_m} \left[\frac{\sin b_m}{b_m} - e^{-jb_m} \right] \end{aligned} \quad (40)$$

2.4 COMBINED FIELD FORMULATION

It can be shown [10] that the E-field or H-field equations are not sufficient by themselves to uniquely determine the electric current distribution, \underline{J}_c . That is, they each may have non-trivial homogeneous solutions at

frequencies which correspond to internal eigenfrequencies of the closed contour C. To illustrate this correspondence, consider the TE interior problem, where the total electric field \underline{E} inside C must satisfy

$$(\nabla_t^2 + k^2) \underline{E} = 0 \quad \text{inside C} \quad (41)$$

subject to the boundary condition

$$\underline{E}_t = 0 \quad \text{on C} \quad (42)$$

This is mathematically identical to the external problems:

- ° H-field formulation, TM case
- ° E-field formulation, TE case

Thus, these problems have the same eigenfrequencies. Similarly, for the TM interior problem, the total electric field, \underline{E}_z , inside C satisfies

$$(\nabla_t^2 + k^2) E_z = 0 \quad \text{inside C} \quad (43)$$

subject to the boundary condition

$$E_z = 0 \quad \text{on C} \quad (44)$$

This problem is mathematically identical to the external problems

- ° E-field formulation, TM case
- ° H-field formulation, TE case

Thus, at or near these internal resonant frequencies, the E-field and H-field matrices become ill-behaved. To remedy this situation, a linear combination of the E- and H-field equations is formed:

$$-k \hat{\underline{n}} \times \hat{\underline{H}}^S(\underline{J}_c) - \beta \frac{k}{\eta} \hat{\underline{E}}_t^S(\underline{J}_c) = k \hat{\underline{n}} \times \underline{H}^i + \beta \frac{k}{\eta} \underline{E}_t^i \quad (45)$$

This equation is referred to as the combined field formulation and it can be shown [10] that Equation (45) has a unique solution for \underline{J}_c for any contour C at all frequencies as long as β is a positive real number. In matrix form, Equation (45) is written as

$$[T^e + \beta Z^e] \vec{I}^e = \vec{I}^{ie} + \beta \vec{V}^{ie} \quad (46)$$

for the TM case, and

$$[T^h + \beta Z^h] \vec{I}^h = \vec{I}^{ih} + \beta \vec{V}^{ih} \quad (47)$$

for the TE case. The formulas for these matrix elements are given in Subsections 2.2 and 2.3.

2.5 FORMULAS FOR SCATTERING CROSS SECTION

Once the electric current \underline{J}_c is found, the scattered field ($\underline{E}^S, \underline{H}^S$) is readily computed from Equations (8) through (10). In the far-field, $|\underline{r}| \gg \lambda$, there are two quantities of interest which are computed from \underline{J}_c . One is the normalized scattered field pattern. This is simply a plot of $|E_z^S/E_z^S \max|$ versus ϕ for the TM case and $|H_z^S/H_z^S \max|$ versus ϕ for the TE case. The denominator is the maximum value of scattered field. The second quantity of interest is the scattering cross section. For the TM case, this is defined by the equation [2]

$$\sigma(\phi) = \lim_{r \rightarrow \infty} 2\pi r \left| \frac{E_z^S(r, \phi)}{E_z^i} \right|^2 \quad (48)$$

Using Equation (3) with $ae^{j\alpha} = 1$ and specializing $H_o^{(2)}(k|\underline{r} - \underline{r}'|)$ to large \underline{r} , we obtain

$$\sqrt{\sigma/\lambda} = \frac{1}{\sqrt{8\pi}} \left| k \int_C J_z e^{jk(\hat{k} \cdot \underline{r}')} dt' \right| \quad (49)$$

After Equation (15) is used for J_z , this may be rewritten as

$$\sqrt{\sigma/\lambda} = \frac{1}{\sqrt{8\pi}} \left| \tilde{v}^{me} \tilde{I}^e \right| \quad (50)$$

where the tilda denotes transpose and \tilde{v}^{me} is a "measurement" vector whose elements are defined by

$$v_m^{me}(\phi) = k \int_{t_m}^{t_{m+1}} p_m(t) e^{jk(\hat{k} \cdot \underline{r}')} dt' \quad (51)$$

For the TE case we have

$$\sigma(\phi) = \lim_{r \rightarrow \infty} 2\pi r \left| \frac{H_z^S(r, \phi)}{H_z^I} \right|^2 \quad (52)$$

Using Equation (6) with $be^{j\beta} = 1$ and again specializing $H_o^{(2)}(k|\underline{r} - \underline{r}'|)$ to large \underline{r} we have

$$\sqrt{\sigma/\lambda} = \frac{1}{\sqrt{8\pi}} \left| k \int_C J_t(t') (\hat{n} \cdot \hat{k}) e^{jk(\hat{k} \cdot \underline{r}')} dt' \right| \quad (53)$$

This is also written in terms of a TE measurement vector, \tilde{v}^{mh} , as

$$\sqrt{\sigma/\lambda} = \frac{1}{\sqrt{8\pi}} \left| \tilde{v}^{mh} \tilde{I}^h \right| \quad (54)$$

where the elements of \tilde{v}^{mh} are defined by

$$v_m^{mh} = k \int_{t_{m-1}}^{t_{m+1}} \tau_m(t') (\hat{n} \cdot \hat{k}) e^{jk(\hat{k} \cdot \underline{r}')} dt' \quad (55)$$

Note that \vec{V}^{mh} and \vec{V}^{me} are identical to the E-field excitation vectors \vec{V}^{ih} and \vec{V}^{ie} , respectively, for measurement angle $\phi = \phi^i$.

2.6 EXACT SERIES SOLUTION

Here the cylinder is defined by a contour C which is a circle of radius a. The angle of incidence will be chosen at $\phi^i = 0$. Thus for the TM case, the incident field at a point \underline{r} is expanded as [6]

$$\begin{aligned} E_z^i &= \eta e^{jkx} \\ &= \eta e^{jkr \cos \phi} \\ &= \eta \sum_{n=0}^{\infty} \epsilon_n j^n J_n(kr) \cos n\phi \end{aligned} \quad (56)$$

Neumann's number ϵ_n is defined by

$$\epsilon_n = \begin{cases} 1 & \text{for } n = 0 \\ 2 & \text{for } n > 0 \end{cases} \quad (57)$$

For the TE case, the incident field on C is expanded similarly as

$$\begin{aligned} H_z^i &= e^{jkx} \\ &= \sum_{n=0}^{\infty} \epsilon_n j^n J_n(kr) \cos n\phi \end{aligned} \quad (58)$$

Writing \underline{J}_c in Equation (13) in terms of its components on C we have

$$\underline{J}_c = J_z \hat{z} + J_\phi \hat{\phi} \quad (59)$$

where J_z and J_ϕ may be expanded in a Fourier series on C of the form

$$J_z(\phi) = \frac{2}{\pi ka} \left[a_0 + 2 \sum_{n=1}^{\infty} a_n \cos n\phi \right] \quad (60)$$

and

$$J_\phi(\phi) = \frac{2j}{\pi ka} \left[c_0 + 2 \sum_{n=1}^{\infty} c_n \cos n\phi \right] \quad (61)$$

The coefficients are obtained by enforcing the boundary conditions on the tangential components of $\underline{E}^i + \underline{E}^S$ and $\underline{H}^i + \underline{H}^S$ at $r = a$. They are given by [6,11]

$$\begin{aligned} a_0 &= \frac{1}{H_0^{(2)}(ka)} & c_0 &= \frac{1}{H_0^{(2)'}(ka)} \\ a_n &= \frac{(-j)^n}{H_n^{(2)}(ka)} & c_n &= \frac{(-j)^n}{H_n^{(2)'}(ka)} \end{aligned} \quad (62)$$

Note that, in the above expansion for J_ϕ , $\hat{\phi} = -\hat{t}$.

Formulas for the normalized scattered field pattern are given by

$$\sqrt{\sigma/\lambda} = \sqrt{2/\pi} \left| b_0 + 2 \sum_{n=1}^{\infty} b_n \cos n\phi \right| \quad (63)$$

for the TM case and

$$\sqrt{\sigma/\lambda} = \sqrt{2/\pi} \left| d_0 + 2 \sum_{n=1}^{\infty} d_n \cos n\phi \right| \quad (64)$$

for the TE case. The coefficients are given by

$$\begin{aligned}
 b_0 &= \frac{J_0(ka)}{H_0^{(2)}(ka)} & d_0 &= \frac{J_0'(ka)}{H_0^{(2)'}(ka)} \\
 b_n &= (-1)^n \frac{J_n(ka)}{H_n^{(2)}(ka)} & d_n &= (-1)^n \frac{J_n'(ka)}{H_n^{(2)'}(ka)}
 \end{aligned}
 \tag{65}$$

2.7 OBLIQUE INCIDENCE

A plane wave which is incident at an angle θ^i from the x axis and ϕ^i from the z axis of Fig. 2-1 is written in the form

$$\underline{E}^i = \underline{E}_0 e^{jk(\hat{k}_t + k_z \hat{z}) \cdot \underline{r}}
 \tag{66}$$

where the argument of the exponential is defined by

$$\begin{aligned}
 k &= 2\pi/\lambda = \omega \sqrt{\mu\epsilon} \\
 \underline{k}_t &= \sin \theta^i \cos \phi^i \hat{x} + \sin \theta^i \sin \phi^i \hat{y} \\
 k_z &= \cos \theta^i \\
 \underline{r} &= x \hat{x} + y \hat{y}
 \end{aligned}
 \tag{67}$$

The z dependence of the incident field gives rise to a z-dependent scattered field and it is no longer possible to decouple the z-directed and transverse-directed components of \underline{J}_c . The E-field integral equation is now written as

$$\underline{E}_t^S(r, z) = -\underline{E}_t^i(r, z) \quad r \text{ on } C \text{ for all } z
 \tag{68}$$

which must be satisfied everywhere on C. We define the Fourier transform pairs

$$\underline{E}(r, z) = \frac{1}{\sqrt{2\pi}} \int_{-\infty}^{\infty} \underline{E}(r, k_z) e^{jk_z z} dk_z \quad (69)$$

and

$$\underline{E}(r, k_z) = \frac{1}{\sqrt{2\pi}} \int_{-\infty}^{\infty} \underline{E}(r, z) e^{-jk_z z} dz \quad (70)$$

Taking the transform of Equation (68) gives

$$\underline{E}_t^S(r, k_z) = -\underline{E}_t^i(r, k_z) \quad \text{on C} \quad (71)$$

The scattered field \underline{E}^S is caused by an equivalent electric current $\underline{J}(r', z')$ and is written as

$$\underline{E}^S(r, z) = -j\eta \left[k \int_C \int_{z'} \underline{J} G dt' dz' + \frac{1}{k} \underline{\nabla} \cdot \int_C \int_{z'} \underline{J} G dt' dz' \right] \quad (72)$$

where G is the Green's function defined by

$$G(r, z, r', z') = \frac{e^{-jk \sqrt{|\underline{r} - \underline{r}'|^2 + (z - z')^2}}}{4\pi \sqrt{|\underline{r} - \underline{r}'|^2 + (z - z')^2}} \quad (73)$$

The $\underline{\nabla} \cdot$ operator in the second term is taken inside to give

$$\underline{E}^S(r, z) = -j\eta \left[k \int_C \int_{z'} \underline{J} G dt' dz' + \frac{1}{k} \underline{\nabla} \int_C \int_{z'} \underline{\nabla}' \cdot \underline{J} G dt' dz' \right] \quad (74)$$

The transform of Equation (74) is

$$\begin{aligned} \underline{E}^S(r, k_z) = & -\frac{j\eta}{\sqrt{2\pi}} \left[k \int_C \int_{z'} \underline{J} \left(\int_{-\infty}^{\infty} G e^{-jk_z z} dz \right) dt' dz' \right. \\ & \left. + \frac{1}{k} \int_C \int_{z'} (\underline{\nabla}' \cdot \underline{J}) \left(\int_{-\infty}^{\infty} G e^{-jk_z z} dz \right) dt' dz' \right] \end{aligned} \quad (75)$$

To do the first integral, note that G satisfies

$$\nabla^2 G + k^2 G = -\delta(\underline{r} - \underline{r}') \quad (76)$$

This is rewritten in the form

$$\nabla_t^2 G + \frac{\partial^2 G}{\partial z^2} + k^2 G = -\delta(\underline{R}) \delta(z - z') \quad (77)$$

where $\underline{R} = (x - x') \hat{x} + (y - y') \hat{y}$. The transform of Equation (77) with respect to $(z - z')$ is

$$(\nabla_t^2 + k_t^2) \hat{G} = -\delta(\underline{R}) \quad (78)$$

where

$$\hat{G} = \frac{1}{\sqrt{2\pi}} \int_{-\infty}^{\infty} G e^{-jk_z(z - z')} d(z - z') \quad (79)$$

and

$$k_t^2 = k^2 - k_z^2 \quad (80)$$

The solution to Equation (78) is

$$\hat{G} = \frac{1}{4j} H_0^{(2)}(k|\underline{R}|) \quad (81)$$

Thus we have

$$\int_{-\infty}^{\infty} G e^{-jk_z z} dz = e^{-jk_z z'} \hat{G} \quad (82)$$

The second integral in Equation (75) is aided by the identity

$$\underline{\nabla} \int_{-\infty}^{\infty} G e^{-jk_z z} dz = e^{-jk_z z'} \underline{\nabla}_t \hat{G} - j k_z \hat{G} \hat{z} \quad (83)$$

Thus we have, after writing $\underline{J} = \underline{J}_t + \hat{z} J_z$,

$$\begin{aligned} \underline{E}^S(r, k_z) = & -\frac{j\eta}{\sqrt{2\pi}} \left\{ k \int_C \int_{-\infty}^{\infty} (\underline{J}_t + \hat{z} J_z) e^{-jk_z z'} \hat{G} dt' dz' \right. \\ & \left. + \frac{1}{k} \int_C \int_{-\infty}^{\infty} (\underline{\nabla}' \cdot \underline{J}) \left[e^{-jk_z z'} \underline{\nabla}_t \hat{G} - j k_z \hat{G} \hat{z} \right] dt' dz' \right\} \end{aligned} \quad (84)$$

Now let

$$\underline{g}(t', k_z) = \frac{1}{\sqrt{2\pi}} \int_{-\infty}^{\infty} \underline{J}(t', z') e^{-jk_z z'} dz' \quad (85)$$

and

$$\underline{J}(t', z') = \frac{1}{\sqrt{2\pi}} \int_{-\infty}^{\infty} \underline{J}(t', k_z) e^{jk_z z'} dk_z \quad (86)$$

Expanding the divergence of \underline{J} gives

$$\underline{\nabla}' \cdot \underline{J}(t', z') = j k_z \underline{J}(t', z') + \frac{\partial}{\partial t'} \underline{J}(t', z') \quad (87)$$

Substituting Equation (87) into Equation (84), one obtains

$$\begin{aligned} \underline{E}^S(r, k_z) = & -j\eta \left[k \int_C \underline{J}_t \hat{G} dt' + \frac{1}{k} \int_C \left(\frac{\partial}{\partial t'} \underline{J}_t(t', k_z) \right. \right. \\ & \left. \left. + j k_z \underline{J}_t(t', k_z) \right) \cdot \underline{\nabla}'_t \hat{G} dt' \right] \\ & + \hat{z} \left[k \int_C \underline{J}_z \hat{G} dt' + \frac{1}{k} \int_C \left(j k_z \underline{J}_z(t', k_z) \right. \right. \\ & \left. \left. + \frac{\partial}{\partial t'} \underline{J}_z \right) (-j k_z) \hat{G} dt' \right] \end{aligned} \quad (88)$$

Thus putting Equation (71) into matrix form would yield the following:

$$\begin{bmatrix} Z_{zz} & Z_{zt} \\ Z_{tz} & Z_{tt} \end{bmatrix} \begin{bmatrix} \vec{I}_z \\ \vec{I}_t \end{bmatrix} = \begin{bmatrix} \vec{V}_z \\ \vec{V}_t \end{bmatrix} \quad (89)$$

where the elements of the submatrices, Z , are found from Equation (88).

2.8 CURRENT DISTRIBUTION ON CONDUCTOR DUE TO IMPRESSED LONGITUDINAL CURRENT

In the preceding sections, formulations were presented for determining the induced surface current distribution on perfect conducting cylinders of arbitrary cross section and infinite length. The excitation was taken to be a uniform plane wave. Here we consider a different type of excitation, namely, that of a steady-state current which flows axially along the cylinder. If the cylinder contour C is not circular, the current density on C is distributed around the contour due to inductive effects. It is this current redistribution which is solved for here by an integral equation formulation.

The perfect electric conductor C is infinite in the z direction and carries a total current I_z amp. Let the surface current density on C be denoted by J_z amp/m. Then

$$\int_C J_z \, dc = I \quad (90)$$

where dc is the elemental arc length on C . Since I is independent of frequency, there is no electric field. Thus the magnetic field satisfies the equations:

$$\underline{\nabla} \cdot \underline{H} = 0 \text{ everywhere} \quad (91)$$

$$\underline{\nabla} \times \underline{H} = \begin{cases} \underline{J}_z \text{ on } C \\ \underline{0} \text{ in } R_o \text{ and } R_i \end{cases} \quad (92)$$

Since C is a perfect conductor, $\underline{H} = 0$ in the internal region, R_i , shown in Fig. 2-3. For the region, R_o , \underline{H} may be written as [from Equation (92)]

$$\underline{H} = \underline{\nabla} \times \underline{A} \quad (93)$$

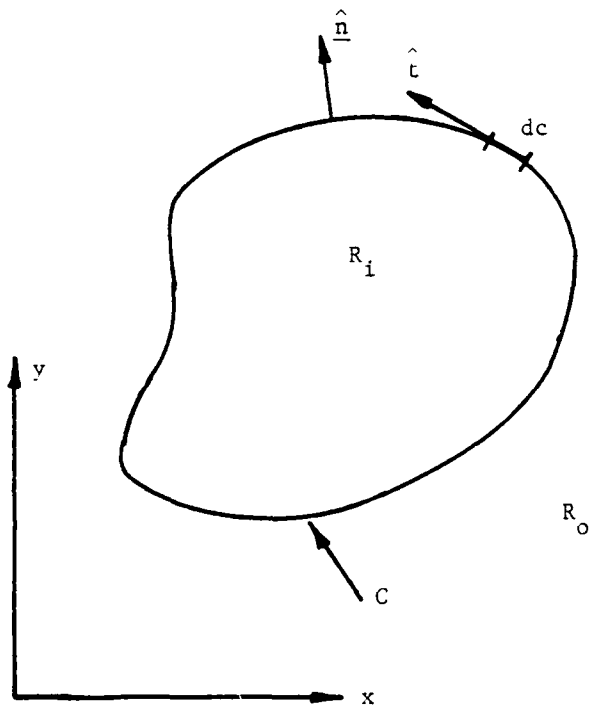


Figure 2-3. Contour C Carrying Total z -Directed Current I_z

where \underline{A} satisfies

$$\underline{\nabla} \times \underline{\nabla} \times \underline{A} = \underline{J}_z = \underline{\nabla}(\underline{\nabla} \cdot \underline{A}) - \nabla^2 \underline{A} \quad (94)$$

\underline{A} is in the z direction only and independent of z so

$$\nabla^2 A_z = -J_z \quad (95)$$

The boundary condition that \underline{H} satisfies is [from Equation (91)]

$$\hat{n} \cdot \underline{H} = 0 \quad \text{on } C \quad (96)$$

This is rewritten in terms of A_z as

$$\frac{\partial A_z}{\partial c} = 0 \quad \text{on } C \quad (97)$$

where we have used the fact that $\hat{n} \times \hat{t} = \hat{z}$. The solution to Equation (95) may be written as

$$A_z = -\frac{1}{2\pi} \int_C J_z(c') \ln |\underline{r} - \underline{r}'| dc' \quad (98)$$

where \underline{r} is a point in R_0 and $\underline{r}' = \underline{r}'(c')$ is a point on C . Now Equation (97) implies that $A_z = \text{constant}$ on C . Thus the integral equation that J_z satisfies is

$$-\frac{1}{2\pi} \int_C J_z(c') \ln |\underline{r} - \underline{r}'| dc' = K \quad (99)$$

subject to the constraint of Equation (90). K is a constant which depends on the geometry of C . For a circle of radius a ,

$$K = \frac{I}{2\pi a^2 \ln 2a} \quad (100)$$

Equation (99) may be solved by choosing $K = -1/2\pi$. Proceeding as in the previous sections, we break C up into N subsections. Over each subsection, J_z is assumed constant. This is equivalent to using the pulse basis defined by Equation (15). Thus we have

$$J_z = \sum_{j=1}^N \alpha_j P_j(t) \quad (101)$$

where α_j are unknown coefficients. This is substituted into Equation (99) to obtain

$$\sum_{j=1}^N \alpha_j \int_{-\Delta_j/2}^{\Delta_j/2} \ln(|\underline{r} - \underline{r}_j - t \hat{\underline{t}}_j|) dt = 1 \quad (102)$$

For computational simplicity, a point-matching procedure is used where the impulse functions

$$\delta_j(\underline{r}) = \begin{cases} 1 & \text{if } \underline{r} \text{ is on } \Delta_j \\ 0 & \text{if } \underline{r} \text{ is elsewhere on } C \end{cases} \quad (103)$$

are used for testing. The resulting matrix equation is given by

$$[M] \vec{\alpha} = \vec{K} \quad (104)$$

where

$$M_{ij} = \frac{\Delta_j}{2} \int_{-1}^1 \ln \left| \underline{r}_i - \underline{r}_j - t \frac{\Delta_j}{2} \hat{\underline{t}}_j \right| dt \quad (105)$$

Equation (105) can be evaluated analytically and is given by

$$M_{ij} = \begin{cases} \Delta_i \left[\ln \frac{\Delta_i}{2} - 1 \right] & \text{if } i = j \\ \frac{\Delta_j}{4} \ln (RU \cdot RL) - \frac{\hat{t}_j \cdot \underline{R}}{2} \ln (RU/RL) - \Delta_j \\ + |\hat{n}_j \cdot \underline{R}| \left\{ \tan^{-1} \left[\frac{\frac{\Delta_j}{2} - \hat{t}_j \cdot \underline{R}}{|\hat{n}_j \cdot \underline{R}|} \right] - \tan^{-1} \left[\frac{\frac{\Delta_j}{2} - \hat{t}_j \cdot \underline{R}}{|\hat{n}_j \cdot \underline{R}|} \right] \right\} & \text{if } i \neq j \end{cases} \quad (106)$$

where the following notation is used:

$$\underline{r}_i = \text{vector from origin to midpoint of } \Delta_i$$

$$\underline{r}_i - \underline{r}_j = R_x \hat{x} + R_y \hat{y} = \underline{R}$$

$$\hat{t}_i \times \hat{n}_i = \hat{z} \implies \begin{cases} t_x = n'_y \\ t_y = -n'_x \end{cases}$$

$$\hat{t}_j = t_{jx} \hat{x} + t_{jy} \hat{y}$$

$$RU = \left(R_x - \frac{\Delta_j}{2} t_{jx} \right)^2 + \left(R_y - \frac{\Delta_j}{2} t_{jy} \right)^2$$

$$RL = \left(R_x + \frac{\Delta_j}{2} t_{jx} \right)^2 + \left(R_y + \frac{\Delta_j}{2} t_{jy} \right)^2$$

2.9 References

- [1] R.F. Wallenberg, "Two-Dimensional Scattering and Radiation from Perfectly Conducting Cylinders of Arbitrary Shape", PhD Dissertation, Syracuse University, Syracuse, New York, March 1968.
- [2] R.F. Harrington, "Field Computation by Moment Methods", Reprinted by the author, 1968.
- [3] D.T. Auckland and R.F. Harrington, "Moment Solution for Radiation and Scattering from Conducting Cylinders, TM Case", Syracuse University Technical Report TR-75-8, July 1975. Also as a computer program description in IEEE Trans. on Ant. and Prop., July 1976.
- [4] J.H. Richmond, "An Integral-Equation Solution for TE Radiation and Scattering from Conducting Cylinders", Interaction Note 201, April 1973.
- [5] K. Rektorys, "Variational Methods in Mathematics, Science, and Engineering", D. Reidel Publishing Co., Dordrecht, Holland, 1977, Chapter 14.
- [6] R.F. Harrington, "Time-Harmonic Electromagnetic Fields", McGraw-Hill Book Company, New York, 1961, Section 3.12.
- [7] M. Abramowitz and I. Stegun, "Handbook of Mathematical Functions", Dover Publications, Inc., New York, 1965.
- [8] V.I. Krylov, "Approximate Calculation of Integrals", translated by A.H. Stroud, The Macmillan Co., New York, 1962, pp. 107-122.
- [9] D.T. Auckland and R.F. Harrington, "Electromagnetic Transmission Through a Filled Slit of Arbitrary Cross Section in a Conducting Plane of Finite Thickness", Syracuse University Technical Report TR-79-7, Syracuse, New York, May 1979.
- [10] J.R. Mautz and R.F. Harrington, "E-Field, H-Field, and Combined-Field Solutions for Bodies of Revolution", Syracuse University Technical Report TR-77-2, Syracuse, New York, February 1977.
- [11] Ruck, et. al., "Radar Cross Section Handbook", Volume 1, Plenum Press, New York, 1970, Chapter 4.
- [12] D.T. Auckland and R.F. Harrington, "Computer Programs for Thick Slits", Syracuse University Technical Report.

SECTION 3

THIN SHELLS OF ARBITRARY CROSS SECTION AND FINITE CONDUCTIVITY

Two approximate methods are presented here for computer-aided analysis of field penetration into cylindrical shells. The first method effectively replaces the shell by an equivalent impedance sheet boundary condition which results in a modified E-field integral equation. The second method utilizes a transmission line analysis to derive a surface load impedance to be used in a loaded body E-field integral equation. The E-field operator developed in Section 2 for both polarizations is used. The adjective "thin", as used here, means the shell thickness is small with respect to a wavelength in the surrounding medium but may be appreciable with respect to the shell material wavelength.

3.1 INTRODUCTION

The primary purpose of this section is to develop some approximate techniques for computing the electromagnetic scattering and penetration properties of two-dimensional shells of an arbitrary cross section and having finite conductivity. Quantities of interest are thus scattering cross section and near fields inside the shell. The latter are characterized by the "shielding effectiveness" of the shell which is defined here as [1]

$$SE = 20 \log \left| \frac{\underline{F}^{NS}}{\underline{F}^S} \right| \text{ (dB)} \quad (1)$$

where \underline{F}^{NS} and \underline{F}^S are fields computed at a point without and with the shell present, respectively.

The original problem is shown in Fig. 3-1 where a plane wave illuminates a shell of thickness d . The shell is made up of material with constitutive parameters μ_0 , ϵ , σ and the surrounding material is free space (μ_0 , ϵ_0).

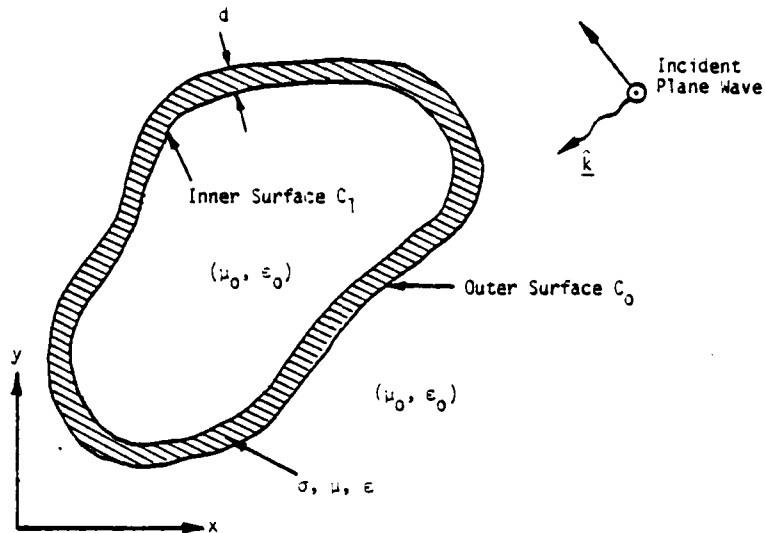


Figure 3-1. Original Problem: Plane Wave Illuminating a Shell of Uniform Thickness d

The conductivity σ may also be a function of position in the shell. The thickness d is assumed to be much less than the wavelength of free space, λ_0 . Thus, as far as the surrounding medium is concerned, the shell may be replaced by a single contour, C . This contour is further approximated by a finite number of straight line segments ΔC_i for $i = 1, 2, \dots, NC$. This is shown in Fig. 3-2. The original properties of the shell are accounted for by assigning to each segment ΔC_i a value of d and σ . Each line segment has length Δ_i and unit vectors \hat{t}_i and \hat{n}_i such that $\hat{t}_i \times \hat{n}_i = \hat{z}$. The excitation consists of two types of plane waves, each to be considered separately. These are the TE case (z component of magnetic field only) and the TM case (z component of electric field only).

A general formulation of the problem in Fig. 3-1 requires the use of equivalent electric and magnetic currents on the inner and outer surfaces

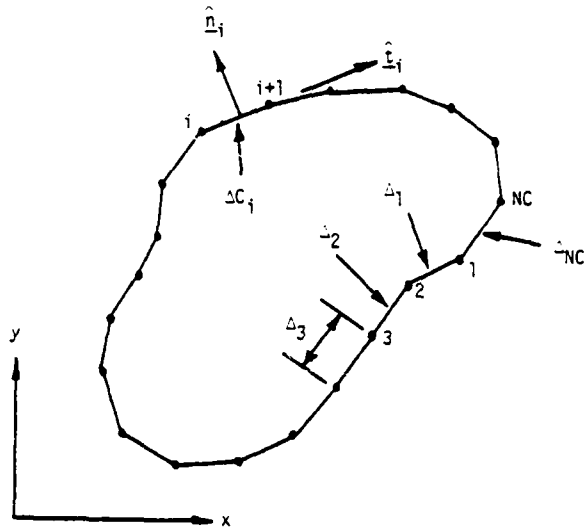


Figure 3-2. Approximation of Shell by Contour C

of the shell. This is given in [2] and will not be discussed here. Instead, some approximate formulations will be developed which are valid for certain types of shells. As a starting point, the shell material is assumed to be a fairly good conductor. If d is also much less than the wavelength in the shell, λ_b , then an impedance sheet approximation may be used [3]. The derivation of this formulation is summarized in Subsection 3.2 for use in computer program 1. If the frequency is higher, so that d is then comparable to λ_b , the shell material may be assumed to support traveling waves. Here a transmission line analysis is presented in Subsection 3.3 for use in computer program 2. Lastly, if the shell is circular then an infinite series solution is possible using Bessel functions [4]. This is presented in Section 4 for use in computer program 3. The desired quantity in all three formulations is the field at points interior to the shell. This may be expressed as an integral over electric and magnetic currents on C and procedures for this computation are given in Subsection 3.4. Descriptions of the computer programs as well as sample input/output data are given in Appendix B.

3.2 IMPEDANCE SHEET APPROXIMATION

The total field everywhere in Fig. 3-1 is the sum of the incident field ($\underline{E}^i, \underline{H}^i$) and a secondary field ($\underline{E}^S, \underline{H}^S$) due to the presence of the shell. This secondary field may be generated by an equivalent electric polarization current which effectively replaces the shell. This current is given by [5]

$$\underline{J} = \begin{cases} [j\omega(\epsilon - \epsilon_0) + \sigma] \underline{E} & \text{in } S \\ \underline{0} & \text{outside } S \end{cases} \quad (2)$$

where \underline{E} is the total electric field ($\underline{E}^i + \underline{E}^S$). Equation (2) may be rewritten as

$$-\hat{\underline{E}}^S(\underline{J}_C) + \frac{\underline{J}}{j\omega(\epsilon - \epsilon_0) + \sigma} = \underline{E}^i \quad \text{in } S \quad (3)$$

where $\hat{\underline{E}}^S$ is an electric field operator defined by Equation (8) of [6]. If the shell thickness d is much less than the wavelength in region b , λ_b , then one may approximate Equation (3) by specializing it to the contour C in Fig. 3-2 and replacing the volume current \underline{J} with a surface current \underline{J}_C . One then obtains the loaded body equation [7]

$$-\frac{k_o}{\eta_o} \hat{\underline{E}}_t^S(\underline{J}_C) + Z_L \underline{J}_C = \frac{k_o}{\eta_o} \underline{E}_t^i \quad \text{on } C \quad (4)$$

where the factor of k_o/η_o has been multiplied through for later convenience. The subscript t denotes tangential component evaluated on C .

The normalized impedance load Z_L is given by

$$Z_L = \frac{1}{jd \left[\left(\frac{\epsilon}{\epsilon_o} - 1 \right) - j \frac{\sigma}{\omega \epsilon_o} \right]} \quad (5)$$

which, if $\epsilon = \epsilon_0$, reduces to

$$Z_L = \frac{\epsilon_0}{\sigma t} \quad (6)$$

This is the low frequency limit used in [1]. Equation (4) is solved by a moment method procedure as in Section 2 [6] where the matrix equations are written as

$$\left[Z^e + Z_L^e \right] \vec{I}^e = \vec{V}^{ie} \quad (7)$$

for the TM case and

$$\left[Z^h + Z_L^h \right] \vec{I}^h = \vec{V}^{ih} \quad (8)$$

for the TE case. The matrices $[Z^e]$, $[Z^h]$ and vectors \vec{V}^{ie} , \vec{V}^{ih} are exactly the same as those in Section 2. The vectors \vec{I}^e and \vec{I}^h contain the coefficients of expansion for \underline{J}_c in the TM and TE cases, respectively, which is the same as that used for \underline{J}_c in [6]. For the TM case, the elements of Z_L^e are given by

$$(Z_L^e)_{mn} = \begin{cases} \frac{k_o \Delta_m}{\beta} & \text{if } m = n \\ 0 & \text{if } m \neq n \end{cases} \quad (9)$$

where β is defined by

$$\beta = jk_o d \left[\left(\frac{\epsilon}{\epsilon_0} - 1 \right) - j \frac{\sigma}{\omega \epsilon_0} \right] \quad (10)$$

For the TE case, the elements of Z_L^h are given by

$$(Z_L^h)_{mn} = \begin{cases} \frac{1}{3} \frac{k_o}{\beta} (\Delta_{m-1} + \Delta_m) & \text{if } m = n \\ \frac{k_o}{\beta} \frac{\Delta_m}{6} & \text{if } m = n-1 \\ & \text{or } n+1 - NC \\ \frac{k_o \Delta_n}{\beta 6} & \text{if } m = n+1 \\ & \text{or } n-1 + NC \end{cases} \quad (11)$$

Note that in this formulation \underline{J} is assumed tangential to C. Any normal component which the actual polarization current may have has been neglected. This is probably acceptable for the TM case since \underline{J} is z directed. For the TE case, however, this assumption is no good unless $k_b d \ll 1$ and even then depends upon the incident field. For example, the configuration in Fig. 3-3 would produce erroneous results by the above formulation. A more accurate solution could be obtained by allowing both components of the polarization current [8,9].

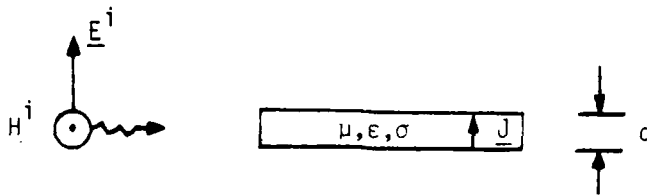


Figure 3-3. Incident Field Causing Normal Component of Polarization Current

3.3 TRAVELING WAVE APPROXIMATION

The problem in Fig. 3-1 may also be looked at as a three-region problem, where equivalent electric and magnetic currents are assumed to exist on surfaces C_0 and C_1 . [2]. This formulation will not be presented here, but for the purposes of discussion, let "a", "b", and "c" denote the regions outside C_0 , between C_0 and C_1 , and inside C_1 , respectively. The total field in region "a" now may be expressed as the sum of the incident field and a secondary field arising from electric and magnetic current sources on C_0 . Now if the shell is a good conductor, then the magnetic current on C_0 will be negligible. Secondly, if the shell surface has no abrupt changes in curvature [10] one may assume that an impedance relationship exists between the total tangential component of the electric field in region "a" and the electric current on C_0 . Again, since $k_0 d \ll 1$, we replace C_0 and C_1 by C in Fig. 3-2. The condition that $|k_b d| \ll 1$ as in Subsection 3.2 need not apply here. Hence, we write

$$\underline{E}_t^a = Z_L \underline{J}_{-0} \quad \text{on } C \quad (12)$$

where \underline{E}^a is the total electric field in region a. Equation (12) is rewritten as

$$-\hat{\underline{E}}_t^a(\underline{J}_{-0}) + Z_L(\underline{J}_{-0}) = \underline{E}_t^i \quad \text{on } C \quad (13)$$

which is again the loaded body equation of Subsection 3.2.

The load impedance, Z_L , this time will be determined by assuming that, inside region "b", each subsection of C appears locally planar. Traveling waves are then assumed to exist in region "b" which reflect the impedance seen at C_1 looking into region "c" back to region "a". Standard transmission line techniques may thus be used to obtain Z_L .

First consider the infinite slab shown in Fig. 3-4 where a local (u,v,w) coordinate system is used. The electric surface current \underline{J}_0 exists everywhere on the plane $u = 0$ and is constant over all v. This gives rise to

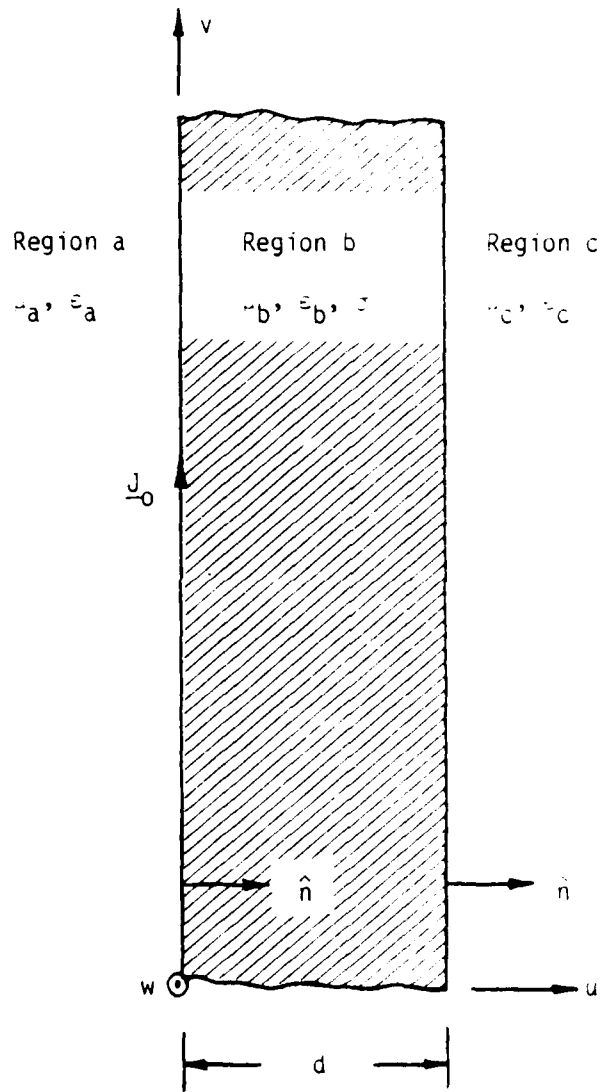


Figure 3-4. Infinite Slab Representation of Shell Subsection

plane waves in all three regions which have no u components. The electric field is written as

$$\underline{E}_t^a = A \hat{t} e^{jk_a u} \quad (-\hat{u} \text{ traveling plane waves}) \quad (14)$$

$$\underline{E}_t^b = B \hat{t} e^{-jk_b u} + C \hat{t} e^{jk_b u} \quad (+\hat{u} \text{ traveling plane waves}) \quad (15)$$

$$\underline{E}_t^c = D \hat{t} e^{-jk_c(u-d)} \quad (+\hat{u} \text{ traveling plane waves}) \quad (16)$$

The transverse unit vector \hat{t} lies in the v-w plane. The magnetic field is obtained from the Maxwell curl equation

$$\hat{n} \times \frac{\partial \underline{E}_t}{\partial u} = -jk \eta \underline{H}_t \quad (17)$$

which has been specialized to $+\hat{u}$ traveling plane waves. Thus we obtain

$$\underline{H}_t^a = -\frac{j}{\eta_a} (\hat{n} \times \hat{t}) e^{jk_a u} \quad (18)$$

$$\underline{H}_t^b = \frac{(\hat{n} \times \hat{t})}{\eta_b} \left[B e^{-jk_b u} - C e^{jk_b u} \right] \quad (19)$$

$$\underline{H}_t^c = \frac{\hat{n} \times \hat{t}}{\eta_c} D e^{-jk_c(u-d)} \quad (20)$$

The boundary conditions which must be satisfied are

$$\hat{n} \times [\underline{H}^b - \underline{H}^a] = \underline{J}_s \quad \text{at } u = 0 \quad (21)$$

$$\underline{E}_t^a = \underline{E}_t^b \quad \text{at } u = 0 \quad (22)$$

$$\underline{H}_t^b = \underline{H}_t^c \quad \text{at } u = d \quad (23)$$

$$\underline{E}_t^b = \underline{E}_t^c \quad \text{at } u = d \quad (24)$$

Now, since $\underline{H}_t = -\hat{n} \times \hat{n} \times \underline{H}$, Equation (20) is rewritten as

$$\underline{H}_t^a - \underline{H}_t^b = \hat{n} \times \underline{J}_o \quad \text{at } u = 0 \quad (25)$$

Solving Equations (22) through (25) simultaneously for the coefficients A, B, C, and D, one obtains

$$A = \frac{\eta_a J_{ot}}{\Delta} \left[-2j r_2 \sin k_b d - 2 \cos k_b d \right] \quad (26)$$

$$B = -\frac{\eta_a J_{ot}}{\Delta} (1 + r_2) e^{jk_b d} \quad (27)$$

$$C = -\frac{\eta_a J_{ot}}{\Delta} (1 - r_2) e^{-jk_b d} \quad (28)$$

$$D = -\frac{2 \eta_a J_{ot}}{\Delta} \quad (29)$$

where Δ is given by

$$\Delta = 2(1 + r_1 r_2) \cos k_b d + 2j (r_1 + r_2) \sin k_b d \quad (30)$$

and $r_1 = \eta_a/\eta_b$, $r_2 = \eta_b/\eta_c$. In the above, \underline{J}_o is in the $\hat{\underline{t}}$ direction so that $\underline{J}_o = J_{ot}\hat{\underline{t}}$. In the actual problem, \underline{E}_t and \underline{H}_t must be continuous across C_o so the load impedance Z_L is determined by the ratio

$$Z_L = \frac{\hat{\underline{n}} \times \underline{E}_t^b}{\underline{H}_t^b} \Big|_{u=0} = \eta_b \left[\frac{\cos k_b d + j r_2 \sin k_b d}{j \sin k_b d + r_2 \cos k_b d} \right] \quad (31)$$

The following limiting cases of Equation (31) may be used when applicable:

$$Z_L \rightarrow \begin{cases} \eta_b \left[\frac{1 + j r_2 k_b d}{r_2 + j k_b d} \right] & |k_b d| \rightarrow 0 \\ \frac{1}{\sigma d} & |k_b d| \rightarrow 0 \text{ and } |\eta_b| \ll \eta_c \\ -j \eta_b \cot k_b d & |\eta_b| \ll \eta_c \\ \eta_b & |k_b d| \rightarrow \infty \text{ and } |\eta_b| \ll \eta_c \end{cases} \quad (32)$$

The tangential components of field at surface C_1 are given by the expressions

$$\underline{E}_t^c = - \frac{2 \eta_a J_{ot}}{\Delta} \hat{\underline{t}} e^{-jk_c(u-d)} \quad (33)$$

and

$$\underline{H}_t^c = - \frac{(\hat{\underline{n}} \times \hat{\underline{t}})}{\eta_c} \frac{2 \eta_a J_{ot}}{\Delta} e^{-jk_c(u-d)} \quad (34)$$

These fields may be thought of as arising from surface electric and magnetic currents at $u = d$ defined by

$$\underline{M}_1 = \underline{E}^c \times \hat{n} = (\hat{n} \times \underline{J}_0) \frac{\eta_a}{(1 + r_1 r_2) \cos k_b d + j(r_1 + r_2) \sin k_b d} \quad (35)$$

and

$$\underline{J}_1 = \underline{J}_0 \frac{\eta_a}{\eta_c} \frac{1}{(1 + r_1 r_2) \cos k_b d + j(r_1 + r_2) \sin k_b d} \quad (36)$$

Again, as $\eta_b \ll \eta_a$ or η_c , we have

$$\underline{M}_1 \rightarrow (\hat{n} \times \underline{J}_0) \frac{\eta_b}{j \sin k_b d} \quad (37)$$

$$\underline{J}_1 \rightarrow \underline{J}_0 \frac{\eta_b}{\eta_c j \sin k_b d} \quad (38)$$

In the above, we have assumed that the field in region c is a plane wave. This, of course, is not exactly true so the approximation will probably fail unless region c is electrically large. Note that the normal unit vector \hat{n} used here is opposite to that used in Figs. 3-1 and 3-2.

3.4 COMPUTATION OF FIELDS DUE TO TWO-DIMENSIONAL CURRENT DISTRIBUTIONS

Expressions are presented here for the field at points interior to the shell, denoted by region c in [2]. For the formulation of Subsection 3.2, the total field in region c is due to an incident field plus a secondary field which is caused by a two-dimensional electric current distribution on C . For the formulation of Subsection 3.3, the total field in region c is due to electric and magnetic currents on C . In both cases these current distributions radiate in unbounded space filled with μ_c, ϵ_c . Hence, we represent the fields by a potential integral formula [14].

The actual fields computed are the z components of electric field in the TM case and magnetic field in the TE case. These are written as

$$\frac{E_z^c}{\eta_c} = \frac{E_z^i}{\eta_c} - \hat{z} \cdot [j k_c \underline{A} + \underline{\nabla} \times \underline{F}] \quad (39)$$

and

$$H_z^c = H_z^i + \hat{z} \cdot [\underline{\nabla} \times \underline{A} - j k_c \underline{F}] \quad (40)$$

where the electric and magnetic vector potentials are defined by

$$\underline{A} = \frac{1}{4j} \int_C \underline{J}(t') H_0^{(2)}(k_c |\underline{r} - \underline{r}'(t')|) dt' \quad (41)$$

$$\underline{F} = \frac{1}{4j} \int_C \underline{M}(t') H_0^{(2)}(k_c |\underline{r} - \underline{r}'(t')|) dt' \quad (42)$$

In the above, the electric field and magnetic current have been normalized by η_c for computational convenience. Both terms in Equations (39) and (40) are used in the formulation of Subsection 3.2 and the last terms

only are used for the formulation of Subsection 3.3. Equations (39) and (40) at a point \underline{r} in region c where $\underline{r}'(t')$ is a point on C where arc length is parametrically expressed in terms of t' . The electric and magnetic currents are expanded as

$$\underline{J} = \sum_{n=1}^{NC} I_n^h \underline{r}_n(t) + I_n^e \underline{p}_n(t) \quad (43)$$

$$\frac{1}{\eta_c} \underline{M} = \sum_{n=1}^{NC} V_n^h \underline{p}_n(t) + V_n^e \underline{r}_n(t) \quad (44)$$

where \underline{p}_n and \underline{r}_n are defined by Equations (14) and (15) of [6]. I_n^h and V_n^h are complex coefficients for the TE case and I_n^e and V_n^e are complex coefficients for the TM case. Equations (39) and (40) may be conveniently rewritten in terms of near-field measurement vectors as

$$\frac{E_z^c}{\eta_c} = \frac{E_z^i}{\eta_c} + \tilde{Q} \tilde{I}^e + \tilde{P} \tilde{V}^e \quad (45)$$

$$H_z^c = H_z^i - \tilde{P} \tilde{I}^h + \tilde{Q} \tilde{V}^h \quad (46)$$

where the tilda (\sim) denotes transpose.

3.4.1 Formulas for Near-Field Measurement Vector, \vec{Q}

Each element Q_n of \vec{Q} actually represents the electric (magnetic) field due to a \hat{z} directed electric (magnetic) current of amplitude $1/\eta_c$ (η_c) with a pulse function distribution on subinterval, ΔC_n . The field point is denoted by \underline{r} and \underline{r}' denotes a point on ΔC_n . Thus one may write

$$Q_n = -\frac{k_c}{4} \int_{t_n}^{t_{n+1}} P_n(t') H_o^{(2)}(k_c |\underline{r} - \underline{r}'(t')|) dt' \quad (47)$$

Let \underline{r}_n be a vector from the origin to the midpoint of ΔC_n and define $\underline{R}_n(t')$ as

$$\underline{R}_n(t') = \underline{r} - \underline{r}_n - \frac{\Delta_n}{2} t \hat{\underline{t}}_n \quad (48)$$

which is shown in Fig. 3-5, where $-1 \leq t \leq 1$. Then Equation (47) may be transformed to

$$Q_n = -\frac{k_c \Delta_n}{8} \int_{-1}^1 H_0^{(2)}(k_c |\underline{R}_n(t')|) dt' \quad (49)$$

The integrand of Equation (49) becomes singular when $|\underline{R}_n(t')| \rightarrow 0$. To remedy the numerical difficulty encountered when this happens, we rewrite Equation (49) as

$$Q_n = -\frac{k_c \Delta_n}{8} \int_{-1}^1 \left[H_0^{(2)}(k_c |\underline{R}_n(t')|) + \frac{2j}{\pi} \ln \frac{\gamma k_c |\underline{R}_n(t')|}{2} \right] dt' \quad (50)$$

$$+ \frac{k_c \Delta_n}{8} \int_{-1}^1 \frac{2j}{\pi} \ln \frac{\gamma k_c |\underline{R}_n(t')|}{2} dt'$$

whenever $|\underline{R}_n(t')| < \epsilon$ for some small number $\epsilon > 0$ and subinterval Δ_n . The first integral can be done accurately by a quadrature rule as long as the integrand is never evaluated exactly where $|\underline{R}_n(t')| = 0$. The second integral can be done analytically and the following substitutions are made:

$$\underline{r} = x \hat{\underline{x}} + y \hat{\underline{y}}$$

$$\hat{\underline{t}}_n = t_{nx} \hat{\underline{x}} + t_{ny} \hat{\underline{y}}$$

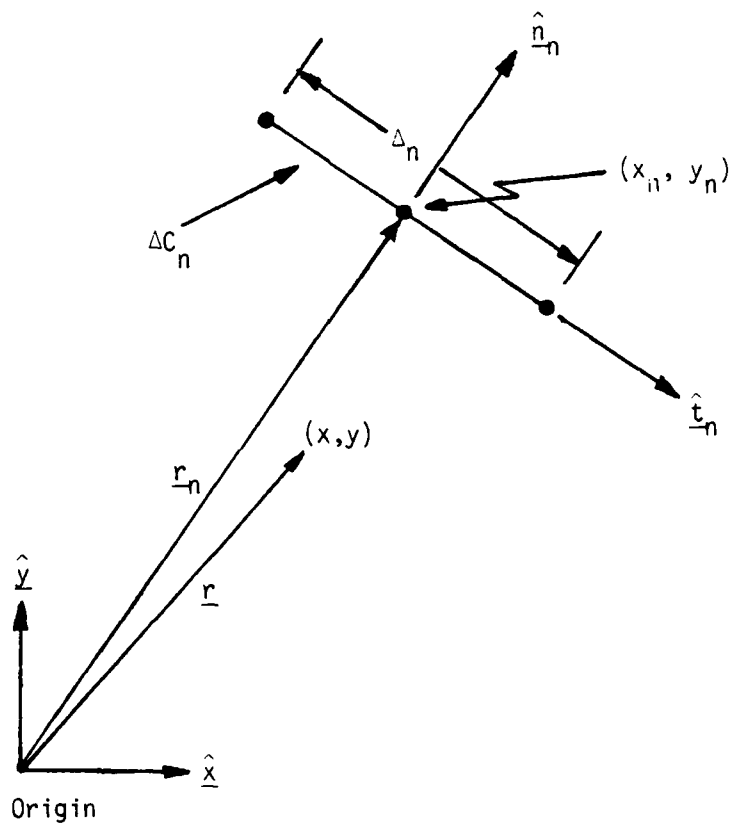


Figure 3-5. Geometry Relating to the Computation of \vec{Q} and \vec{P}

$$\underline{r}_n = x_n \hat{x} + y_n \hat{y}$$

$$a_n = (\Delta_n/2)^2$$

$$b_n = -\Delta_n [(x - x_n) t_{nx} + (y - y_n) t_{ny}]$$

$$c_n = (x - x_n)^2 + (y - y_n)^2$$

$$D_n = b_n^2 - 4 a_n c_n = 2\Delta_n^2 (x - x_n)(y - y_n) t_{nx} t_{ny}$$

Then $|R_n(t')|$ becomes

$$|R_n(t')| = \sqrt{a_n t'^2 + b_n t' + c_n}$$

and the second term in Equation (50) is written as

$$\begin{aligned} & \frac{k_c \Delta_n}{4} \frac{j}{\pi} \left[\ln \left\{ \left(\frac{\gamma k_c}{2} \right)^2 \sqrt{(a_n + b_n + c_n)(a_n - b_n + c_n)} \right\} \right. \\ & \quad \left. + \frac{b_n}{4 a_n} \ln \left[\frac{a_n + b_n + c_n}{a_n - b_n + c_n} \right] - 2 \right. \\ & \quad \left. + \frac{\sqrt{D_n}}{2 a_n} \left(\tan^{-1} \frac{2 a_n + b_n}{\sqrt{D_n}} - \tan^{-1} \frac{b_n - 2 a_n}{\sqrt{D_n}} \right) \right] \end{aligned} \quad (51)$$

for $D_n < 0$. If $D_n > 0$, D_n is replaced by $-D_n$ and \tan^{-1} is replaced by \tanh^{-1} .

3.4.2 Formulas for Near-Field Measurement Vector, \vec{P}

The element P_n represents the magnetic (electric) field due to a $-\hat{t}$ (\hat{t})-directed electric (magnetic) current of unit amplitude with a triangle function distribution over the interval $\Delta C_{n-1} \cup \Delta C_n$. Thus we have

$$\begin{aligned}
 P_n &= -\frac{1}{4j} \hat{z} \cdot \nabla \times \int_C \tau_n(t') H_0^{(2)}(k_c |\underline{r} - \underline{r}'(t')|) dt' \\
 &= -\frac{k_c}{4j} \int_C \frac{\tau_n(t') \hat{n} \cdot \underline{R}(t')}{|\underline{R}(t')|} H_1^{(2)}(k_c |\underline{R}(t')|) dt'
 \end{aligned} \tag{52}$$

where $\underline{R}(t') = \underline{r} - \underline{r}'(t')$. This may be rewritten as

$$\begin{aligned}
 P_n &= -\frac{1}{4j} \left\{ \frac{k_c \Delta_{n-1}}{2} \int_{-1}^1 \frac{\left(\frac{1}{2} + \frac{t'}{2}\right) \hat{n}_{n-1} \cdot \underline{R}_{n-1}(t')}{|\underline{R}_{n-1}(t')|} H_1^{(2)}(k_c |\underline{R}_{n-1}(t')|) dt' \right. \\
 &\quad \left. + \frac{k_c \Delta_n}{2} \int_{-1}^1 \frac{\left(\frac{1}{2} - \frac{t'}{2}\right) \hat{n}_n \cdot \underline{R}_n(t')}{|\underline{R}_n(t')|} H_1^{(2)}(k_c |\underline{R}_n(t')|) dt' \right\}
 \end{aligned} \tag{53}$$

The integrand of Equation (53) becomes singular when $|\underline{R}_n| \rightarrow 0$. The singularity is integrable, however, and after a similar manipulation to that done in Subsection 3.4.1 one obtains

$$P_n = \hat{P}_{n-1} + S_{n-1} + \hat{P}_n + S_n \tag{54}$$

The \hat{P} and S terms are defined by

$$\hat{P}_{n-1} = -\frac{k_c \Delta_{n-1}}{2} \int_{-1}^1 \frac{\left(\frac{1}{2} + \frac{t}{2}\right) \hat{t}_{n-1} \times R_{n-1}(t)}{|R_{n-1}(t)|} \cdot \left[H_1^{(2)}(k_c |R_{n-1}(t)|) - \frac{2j}{\pi k_c |R_{n-1}(t)|} \right] dt \quad (55)$$

$$S_{n-1} = -\frac{j \Delta_{n-1}}{\pi} \int_{-1}^1 \frac{\left(\frac{1}{2} + \frac{t}{2}\right) \hat{t}_{n-1} \times R_{n-1}(t)}{|R_{n-1}(t)|^2} dt \quad (56)$$

$$\hat{P}_n = -\frac{k_c \Delta_n}{2} \int_{-1}^1 \frac{\left(\frac{1}{2} - \frac{t}{2}\right) \hat{t}_n \times R_n(t)}{|R_n(t)|} \cdot \left[H_1^{(2)}(k_c |R_n(t)|) - \frac{2j}{\pi k_c |R_n(t)|} \right] dt \quad (57)$$

$$S_n = -\frac{j \Delta_n}{\pi} \int_{-1}^1 \frac{\left(\frac{1}{2} - \frac{t}{2}\right) \hat{t}_n \times R_n(t)}{|R_n(t)|^2} dt \quad (58)$$

The terms \hat{P}_{n-1} and \hat{P}_n may be integrated by a quadrature rule with no difficulties as $|R_n| \rightarrow 0$. The terms S_{n-1} and S_n may be integrated analytically to give

$$\begin{aligned}
 S_{n-1} &= -\frac{j \Delta_{n-1}}{2\pi} \int_{-1}^1 \frac{(1+t) d_{n-1}}{a_{n-1} t^2 + b_{n-1} t + c_{n-1}} dt' \\
 &= -\frac{j \Delta_{n-1}}{2\pi} \left\{ \left(1 - \frac{b_{n-1}}{2 a_{n-1}} \right) \frac{4 d_{n-1}}{\sqrt{D_{n-1}}} \tan^{-1} \left(\frac{2 a_{n-1} + b_{n-1}}{\sqrt{D_{n-1}}} \right) \right. \\
 &\quad \left. + \frac{d_{n-1}}{2 a_{n-1}} \ln \left(\frac{a_{n-1} + b_{n-1} + c_{n-1}}{a_{n-1} - b_{n-1} + c_{n-1}} \right) \right\} \quad (59)
 \end{aligned}$$

where $d_n = [t_{nx}(y - y') - t_{ny}(x - x')]$, and

$$\begin{aligned}
 S_n &= -\frac{j \Delta_n}{2\pi} \left\{ \left(1 + \frac{b_n}{2 a_n} \right) \frac{4 d_n}{\sqrt{D_n}} \tan^{-1} \left(\frac{2 a_n + b_n}{\sqrt{D_n}} \right) \right. \\
 &\quad \left. - \frac{d_n}{2 a_n} \ln \left(\frac{a_n + b_n + c_n}{a_n - b_n + c_n} \right) \right\} \quad (60)
 \end{aligned}$$

3.5 REFERENCES

- [1] D. Schieber, "Shielding Performance of Metallic Cylinders", IEEE Trans. on EMC, Vol. EMC-15, No. 1, February 1973, pp 12-16.
- [2] R.F. Harrington, "Penetration of Electromagnetic Waves Through Lossy Shells", Memo to Syracuse Research Corporation, March 1979.
- [3] R.F. Harrington and J.R. Mautz, "An Impedance Sheet Approximation for Thin Dielectric Shells", IEEE Trans. on Ant. and Propagat., July 1975, pp 532-534.
- [4] G.T. Ruck, et al., Radar Cross Section Handbook, Plenum Press, New York, 1970, pp 253-259.
- [5] R.F. Harrington, Field Computation by Moment Methods, The Macmillan Co., New York, 1968.
- [6] D.T. Auckland, "Computer Programs for Scattering by Perfectly Conducting Cylinders of Arbitrary Shape", Syracuse Research Corporation Technical Memo, December 1979. (Section 2 of this report.)
- [7] R.F. Harrington and J.R. Mautz, "Radiation and Scattering from Loaded Bodies of Revolution", Appl. Sci. Res., Vol. 26, June 1971, pp 209-217.
- [8] J.H. Richmond, "Scattering by a Dielectric Cylinder of Arbitrary Cross Section Shape", IEEE Trans. on Ant. and Propagat., pp 334-341.
- [9] J.H. Richmond, "TE-Wave Scattering by a Dielectric Cylinder of Arbitrary Cross Section Shape", IEEE Trans. on Ant. and Propagat., July 1966, pp 460-464.
- [10] K.M. Mitzner, "Effective Boundary Conditions for Reflection and Transmission by an Absorbing Shell of Arbitrary Shape", IEEE Trans. on Ant. and Propagat., November 1968, pp 706-712.
- [11] T.K. Wu and L.L. Tsai, "Shielding Properties of Thick Conducting Cylindrical Shells", IEEE Trans. on EMC, November 1974, pp 201-204.
- [12] T.K. Wu and L.L. Tsai, "Shielding Properties of Thick Conducting Cylindrical Shells with an Obliquely Incident Plane Wave", IEEE Trans. on EMC, August 1975, pp 189-193.
- [13] D.N. Filipovic and R.F. Harrington, "On a Transmission Matrix Approximation for Scattering by a Highly Conducting Cylindrical Shell", Syracuse University Technical Report TR-76-7, June 1976.
- [14] R.F. Harrington, Time Harmonic Electromagnetic Fields, McGraw-Hill Book Co., New York, 1961.

SECTION 4

SHELLS OF CIRCULAR CROSS SECTION AND FINITE CONDUCTIVITY

When the shell has a circular cross section, the Helmholtz wave equation is separable in cylindrical coordinates. An expansion of the fields in each region is then possible in terms of the solutions to the homogeneous wave equation. The unknown coefficients of expansion are found by ensuring continuity of tangential fields across the inside and outside shell surfaces.

4.1 INTRODUCTION

An exact-series solution [1, 2] for the penetration fields inside circular shells is presented here. This is useful in testing the approximate solutions developed in Section 3. This solution is especially useful in developing low-frequency approximations to the interior penetration fields, i.e., when the overall dimension of the shell cross section is small with respect to a wavelength. The interior fields are shown to be uniform in this limit and a convenient equivalent circuit model is valid for the coupling mechanism.

4.2 GENERAL SOLUTION

Consider the problem shown in Fig. 4-1. For the TE case, the incident field is

$$\begin{aligned} H_z^i &= e^{jk_0 x} = e^{jk_0 r \cos \phi} \\ &= \sum_{-\infty}^{\infty} j^n J_n(k_0 r) e^{jn\phi} \end{aligned} \quad (1)$$

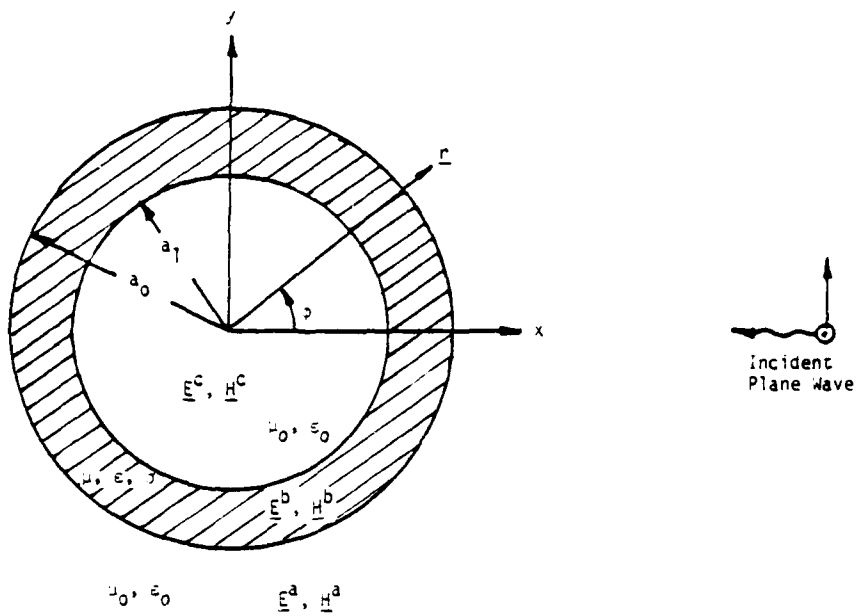


Figure 4-1. Plane Wave Incident Upon a Circular Shell

The z component of magnetic field in each region is expressed as

$$H_z^a = \sum_{-\infty}^{\infty} j^n a_n^{\text{TE}} H_n(k_o r) e^{jn\phi} + H_z^i$$

$$H_z^b = \sum_{-\infty}^{\infty} j^n \left[b_n^{\text{TE}} J_n(k_b r) + c_n Y_n^{\text{TE}}(k_b r) \right] e^{jn\phi} \quad (2)$$

$$H_z^c = \sum_{-\infty}^{\infty} j^n d_n^{\text{TE}} J_n(k_o r) e^{jn\phi}$$

where $H_n(x) = J_n(x) - j Y_n(x)$.

The ϕ component of electric field is obtained from

$$E_\phi = -\frac{n}{jk} \frac{\partial H_z}{\partial r} \quad (3)$$

Hence

$$E_\phi^a = j \eta_o \sum_{-\infty}^{\infty} j^n \left[a_n^{\text{TE}} H_n'(k_o r) + J_n'(k_o r) \right] e^{jn\phi}$$

$$E_\phi^b = j \eta_b \sum_{-\infty}^{\infty} j^n \left[b_n^{\text{TE}} J_n'(k_b r) + c_n^{\text{TE}} Y_n'(k_b r) \right] e^{jn\phi} \quad (4)$$

$$E_\phi^c = j \eta_o \sum_{-\infty}^{\infty} j^n d_n^{\text{TE}} J_n'(k_o r) e^{jn\phi}$$

Matching tangential components of \underline{E} and \underline{H} at $r = a_1, a_0$ leads to

$$\begin{bmatrix} H_n(k_0 a_0) & -J_n(k_b a_0) & -Y_n(k_b a_0) & 0 \\ 0 & J_n(k_b a_1) & Y_n(k_b a_1) & -J_n(k_0 a_1) \\ H'_n(k_0 a_0) & -\xi J'_n(k_b a_0) & -\xi Y'_n(k_b a_0) & 0 \\ 0 & \xi J'_n(k_b a_1) & \xi Y'_n(k_b a_1) & -J'_n(k_0 a_1) \end{bmatrix} \begin{bmatrix} a_n^{TE} \\ b_n^{TE} \\ c_n^{TE} \\ d_n^{TE} \end{bmatrix} = \begin{bmatrix} -J_n(k_0 a_0) \\ 0 \\ -J'_n(k_0 a_0) \\ 0 \end{bmatrix} \quad (5)$$

where $\xi = \eta_b/\eta_0$. This system has the determinant:

$$\Delta_n^{TE} = \frac{2\xi}{\pi k_b a_1} \left\{ H_n(k_0 a_0) \left[J'_n(k_0 a_1) T_{n11} + \xi J_n(k_0 a_1) T_{n12} \right] - H'_n(k_0 a_0) \left[\frac{1}{\xi} J'_n(k_0 a_1) T_{n21} + J_n(k_0 a_1) T_{n22} \right] \right\} \quad (6)$$

where

$$\begin{aligned} T_{n11} &= \frac{\pi k_b a_1}{2} \left[J_n(k_b a_1) Y'_n(k_b a_0) - J'_n(k_b a_0) Y_n(k_b a_1) \right] \\ T_{n12} &= -\frac{\pi k_b a_1}{2} \left[J'_n(k_b a_0) Y'_n(k_b a_1) - J'_n(k_b a_1) Y'_n(k_b a_0) \right] \\ T_{n21} &= \frac{\pi k_b a_1}{2} \left[J_n(k_b a_1) Y_n(k_b a_0) - J_n(k_b a_0) Y_n(k_b a_1) \right] \\ T_{n22} &= \frac{\pi k_b a_1}{2} \left[J_n(k_b a_0) Y'_n(k_b a_1) - J'_n(k_b a_1) Y_n(k_b a_0) \right] \end{aligned} \quad (7)$$

Solving for a_n^{TE} and d_n^{TE} , one obtains

$$a_n^{TE} = \frac{2\xi}{\pi k_b a_1 \Delta_n^{TE}} \left\{ -J_n(k_o a_o) \left[J_n'(k_o a_1) T_{n11} + \xi J_n(k_o a_1) T_{n12} \right] \right. \\ \left. + J_n'(k_o a_o) \left[\frac{1}{\xi} J_n'(k_o a_1) T_{n21} + J_n(k_o a_1) T_{n22} \right] \right\} \quad (8)$$

$$d_n^{TE} = \frac{4j \xi}{\Delta_n^{TE} \pi^2 k_o a_o k_b a_1} \quad (9)$$

These coefficients allow one to compute the total fields external to and internal to the shell.

In a similar procedure for TM excitation, one obtains:

$$E_z^i = e^{jk_o x} = \sum_{-\infty}^{\infty} j^n J_n(k_o r) e^{jn\phi} \quad (10)$$

The z component of electric field in each region is expressed as

$$E_z^a = \sum_{-\infty}^{\infty} j^n \left[a_n^{TM} H_n(k_o r) + J_n(k_o r) \right] e^{jn\phi} \\ E_z^b = \sum_{-\infty}^{\infty} j^n \left[b_n^{TM} J_n(k_b r) + c_n^{TM} Y_n(k_b r) \right] e^{jn\phi} \quad (11) \\ E_z^c = \sum_{-\infty}^{\infty} j^n d_n^{TM} J_n(k_o r) e^{jn\phi}$$

The ϕ component of magnetic field is obtained from:

$$H_\phi = \frac{1}{jk\eta} \frac{\partial E_z}{\partial r} \quad (12)$$

Hence:

$$\begin{aligned}
 H_{\phi}^a &= \frac{1}{j\eta_0} \sum_{-\infty}^{\infty} j^n \left[a_n^{\text{TM}} H'_n(k_0 r) + J'_n(k_0 r) \right] e^{jn\phi} \\
 H_{\phi}^b &= \frac{1}{j\eta_b} \sum_{-\infty}^{\infty} j^n \left[b_n^{\text{TM}} J'_n(k_b r) + c_n^{\text{TM}} Y'_n(k_b r) \right] e^{jn\phi} \\
 H_{\phi}^c &= \frac{1}{j\eta_0} \sum_{-\infty}^{\infty} j^n d_n^{\text{TM}} J'_n(k_0 r) e^{jn\phi}
 \end{aligned} \tag{13}$$

Again, matching tangential components of \underline{E} and \underline{H} at $r = a, a_0$ leads to

$$\begin{bmatrix}
 H'_n(k_0 a_0) & - J'_n(k_b a_0) & - Y'_n(k_b a_0) & 0 \\
 0 & J'_n(k_b a_1) & Y'_n(k_b a_1) & - J'_n(k_0 a_1) \\
 H'_n(k_0 a_0) & - \frac{1}{\xi} J'_n(k_b a_0) & - \frac{1}{\xi} Y'_n(k_b a_0) & 0 \\
 0 & \frac{1}{\xi} J'_n(k_b a_1) & \frac{1}{\xi} Y'_n(k_b a_1) & - J'_n(k_0 a_1)
 \end{bmatrix}
 \begin{bmatrix}
 a_n^{\text{TM}} \\
 b_n^{\text{TM}} \\
 c_n^{\text{TM}} \\
 d_n^{\text{TM}}
 \end{bmatrix}
 =
 \begin{bmatrix}
 - J'_n(k_0 a_0) \\
 0 \\
 - J'_n(k_0 a_0) \\
 0
 \end{bmatrix} \tag{14}$$

where again $\xi = \eta_b / \eta_0$. Comparison with Equation (5) leads to the result that Δ_n^{TM} , a_n^{TM} , and d_n^{TM} are given by Equations (6), (8), and (9) with ξ replaced by $1/\xi$.

4.3 LOW FREQUENCY APPROXIMATION

Of particular interest is the case when the shell geometry of Fig. 4-1 is "quasistatic". This is the case when $k_0 a_0 \ll 1$. After using the first few terms in the series for $J_n(k_0 r)$ and neglecting terms of order $(k_0 r)^2$ and higher, one obtains the following formulas for the fields interior to the shell:

$$\begin{aligned}
 H_z^c &\approx d_0^{TE} + j d_1^{TE} k_0 r \cos \phi \\
 E_\phi^c &\approx -j \eta_0 d_0^{TE} \frac{k_0 r}{2} - \eta_0 d_1^{TE} \cos \phi - \eta_0 d_2^{TE} \frac{k_0 r}{2} \cos 2\phi \\
 E_r^c &= \frac{\eta_0}{j k_0 r} \frac{\partial H_z^c}{\partial \phi} \\
 &\approx -\eta_0 d_1^{TE} \sin \phi + j \eta_0 d_2^{TE} \frac{k_0 r}{2} \sin 2\phi \\
 E_z^c &\approx d_0^{TM} + j d_1^{TM} k_0 r \cos \phi \tag{15} \\
 H_\phi^c &\approx \frac{j}{\eta_0} d_0^{TM} \frac{k_0 r}{2} + \frac{d_1^{TM}}{\eta_0} \cos \phi + \frac{d_2^{TM}}{\eta_0} \frac{k_0 r}{2} \cos 2\phi \\
 H_r^c &= -\frac{1}{j k_0 \eta_0 r} \frac{\partial E_z^c}{\partial \phi} \\
 &\approx \frac{d_1^{TM}}{\eta_0} \sin \phi - \frac{j}{\eta_0} d_2^{TM} \frac{k_0 r}{2} \sin 2\phi
 \end{aligned}$$

We see from the above that, when $k_0 r \ll 1$, the fields interior to the shell are uniform and are given by:

$$\begin{aligned} H_z^c &= d_0^{TE} \\ E_y^c &= -\eta_0 d_1^{TE} \\ E_x^c &= 0 \end{aligned} \tag{16}$$

for the TE case [Fig. 4-2(a)] and

$$\begin{aligned} E_z^c &= d_0^{TM} \\ H_y^c &= \frac{1}{\eta_0} d_1^{TM} \\ H_x^c &= 0 \end{aligned} \tag{17}$$

for the TM case [Fig. 4-2(b)]. It is now necessary to examine expressions for the coefficients d_0 , d_1 , and hence the determinants Δ . To do this, we confine ourselves to shells which are good conductors, i.e.,

$$\begin{aligned} k_b &\approx \sqrt{-j\omega\mu\sigma} \\ \eta_b &\approx \sqrt{\frac{j\omega\mu}{\sigma}} \end{aligned} \tag{18}$$

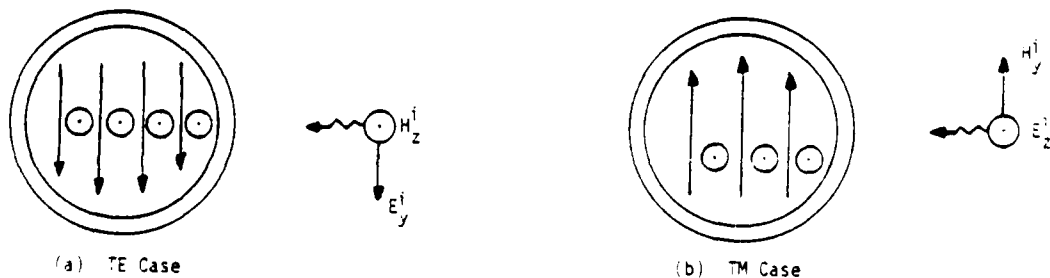


Figure 4-2. Interior Fields

Thus, in general, $|k_b| \gg k_0$ and $|\xi| \ll 1$ and hence $|k_b a_1|$ and $|k_b a_0|$ will be quite large. The following limiting forms for the Bessel functions are then quite useful [3]:

As $x \rightarrow 0$,

$$\begin{aligned}
 J_0(x) &\rightarrow 1 - \left(\frac{x}{2}\right)^2 \\
 J_1(x) &\rightarrow \frac{x}{2} - \frac{1}{2!} \left(\frac{x}{2}\right)^3 \\
 J'_0(x) &\rightarrow -\frac{x}{2} \\
 J'_1(x) &\rightarrow \frac{1}{2} - \frac{3}{4} \left(\frac{x}{2}\right)^2 \\
 H_0(x) &\rightarrow 1 - \frac{j2}{\pi} \ln \frac{\gamma x}{2} \\
 H_1(x) &\rightarrow \frac{x}{2} + \frac{2j}{\pi x} \\
 H'_0(x) &\rightarrow -\frac{x}{2} - \frac{j2}{\pi x} \\
 H'_1(x) &\rightarrow \frac{1}{2} - \frac{2j}{\pi} \left(\ln \frac{\gamma x}{2} + \frac{1}{x^2} \right)
 \end{aligned} \tag{19}$$

As $|x| \gg 1$ and $|x| \gg n$, we have

$$\begin{aligned}
 J_n(x) &\rightarrow \sqrt{\frac{2}{\pi x}} \cos \left(x - \frac{n\pi}{2} - \frac{\pi}{4} \right) \\
 Y_n(x) &\rightarrow \sqrt{\frac{2}{\pi x}} \sin \left(x - \frac{n\pi}{2} - \frac{\pi}{4} \right)
 \end{aligned} \tag{20}$$

The T_n matrix elements become:

$$\begin{aligned}
 T_{n11} &= \sqrt{\frac{a_1}{a_0}} \cos k_b d \\
 T_{n12} &= -\sqrt{\frac{a_1}{a_0}} \sin k_b d \\
 T_{n21} &= \sqrt{\frac{a_1}{a_0}} \sin k_b d \\
 T_{n22} &= \sqrt{\frac{a_1}{a_0}} \cos k_b d
 \end{aligned} \tag{21}$$

where $d = a_0 - a_1$ is the shell thickness. To simplify the results we assume that $d \ll a_0$ or a_1 and hence $a_0 \approx a_1 \equiv b$. This can be taken as the mean radius of the shell. After using Equations (19) through (21) in the formulas for the coefficients d^{TE} and d^{TM} we obtain

$$d_o^{TE} \rightarrow \frac{1}{\cos k_b d - \frac{k_o b}{2\xi} \sin k_b d} \tag{22}$$

$$d_l^{TE} \rightarrow \frac{2 k_o b}{2 k_o b \cos k_b d + \frac{1}{\xi} \sin k_b d} \tag{23}$$

for the TE case and

$$d_o^{TM} \rightarrow \frac{1}{\cos k_b d + \frac{k_o b}{\xi} \gamma \frac{k_o b}{2} \sin k_b d} \tag{24}$$

$$d_l^{TM} \rightarrow \frac{1}{\cos k_b d + \frac{1}{2} \left(\frac{\xi}{k_o b} - \frac{k_o b}{\xi} \right) \sin k_b d} \tag{25}$$

for the TM case.

If the thickness d is such that $|k_b d| \ll 1$, then the following low-frequency behavior for the interior field coefficients is obtained:

$$d_o^{TE} \approx \frac{1}{1 - j\omega\mu_o b \frac{\sigma d}{2}} \quad (26)$$

$$d_1^{TE} \approx \frac{1}{1 + \frac{\sigma d}{2} \frac{1}{j\omega\epsilon_o b}} \quad (27)$$

$$d_o^{TM} \approx \frac{1}{1 + j\omega \left(\mu_o b \ln \frac{\gamma k_o b}{2} \right) \sigma d} \quad (28)$$

$$d_1^{TM} \approx \frac{1}{1 + \frac{\mu d}{2\mu_o b} - j \frac{\omega\epsilon_o b}{2} \sigma d} \quad (29)$$

Using Equations (16) and (17), the electric and magnetic shielding ratios for the two polarizations can be written as

$$\frac{H_z^c}{H_z^i} = d_o^{TE} \quad (30)$$

$$\frac{E_y^c}{E_y^i} = d_1^{TE} \quad (31)$$

for the TE case and

$$\frac{E_z^c}{E_z^i} = d_o^{TM} \quad (32)$$

$$\frac{H_y^c}{H_y^i} = d_1^{TM} \quad (33)$$

for the TM case. The low-frequency behavior of shielding effectiveness can then be inferred from Equations (26) through (29). Of particular interest is the relationship between the interior electric and magnetic fields as the frequency ω becomes small. For the TM case we find that

$$\frac{E_z^c}{H_y^c} \xrightarrow{\omega \rightarrow 0} \eta_o \frac{d_o^{TM}}{d_l^{TM}} \approx \eta_o \left(1 + \frac{ud}{2\mu_o b} \right) \quad (34)$$

Similarly, for the TE case we have

$$\frac{E_y^c}{H_z^c} \xrightarrow{\omega \rightarrow 0} - \frac{\eta_o d_l^{TE}}{d_o^{TE}} \approx 0 \quad (35)$$

4.4 TM LINE SOURCE EXCITATION

Consider the thin circular shell of mean radius a in the presence of an electric line source as shown in Fig. 4-3. The thickness of the shell d is much less than the free space wavelength and also λ_s , the wavelength inside the shell material. If the latter is true then we assume an impedance relation between the total electric field $\underline{E}^i + \underline{E}^s$ and the electric current \underline{J} at $r = a$ where:

- \underline{E}^s = the secondary field due to \underline{J}
- \underline{E}^i = field due to the line source in free space
- \underline{J} = unknown electric polarization current

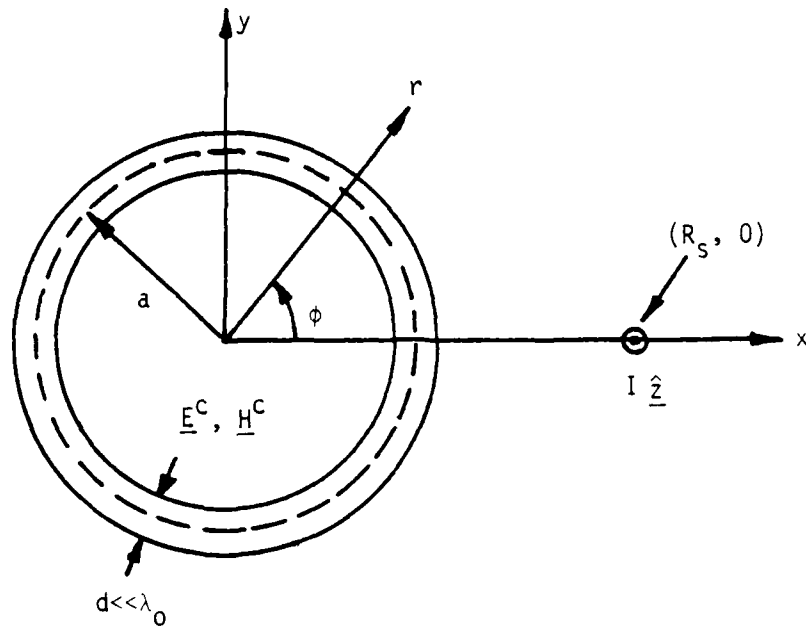


Figure 4-3. Thin Shell in the Presence of a Line Source

This relation is expressed as

$$-\underline{E}_t^s(\underline{J}) + Z_{st}\underline{J} = \underline{E}_t^i \quad (36)$$

where Z_{st} is the surface transfer impedance given by $1/(j\omega(\epsilon - \epsilon_0) + \sigma)d$ for this case. The secondary fields are defined by

$$\begin{aligned} \underline{E}^s(\underline{J}) = & -\frac{k_0 \eta_0}{4} \int_0^{2\pi} a \underline{J}(\phi') H_0^{(2)}(k_0 |\underline{r} - \underline{r}'|) d\phi' \\ & - \frac{\eta_0}{4 k_0} \frac{77}{77} \cdot \int_0^{2\pi} a \underline{J}(\phi') H_0^{(2)}(k_0 |\underline{r} - \underline{r}'|) d\phi' \end{aligned} \quad (37)$$

and

$$\underline{H}^s(\underline{J}) = \frac{1}{4j} \nabla \times \int_0^{2\pi} a \underline{J}(\phi') H_0^{(2)}(k_0 |\underline{r} - \underline{r}'|) \quad (38)$$

Equation (36) will be solved by expanding $\underline{J}(\phi')$ in a Fourier series in ϕ' and specializing the result to the quasi-static case ($\omega \rightarrow 0$). The incident fields are given by

$$\begin{aligned} E_z^i &= -\frac{I k_0 \eta_0}{4} H_0^{(2)}(k_0 |\underline{r} - \underline{R}_s|) \\ H_x^i &= -\frac{I k_0 y}{R} H_1^{(2)}(k_0 |\underline{r} - \underline{R}_s|) \\ H_y^i &= \frac{I k_0 (x - R_s)}{R} H_1^{(2)}(k_0 |\underline{r} - \underline{R}_s|) \\ R &= \sqrt{(x - R_s)^2 + y^2} \end{aligned} \quad (39)$$

with respect to the coordinates of Fig. 4-3. Equation (36) becomes:

$$\begin{aligned} \frac{k_0 \eta_0}{4} \int_0^{2\pi} a \underline{J}(\phi') H_0^{(2)}(k_0 |\underline{r} - \underline{r}'|) d\phi' \\ + Z_{st} \underline{J}(\phi) = -\frac{I k_0 \eta_0}{4} H_0^{(2)}(k_0 |\underline{r} - \underline{R}_s|) \end{aligned} \quad (40)$$

The following addition theorem is now useful [3]:

$$H_0^{(2)}(k_0 |\underline{r} - \underline{r}'|) = \begin{cases} \sum_{-\infty}^{\infty} H_n^{(2)}(k_0 r') J_n(k_0 r) e^{jn(\phi - \phi')} & r < r' \\ \sum_{-\infty}^{\infty} J_n(k_0 r') H_n^{(2)}(k_0 r) e^{jn(\phi - \phi')} & r > r' \end{cases} \quad (41)$$

The Fourier series representation for \underline{J} is written as

$$\underline{J}(\phi') = \sum_{-\infty}^{\infty} c_n e^{jn\phi'} \quad (42)$$

Substituting Equations (41) and (42) into Equation (40) and using the orthogonality of $e^{jn\phi}$ we obtain:

$$c_n = \frac{-\frac{I k_0}{4} H_n^{(2)}(k_0 R_s) J_n(k_0 a)}{\frac{k_0 a \pi}{2} H_n^{(2)}(k_0 a) J_n(k_0 a) + Z'} \quad (43)$$

where $Z' = Z_{st}/\eta_0$. The total field inside the shell is of interest and is obtained by adding \underline{E}^s and \underline{E}^i for $r < a$. Thus we have

$$E_z^c = E_z^s + E_z^i = \frac{I k_0 \eta_0}{4} \sum_{n=0}^{\infty} \epsilon_n H_n^{(2)}(k_0 R_s) J_n(k_0 r) \quad (44)$$

$$\cdot \left[\frac{\frac{k_0 a \pi}{2} J_n(k_0 a) H_n^{(2)}(k_0 a)}{\frac{k_0 a \pi}{2} H_n^{(2)}(k_0 a) J_n(k_0 a) + Z'} - 1 \right] \cdot \cos n\phi$$

This gives the correct result as $Z' \rightarrow 0$ for a perfect conducting shell ($\epsilon_n = 1$ for $n = 0$ and 2 for $n > 0$). Using the formula

$$H_1^{(2)}(k_0' \underline{r} - \underline{r}') = \begin{cases} \sum_{-\infty}^{\infty} H_{n+1}^{(2)}(k_0' r') J_n(k_0' r) e^{jn\phi} & r < r' \\ \sum_{-\infty}^{\infty} H_{n-1}^{(2)}(k_0' r) J_n(k_0' r') e^{jn\phi} & r > r' \end{cases} \quad (45)$$

we obtain the total H-field inside the shell as

$$H_y^c = \frac{I k_0' (x - R_s)}{4j R} \sum_{n=0}^{\infty} H_n^{(2)}(k_0' R_s) J_n(k_0' r) e^{jn\phi} \quad (46)$$

$$\cdot \left[\frac{-Z' \cos n\phi}{\frac{k_0' a \pi}{2} H_n^{(2)}(k_0' a) J_n(k_0' a) + Z'} \right]$$

$$H_x^c = -\frac{I k_0' y}{4j R} \sum_{n=0}^{\infty} H_n^{(2)}(k_0' R_s) J_n(k_0' r) e^{jn\phi} \quad (47)$$

$$\cdot \left[\frac{-Z' \cos n\phi}{\frac{k_0' a \pi}{2} H_n^{(2)}(k_0' a) J_n(k_0' a) + Z'} \right]$$

As the frequency $\omega \rightarrow 0$, the current is approximately given by

$$J_z \approx \frac{-\frac{I\omega}{4} \left(1 - \frac{j^2}{\pi} \ln \frac{R_s}{2} \right)}{\frac{a\pi}{2} \left(1 - \frac{j^2}{\pi} \ln \frac{a}{2} \right) + \frac{\pi}{4} \frac{st}{\mu_0}} - \frac{\frac{I\omega a}{2\pi R_s} \cos \phi}{\frac{j\omega a}{2} + \frac{\pi}{4} \frac{st}{\mu_0}} \quad (48)$$

where

$$\tau_s = \sqrt{\mu_0 \epsilon_0} R_s$$

$$\tau_a = \sqrt{\mu_0 \epsilon_0} a$$

4.5 REFERENCES

- [1] T.K. Wu and L.L. Tsai, "Shielding Properties of Thick Conducting Cylindrical Shells", IEEE Trans. on EMC, November 1974, pp 201-204.
- [2] T.K. Wu and L.L. Tsai, "Shielding Properties of Thick Conducting Cylindrical Shells with an Obliquely Incident Plane Wave", IEEE Trans. on EMC, August 1975, pp 189-193.
- [3] M. Abramowitz and I. Stegun, Handbook of Mathematical Functions, Dover Publications, Inc., New York, 1965.

SECTION 5

DIFFUSION COUPLING MODELS FOR LIGHTNING AND NUCLEAR ELECTROMAGNETIC PULSE

In this section, models for the threats of nearby and direct lightning strikes as well as nuclear electromagnetic pulse (NEMP) radiation are postulated. The diffusion coupling formulas derived by Kaden [1,2] are used to obtain internal penetration fields for homogeneous shells. Modeling the excitation time waveform as a double exponential, an inverse Laplace transform is performed as in [1] to obtain the interior fields as a function of time. These fields are then used to excite transmission lines which reside inside the shell and form the basis of the computer-aided design (CAD) program discussed in Appendix C.

5.1 INTRODUCTION

In the near strike case, the lightning is modeled as a tube of current parallel to the axis of the shell. It produces a transverse magnetic field which penetrates the shell by a diffusive coupling mechanism. The time derivative of this penetration magnetic flux density interacts with a circuit loop area or an equivalent transmission line area to produce a voltage drop across the circuit. At sufficient distances from the lightning current column, the electric and magnetic fields are related by the impedance of free space.

For the case of radiation from a nuclear electromagnetic pulse (NEMP), the incident field is taken to be an incident plane wave. This is exactly what the near strike excitation produces far from its source. The main difference between the two is the frequency content in the spectrum of the incident fields where that of NEMP is much higher. Thus the same diffusion coupling formulas apply for NEMP fields as for the near lightning strike case as long as the shell cross section is electrically small for all frequencies of significance.

In the direct strike case, the lightning current waveform is assumed to distribute itself uniformly about the outside of the shell surface and is in a direction parallel to the axis. It gives rise to an electric field on

the interior of the shell via the surface transfer impedance which is in the same direction as the lightning current and uniform throughout the shell. This electric field gives rise to voltage drops along current paths which lie along it.

5.2 NEAR-STRIKE LIGHTNING

The situation of a lightning bolt striking near an aircraft is shown in Fig. 5-1. The bolt is modeled by a cylindrical tube of current whose time dependence is assumed to be given by

$$I(t) = I_0 \left[e^{-\alpha t} - e^{-\beta t} \right] \quad (1)$$

where

$$\alpha = 1.7 \times 10^4 \text{ s}^{-1}$$

$$\beta = 3.5 \times 10^6 \text{ s}^{-1}$$

$$I_0 = 2 \times 10^5 \text{ amp}$$

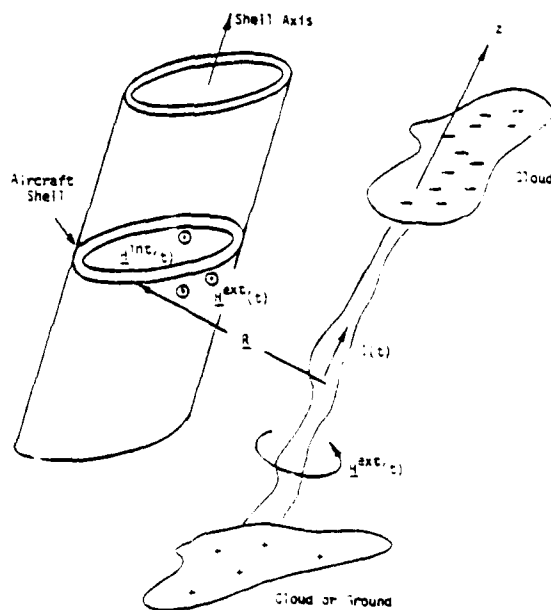


Figure 5-1. Near-Strike Lightning Situation

which are nominal values. The physical length of the bolt will be assumed much longer than the aircraft and the end effects of the clouds are neglected. The bolt, now considered as an infinite tube of current as far as the aircraft is concerned, gives rise to ϕ directed magnetic field lines (because of symmetry) with respect to an axis along the bolt. At a point \underline{R} in the absence of the aircraft, the magnetic field is given by

$$\underline{H}^{\text{ext}}(t) = \frac{I(t)}{2\pi R} \quad (2)$$

which is actually nonuniform. If the aircraft shell is small, however, the external field is usually considered to be uniform over the shell cross section and R is some mean radius from the lightning bolt to the shell.

The spectrum of Equation (1), and hence Equation (2), is shown in Fig. 5-2. It is flat out to approximately 2.7 kHz where it rapidly decreases. Thus, a low-frequency analysis (neglecting the term $j\omega \epsilon_0 E$ in relation to σE) may be applied to the shell to find the internal magnetic field $\underline{H}^{\text{int}}(t)$. The result is given in the frequency domain by

$$T(s) = \frac{H^{\text{int}}(s)}{H^{\text{ext}}(s)} = \frac{1}{\cosh z + \xi z \sinh z} \quad (3)$$

where

- $H^{\text{int}}(s)$ = spectrum of the magnetic field inside shell
- $H^{\text{ext}}(s)$ = spectrum of the magnetic field in the absence of the shell
- z = $\sqrt{s t_d}$
- t_d = diffusion time = $\mu_0 \sigma d^2$
- ξ = $1/d$ x volume to surface ratio for nonmagnetic ($\mu = \mu_0$) shells

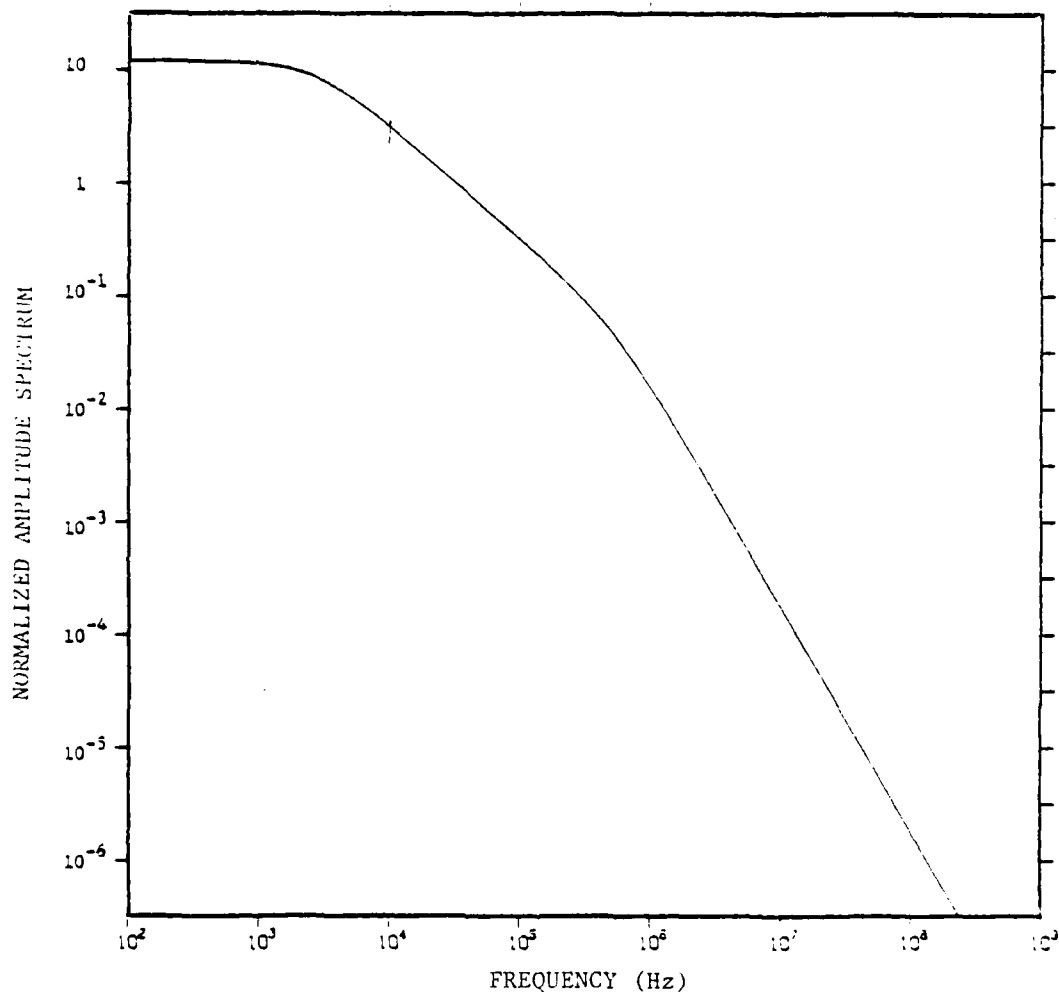


Figure 5-2. Normalized Spectrum of Double Exponential Lightning Waveform

The spectrum of the incident field is given by

$$H^{\text{ext}}(s) = H_0 \frac{\beta - \alpha}{(\alpha + s)(\beta + s)} \quad (4)$$

where $H_0 = I_0/2\pi R$. The spectrum of the internal field is

$$H^{\text{int}}(s) = T(s) H^{\text{ext}}(s) \quad (5)$$

and $H^{\text{int}}(t)$ can be found by simply taking the inverse Laplace transform of Equation (5). Thus, we have

$$H^{\text{int}}(t) = \frac{H_0}{2\pi j} \int_{K-j\infty}^{K+j\infty} \frac{(\beta - \alpha) e^{st} ds}{(\cosh z + \xi z \sinh z)(\alpha + s)(\beta + s)} \quad (6)$$

where K is an arbitrary constant. It is simpler in Equation (6) to use the transformation

$$z = \sqrt{s t_d} \quad (7)$$

to obtain

$$\frac{H^{\text{int}}(t)}{H_0} = 2t_d \frac{(\beta - \alpha)}{2\pi j} \int_{\Omega} \frac{z e^{z^2 t/t_d} dz}{(\cosh z + \xi z \sinh z)(\alpha t_d + z^2)(\beta t_d + z^2)} \quad (8)$$

where Ω is a closed contour in the complex plane [1]. The integrand in Equation (8) has simple poles at

$$z = \pm j \lambda_n \quad (9)$$

where $\cot \lambda_n = \xi \lambda_n$

$$z = \pm j \sqrt{\alpha t_d} \quad (10)$$

and

$$z = \pm j \sqrt{\beta t_d} \quad (11)$$

The poles along the negative $\text{Im}(z)$ axis are discarded due to physical reasons and the contour of integration is the same as that in [1]. Thus Equation (8) may be computed by computing the residues:

$$\frac{H^{\text{int}}(t)}{H_0} = 2(\beta - \alpha) t_d \left[R_\alpha + R_\beta + R_0 + \sum_{n=1}^{\infty} R_n \right] \quad (12)$$

$$R_\alpha = \lim_{z \rightarrow j\sqrt{\alpha t_d}} \frac{(z - j\sqrt{\alpha t_d}) z e^{z^2 t/t_d}}{(\cosh z + \xi z \sinh z)(z^2 + \alpha t_d)(z^2 + \beta t_d)} \quad (13)$$

$$= \frac{e^{-\alpha t}}{2t_d(\beta - \alpha)(\cos \sqrt{\alpha t_d} - \xi \sqrt{\alpha t_d} \sin \sqrt{\alpha t_d})}$$

$$R_\beta = \lim_{z \rightarrow j\sqrt{\beta t_d}} \frac{(z - j\sqrt{\beta t_d}) z e^{z^2 t/t_d}}{(\cosh z + \xi z \sinh z)(z^2 + \alpha t_d)(z^2 + \beta t_d)} \quad (14)$$

$$= \frac{e^{-\beta t}}{2t_d(\alpha - \beta)(\cos \sqrt{\beta t_d} - \xi \sqrt{\beta t_d} \sin \sqrt{\beta t_d})}$$

$$R_0 = \lim_{z \rightarrow j\lambda_0} \frac{(z - j\lambda_0) z e^{z^2 t/t_d}}{(\cosh z + \xi z \sinh z)(z^2 + \alpha t_d)(z^2 + \beta t_d)} \quad (15)$$

Using L'Hospital's rule, the limit in Equation (15) becomes

$$R_0 = \frac{\lambda_0 e^{-\lambda_0^2 t/t_d}}{(\alpha t_d - \lambda_0^2)(\beta t_d - \lambda_0^2)(1 + \xi + (\xi \lambda_0)^2) \sin \lambda_0} \quad (16)$$

The same thing is done for R_n . Now, usually, $\xi \gg 1$ for the shapes to be considered. In this case

$$\lambda_0 \approx \frac{1}{\sqrt{\xi}} \quad (17)$$

$$\lambda_n = n\pi \quad (n \neq 0)$$

This allows us to simplify R_0 and R_n , thus giving:

$$\begin{aligned} \frac{H^{int}(t)}{H_0} &= \frac{e^{-\alpha t}}{\cos \sqrt{\alpha t_d} - \xi \sqrt{\alpha t_d} \sin \sqrt{\alpha t_d}} - \frac{e^{-\beta t}}{\cos \sqrt{\beta t_d} - \xi \sqrt{\beta t_d} \sin \sqrt{\beta t_d}} \\ &+ \frac{(\beta - \alpha) t_d \xi e^{-t/\xi t_d}}{(1 - \xi \alpha t_d)(1 - \xi \beta t_d)} \\ &+ \frac{2(\beta - \alpha) t_d}{\xi} \sum_{n=1}^{\infty} \frac{(-1)^n e^{-n^2 \pi^2 t/t_d}}{(n^2 \pi^2 - \alpha t_d)(n^2 \pi^2 - \beta t_d)} \end{aligned} \quad (18)$$

For voltages induced in loops or transmission lines located at points inside the shell, it is actually the time derivative of the internal magnetic field which is important. This is given by

$$\begin{aligned} \frac{\dot{H}^{int}(t)}{H_0} &= \frac{\beta e^{-\beta t}}{\cos \sqrt{\beta t_d} - \xi \sqrt{\beta t_d} \sin \sqrt{\beta t_d}} - \frac{\alpha e^{-\alpha t}}{\cos \sqrt{\alpha t_d} - \xi \sqrt{\alpha t_d} \sin \sqrt{\alpha t_d}} \\ &- \frac{(\beta - \alpha) e^{-t/\xi t_d}}{(1 - \xi \alpha t_d)(1 - \xi \beta t_d)} \\ &- \frac{2(\beta - \alpha)}{\xi} \sum_{n=1}^{\infty} \frac{(-1)^n e^{-n^2 \pi^2 t/t_d}}{n^2 \pi^2 \left(1 - \frac{\alpha t_d}{n^2 \pi^2}\right) \left(1 - \frac{\beta t_d}{n^2 \pi^2}\right)} \end{aligned} \quad (19)$$

Alternatively, one may obtain Equation (18) by convolving the impulse response $h(t)$ [1] of the shell with the excitation of Equation (2). This is written as

$$H^{int}(t) = h(t) * H^{ext}(t) \quad (20)$$

where

$$h(t) = \frac{H_0}{\xi t_d} \left[e^{-t/\xi t_d} + 2 \sum_{n=1}^{\infty} (-1)^n e^{-(n\pi)^2 t/t_d} \right] \quad (21)$$

The result is given by

$$\begin{aligned}
 H^{int}(t) = & \frac{H_0}{\xi t_d} \left[\frac{1}{\left(\frac{1}{\xi t_d} - \alpha\right)} \left(e^{-\alpha t} - e^{-t/\xi t_d} \right) - \frac{1}{\left(\frac{1}{\xi t_d} - \beta\right)} \left(e^{-\beta t} - e^{-t/\xi t_d} \right) \right. \\
 & + 2 \sum_{n=1}^{\infty} \left\{ \frac{(-1)^n}{\left(\frac{(n\pi)^2}{t_d} - \alpha\right)} \left(e^{-\alpha t} - e^{-\frac{(n\pi)^2 t}{t_d}} \right) \right. \\
 & \left. \left. - \frac{(-1)^n}{\left(\frac{(n\pi)^2}{t_d} - \beta\right)} \left(e^{-\beta t} - e^{-\frac{(n\pi)^2 t}{t_d}} \right) \right\} \right] \quad (22)
 \end{aligned}$$

which is equivalent to Equation (18). From Equation (22) the initial values are easily seen to be

$$\begin{aligned}
 H^{int}(0) &= 0 \\
 \dot{H}^{int}(0) &= 0
 \end{aligned} \quad (23)$$

5.3 NUCLEAR PULSE EXCITATION

The situation of an incident plane wave radiated by a NEMP is shown in Fig. 5-3. The external field time dependence is assumed to be of the form [3]:

$$H^{ext} = H_0 (e^{-\alpha t} - e^{-\beta t}) \quad (24)$$

where typical values are given by

$$\begin{aligned}
 H_0 &= 154 \text{ amps/meter} \\
 \alpha &= 6.3 \times 10^6 \text{ s}^{-1} \\
 \beta &= 1.89 \times 10^8 \text{ s}^{-1}
 \end{aligned}$$

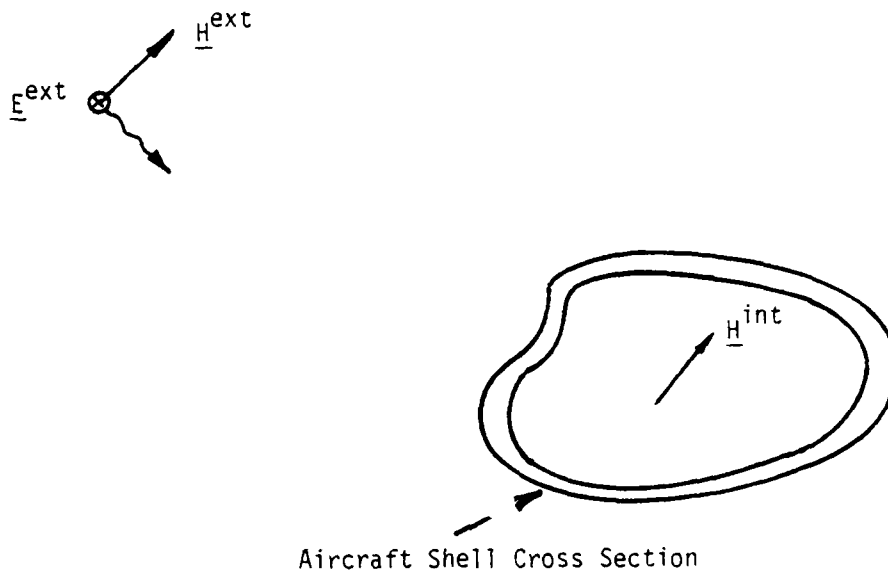


Figure 5-3. NEMP Excitation

This is essentially the same as Equation (1) except that χ and β here are much larger. This accounts for the substantial increase in spectral content of a NEMP waveform compared to the lightning case. The spectrum of Equation (24) is shown in Fig. 5-4. Although the frequency content in \underline{H}^{ext} here is much higher for the near-strike lightning case, the formulas in Subsection 5.2 can still be used if the overall dimension of the shell is small.

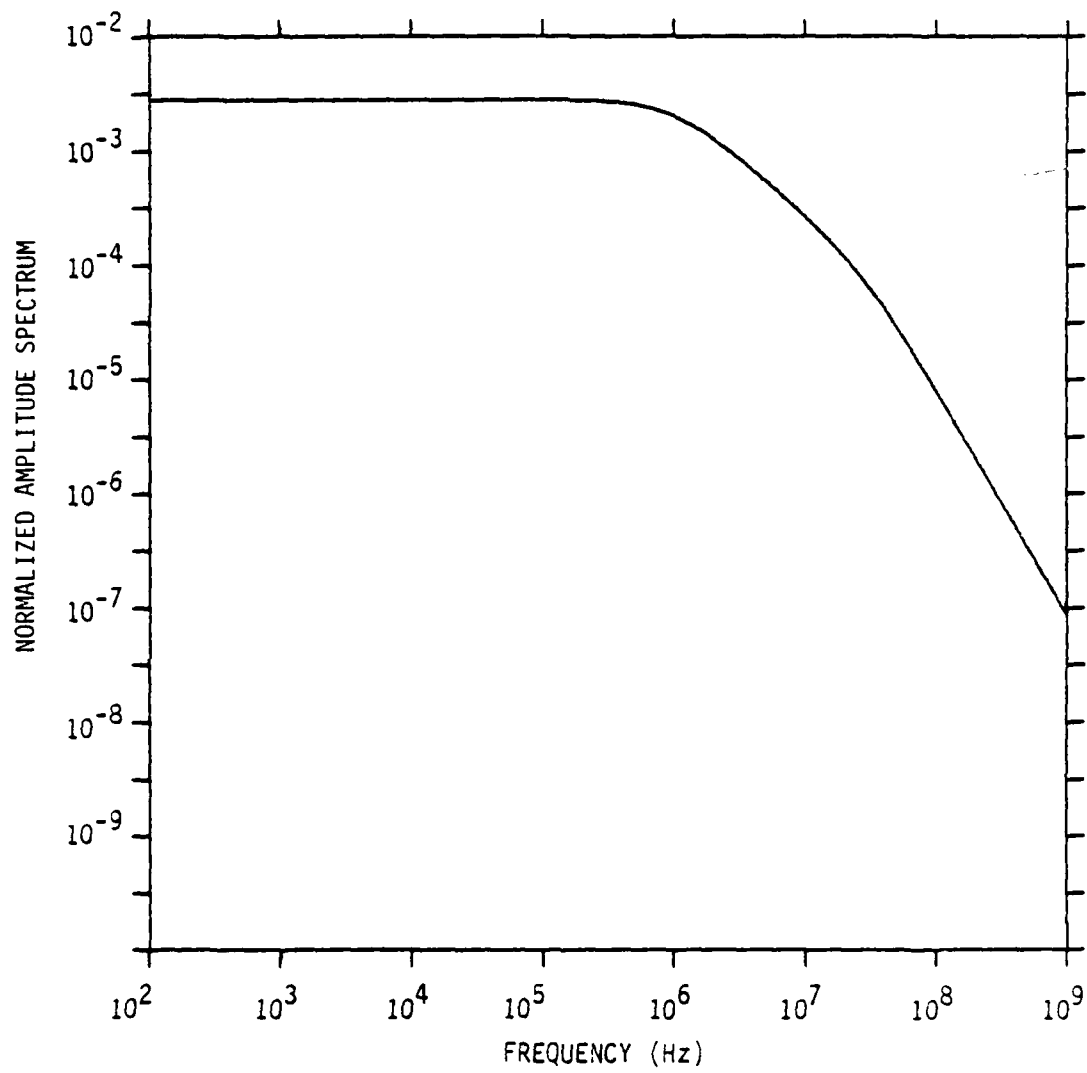


Figure 5-4. Normalized Amplitude Spectrum of the NEMP Double Exponential Waveform

5.4 DIRECT-STRIKE LIGHTNING ATTACHMENT

We assume here, for simplicity, that the attachment current distributes uniformly around the shell cross section shown in Fig. 5-5. The actual distribution can be found by the method of Subsection 2.8. Thus, the surface current density J_s is approximated by

$$J_s(t) = \frac{I(t)}{C} \quad (25)$$

where C is the shell outside circumference and $I(t)$ is given by Equation (1). Coupling to the inside is effected through the surface transfer impedance Z_{st} . Thus, the internal electric field is in the same direction as J_s and is given by

$$E_{int}(s) = J_s(s) Z_{st}(s) \quad (26)$$

in the frequency domain. $Z_{st}(s)$ is given by

$$Z_{st}(s) = \frac{\eta(s)}{\sinh \gamma(s)d} \quad (27)$$

where

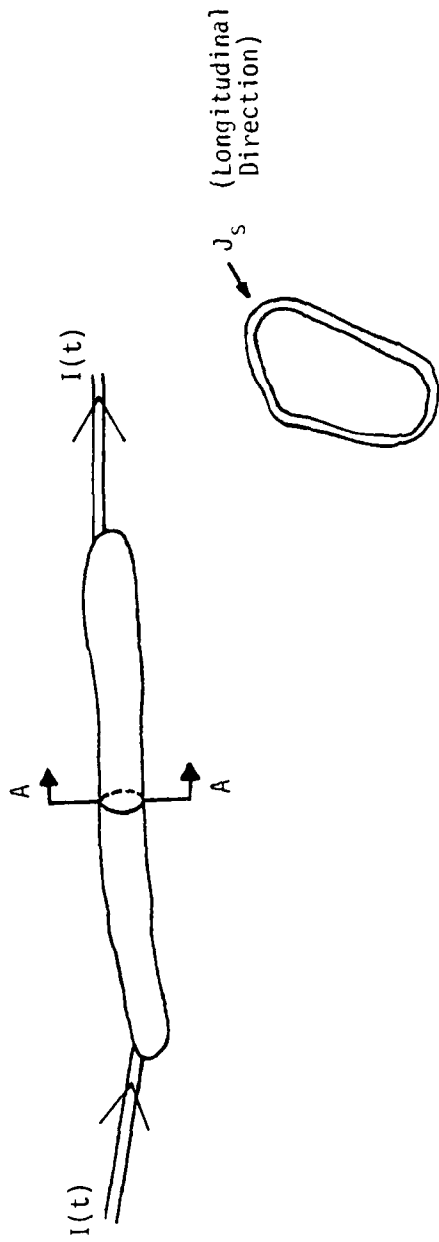
$$\eta(s) = \sqrt{\frac{s\mu}{\sigma}} \quad (s = j\omega)$$

$$\gamma(s) = \sqrt{s\mu\sigma}$$

Now we let $t_d = \mu\sigma d^2$ and the inverse transform of Equation (26) is written as

$$E_{int}(t) = \frac{1}{\sigma d C 2\pi j} \int_{K-j\infty}^{K+j\infty} \frac{I(s) \sqrt{st_d}}{\sinh \sqrt{st_d}} e^{st} ds \quad (28)$$

where K is an arbitrary real constant and Equation (25) has been used.



Section A-A of
Circumference C

Figure 5-5. Direct-Strike Lightning Attachment to Aircraft
Shell Section

To find the step response, let

$$I(t) = \begin{cases} I_0 & t \geq 0 \\ 0 & t < 0 \end{cases}$$

Then $I(s) = I_0/s$. Equation (28) then becomes

$$E_{\text{int}}(t) = \frac{I_0}{\sigma d C 2\pi j} \int_{\Gamma} \frac{z^2 e^{z^2 t/t_d}}{\sinh z} dz \quad (29)$$

where the substitution $s = z^2/t_d$ has been used and Γ is the contour shown in Fig. 5-6. The integral in Equation (29) has simple poles at zero and at

$$z_n = jn\pi \quad ; \quad n = 1, 2, \dots$$

The integral in Equation (29) is thus equal to

$$2\pi j \left[\frac{1}{2} R_0 + \sum_{n=1}^{\infty} R_n \right] \quad (30)$$

where

$$R_0 = 2$$

$$R_n = 2(-1)^n e^{-(n\pi)^2 t/t_d}$$

Thus the step response is given by

$$E_{\text{int}}^{\text{step}}(t) = \frac{I_0}{\sigma d C} \left[1 + 2 \sum_{n=1}^{\infty} (-1)^n e^{-(n\pi)^2 t/t_d} \right] \quad (31)$$

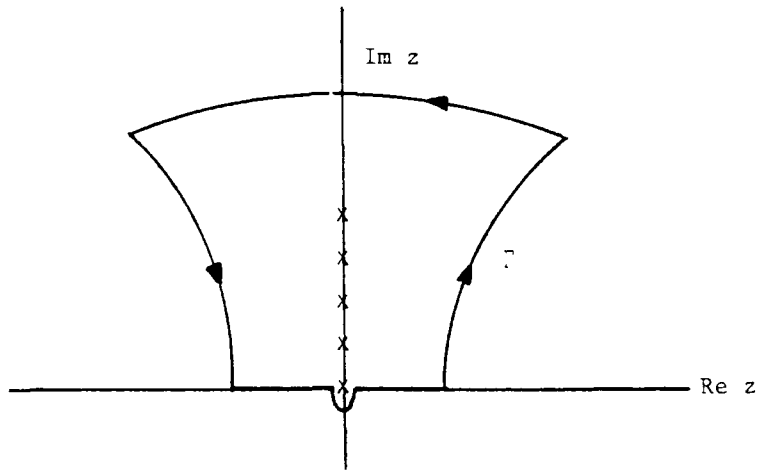


Figure 5-6. Contour in Complex z Plane for Computation of Integral in Equation (29)

The impulse response, obtained by differentiation, is given by

$$E_{int}^{imp}(t) = -\frac{2I_0}{\sigma d C t_d} \sum_{n=1}^{\infty} (-1)^n (n\pi)^2 e^{-(n\pi)^2 t/t_d} \quad (32)$$

Equation (31) is the same as that abstracted in Appendix B of [4] which was for the voltage measured between longitudinally spaced points on the interior surface of the tube due to a current step function.

Now the lightning waveform is modeled by

$$I(t) = I_0 [e^{-\alpha t} - e^{-\beta t}] \quad , \quad t \geq 0 \quad (33)$$

whose spectrum is given by

$$I(s) = I_0 \frac{\beta - \alpha}{(\alpha + s)(\beta + s)} \quad (34)$$

To get the response to Equation (33), we substitute Equation (34) into Equation (28) and obtain

$$E_{int}(t) = \frac{2 I_o (\beta - \alpha)}{\sigma d C 2\pi j} t_d \int_{\Gamma'} \frac{z^2 e^{z^2 t/t_d}}{\sinh z (t_d \alpha + z^2)(t_d \beta + z^2)} dz \quad (35)$$

where simple poles occur at

$$z_n = jn\pi, \quad n = 1, 2, \dots$$

$$z_\alpha = j \sqrt{t_d \alpha}$$

$$z_\beta = j \sqrt{t_d \beta}$$

and Γ' is shown in Fig. 5-7.

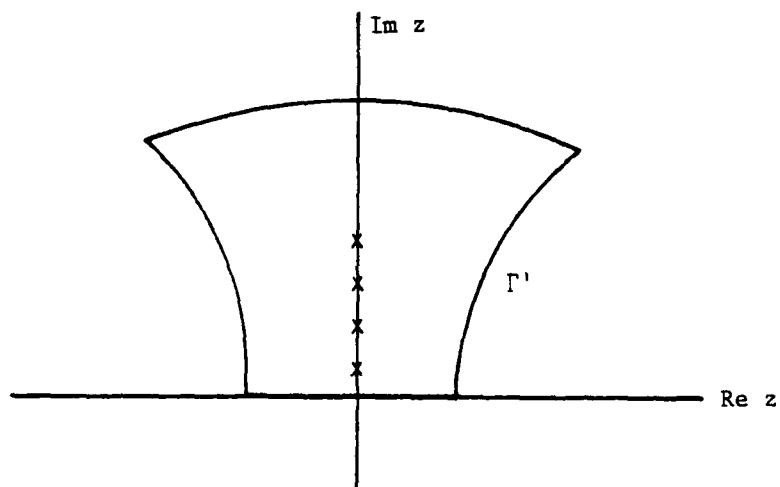


Figure 5-7. Contour in the Complex z Plane Used to Compute the Integral in Equation (35)

The integral in Equation (35) is given by the sum of its residues:

$$2\pi j \left[R_\alpha + R_\beta + \sum_{n=1}^{\infty} R_n \right]$$

where

$$R_\alpha = \frac{e^{-\alpha t}}{2 \sin \sqrt{\alpha t_d}} \frac{1}{(\beta - \alpha)} \sqrt{\alpha/t_d}$$

$$R_\beta = \frac{e^{-\beta t}}{2 \sin \sqrt{\beta t_d}} \frac{1}{(\alpha - \beta)} \sqrt{\beta/t_d}$$

$$R_n = \frac{-(-1)^n (n\pi)^2 e^{-(n\pi)^2 t/t_d}}{(\alpha t_d - (n\pi)^2)(\beta t_d - (n\pi)^2)}$$

Thus Equation (35) can be written as

$$E_{int}(t) = \frac{I_o}{\sigma d C} \left[\frac{\sqrt{\alpha t_d} e^{-\alpha t}}{\sin \sqrt{\alpha t_d}} - \frac{\sqrt{\beta t_d} e^{-\beta t}}{\sin \sqrt{\beta t_d}} - 2(\beta - \alpha) t_d \sum_{n=1}^{\infty} \frac{(-1)^n (n\pi)^2 e^{-(n\pi)^2 t/t_d}}{(\alpha t_d - (n\pi)^2)(\beta t_d - (n\pi)^2)} \right] \quad (36)$$

From [5], we have the sum:

$$S = \sum_{n=1}^{\infty} \frac{\cos nx}{n^2 - a^2} = \frac{1}{2a^2} - \frac{\pi}{2a} \frac{\cos(x - \pi) a}{\sin \pi a}$$

so that

$$\frac{dS}{dx} = - \sum_{n=1}^{\infty} \frac{n \sin nx}{n^2 - a^2} = \frac{a\pi \sin(x - \pi) a}{2a \sin \pi a}$$

and

$$\frac{d^2 S}{dx^2} = - \sum_{n=1}^{\infty} \frac{n^2 \cos nx}{n^2 - a^2} = \frac{a\pi \cos (x - \pi) a}{2 \sin \pi a}$$

Now let $x = \pi$ and we have

$$\frac{a\pi}{2 \sin \pi a} = - \sum_{n=1}^{\infty} \frac{n^2 (-1)^n}{n^2 - a^2}$$

or

$$\frac{u}{\sin u} = - 2 \sum_{n=1}^{\infty} \frac{(-1)^n (n\pi)^2}{(n\pi)^2 - u^2}$$

Thus we also have

$$\frac{\sqrt{\alpha t_d}}{\sin \sqrt{\alpha t_d}} = 2 \sum_{n=1}^{\infty} \frac{(n\pi)^2 (-1)^n}{\alpha t_d - (n\pi)^2}$$

and

$$\frac{\sqrt{\beta t_d}}{\sin \sqrt{\beta t_d}} = 2 \sum_{n=1}^{\infty} \frac{(-1)^n (n\pi)^2}{\beta t_d - (n\pi)^2}$$

Now let $x_{n\alpha} = \alpha t_d - (n\pi)^2$ and $x_{n\beta} = \beta t_d - (n\pi)^2$ then Equation (25) becomes

$$\begin{aligned} E_{int}(t) &= \frac{2 I_0}{\sigma d C} \sum_{n=1}^{\infty} (-1)^n (n\pi)^2 \left\{ \frac{e^{-\alpha t}}{x_{n\alpha}} - \frac{e^{-\beta t}}{x_{n\beta}} + \frac{(x_{n\alpha} - x_{n\beta}) e^{-\frac{(n\pi)^2 t}{t_d}}}{x_{n\alpha} x_{n\beta}} \right\} \\ &= - \frac{2 I_0}{\sigma d C} \sum_{n=1}^{\infty} (-1)^n (n\pi)^2 \left\{ \frac{e^{-\alpha t} - e^{-\frac{(n\pi)^2 t}{t_d}}}{x_{n\alpha}} - \frac{e^{-\beta t} - e^{-\frac{(n\pi)^2 t}{t_d}}}{x_{n\beta}} \right\} \end{aligned} \quad (37)$$

This can also be derived by convolution and is identical to the voltage response derived in [4]. Thus the voltage drop per unit length inside the tube wall along the tube axis is given by

$$E_{int}(t) = \frac{I_0}{C} \left[\frac{\sqrt{\frac{\alpha\mu}{\sigma}}}{\sin \sqrt{\alpha\mu\sigma} d} e^{-\alpha t} - \frac{\sqrt{\frac{\beta\mu}{\sigma}}}{\sin \sqrt{\beta\mu\sigma} d} e^{-\beta t} + 2(\alpha - \beta) t_d \sum_{n=1}^{\infty} \frac{(-1)^n e^{-(n\pi)^2 t/t_d}}{(n\pi)^2 \left(1 - \frac{\alpha t_d}{(n\pi)^2}\right) \left(1 - \frac{\beta t_d}{(n\pi)^2}\right)} \right] \quad (38)$$

5.5 REFERENCES

- [1] K.S.H. Lee and G. Bedrosian, "Diffusive Electromagnetic Penetration into Metallic Enclosures", IEEE Trans. on Ant. and Prop., Vol. AP-27, No. 2, March 1979.
- [2] H. Kaden, Wirbelstrome und Schirmung in der Nachrichtentechnik, Springer-Verlag, Berlin, 1959.
- [3] L.W. Rickett, J.E. Bridges, and J. Miletta, EMP Radiation and Protective Techniques, John Wiley and Sons, 1976.
- [4] "Advanced Composite Aircraft Electromagnetic Design and Synthesis", Syracuse Research Corporation, SRC TR 79-490, April 1980.
- [5] R.E. Collin, Field Theory of Guided Waves, McGraw-Hill Book Co., New York, 1960, p 581.

SECTION 6

INTERIOR FIELD RESULTS AND APPLICATION OF LOW FREQUENCY COUPLING MODELS

6.1 RESULTS AND APPLICATION OF MODELS

Computer programs were written for the E-field and combined-field formulations presented in Section 2 of this report. These are documented in Appendix A where sample output is given for a cylinder of circular cross section with a radius of 0.3828m. The frequency of the incident plane wave is 300 MHz. The TE and TM surface currents of the two formulations are in excellent agreement at all points on the cylinder contour. An additional check is provided by the exact series solution where a computer program along with sample output is also documented in Appendix A. Electric surface currents and scattered far-field patterns for all three methods are in excellent agreement. Several examples of surface current density and scattered field patterns may be found in [1], [2], and [3], so no plots of these quantities are presented here. The main purpose of Section 2 is actually to provide the various E-field impedance operators necessary for the shell penetration formulations of Section 3.

An excitation other than an incident plane wave is considered at the end of Section 2 in which a longitudinal-directed current is assumed to exist on the contour C. This is used as a first-order simulation of a direct-strike lightning (DSL) excitation. If the contour C is not circular, the surface current density is not constant and distributes itself around C inductively. A computer program is documented in Appendix A which is used to compute this distribution. An example of a computation for this excitation is shown in Fig. 6-1 where the cross section of a fuselage station [4] is considered. The numbers near the dots on the contour identify the center of each Δ_j , $j=1, 2, \dots, 28$ (see Fig. 2-2) and the numbers with arrows pointing to the contour indicate surface currents computed at that point. Numbers in parentheses indicate currents computed in [4] by solving Laplace's equation in a finite region surrounding C with the effects of three symmetrically placed return conductors

included. The integral equation solution of Section 2 in effect has the return path at infinity. This accounts for the difference in results obtained by the two methods. Note that the current distribution is symmetric about a vertical centerline of the fuselage section so that only half of the data is shown in the figure.

Computer programs using the impedance sheet approximation of Section 3 and the exact-series solution of Section 4 for a lossy shell (i.e., a shell wall material having finite conductivity σ) are documented in Appendix B. These programs compute an internal z-directed electric field for the TM case and magnetic field for the TE case. Some sample plots of shielding effectiveness (defined by Equation (1) of Section 3) are shown in Figs. 6-2 and 6-3 for a shell of circular cross section. As expected, the impedance sheet approximation gives excellent results in the TM case when compared to the exact-series solution. This comparison is shown in Fig. 6-2 for different conductivities and over a large frequency interval. Here the exact-series solution is represented by the solid lines and the impedance-sheet integral equation solution is represented by circles. The latter becomes suspect at frequencies much higher than 10^8 Hz because the number of subsections with which the circular contour was approximated was held constant ($NC = 16$ for all frequencies). The TE comparison shown in Fig. 6-3 is not as good because for this case there are transverse-directed components of polarization current which are neglected in the impedance sheet formulation.

The results for the TM case indicate that the \hat{z} -directed incident electric field is effectively not shielded at all as the frequency becomes low. This can be seen from the impedance sheet integral equation where the vector potential term becomes negligible as $\omega \rightarrow 0$ and hence $J_z \rightarrow E_z^i / Z_L$. The TM case is somewhat pathological at low frequencies because theoretically no charge separation can occur to create a scattered electric field which tends to produce zero total electric field inside the shell as occurs in the TE case. A physically realizable shell will always have a quasi-static charge separation at low frequencies and thus will tend to shield an incident electric field (more than the TM infinite cylinder result would indicate). As expected, the magnetic field is essentially not shielded at low frequencies regardless of the polarization considered.

Results for the traveling wave approximation to shell penetration developed in Subsection 3.3 are not presented here. A computer program was written which incorporated this formulation but was found to give questionable results at low frequencies. This is because the relationship between the tangential electric and magnetic fields just inside the shell is not given by the characteristic impedance of the material inside the shell. This assumption essentially neglects the inductive reactance caused by the shell geometry which is seen by the electric current used to excite the equivalent transmission line model. The traveling wave approximation, however, does give reasonable results for higher frequencies at which the shell cross section dimension is electrically large.

The various computational methods presented so far allow one to adequately determine the interior fields which penetrate a shell at particular frequencies of an external steady-state electromagnetic field. Thus if the spectrum of the excitation is known, one can characterize the spectrum of the interior field. In Section 5, some expressions are derived for the interior field spectrum, given an assumed external field or excitation. If a low frequency assumption can be made concerning the excitation spectrum, then the interior field can be obtained as a function of time. It is also assumed to be uniform in space over a region which encompasses the shell cross section. The computation of these interior fields which are due to a nuclear electromagnetic pulse (NEMP), near-strike lightning (NSL), or direct-strike lightning (DSL) as they are modeled in Section 5 are performed by the computer program subroutines which are briefly described in Appendix C.

Figure 6-4 shows plots of internal magnetic fields for various lossy cylinders when exposed to an NSL excitation. The lightning current is 100m from the shell and is parallel to the shell axis. As expected, as σ , d , or the volume-to-surface ratio is increased, the rise time of the responding interior field increases. This can be seen from the equivalent circuit analogues to the coupling mechanism. Inside the shell, a circuit or transmission line is exposed to the interior field. A worst-case situation is assumed where the effective area of the transmission line or circuit is maximally coupled to

the transverse component of magnetic flux density. Time derivatives of interior and exterior NSL fields are shown in Fig. 6-5.

Using the transmission line excitation formulas developed in [5], the open-circuit voltage and short-circuit current measurements made for a given loaded transmission line configuration may be computed. An example of these results is shown in Fig. 6-6 where the interior circuit consists of 10m of RG8-A along the cylinder shell axis terminated in a 30-ohm load. The product of the above quantities as a function of time gives an upper bound on the instantaneous transient power possible across the terminals of the load. An example of this is shown in Fig. 6-7. Various parametric curves are of interest from a computer-aided design (CAD) standpoint so that elementary circuits may be constructed which minimize the possibility of component burnout. Examples of these are shown in Figs. 6-8 through 6-11. This type of parametric representation is discussed in more detail in [5].

As mentioned previously, the main difference between NSL and NEMP excitation is the spectral content of the two, that of NEMP being much higher. Some representative interior field coupling examples for NEMP are shown in Figs. 6-12 through 6-14. Note that the time scales are now different and the high-frequency resonance on the transmission line is visible.

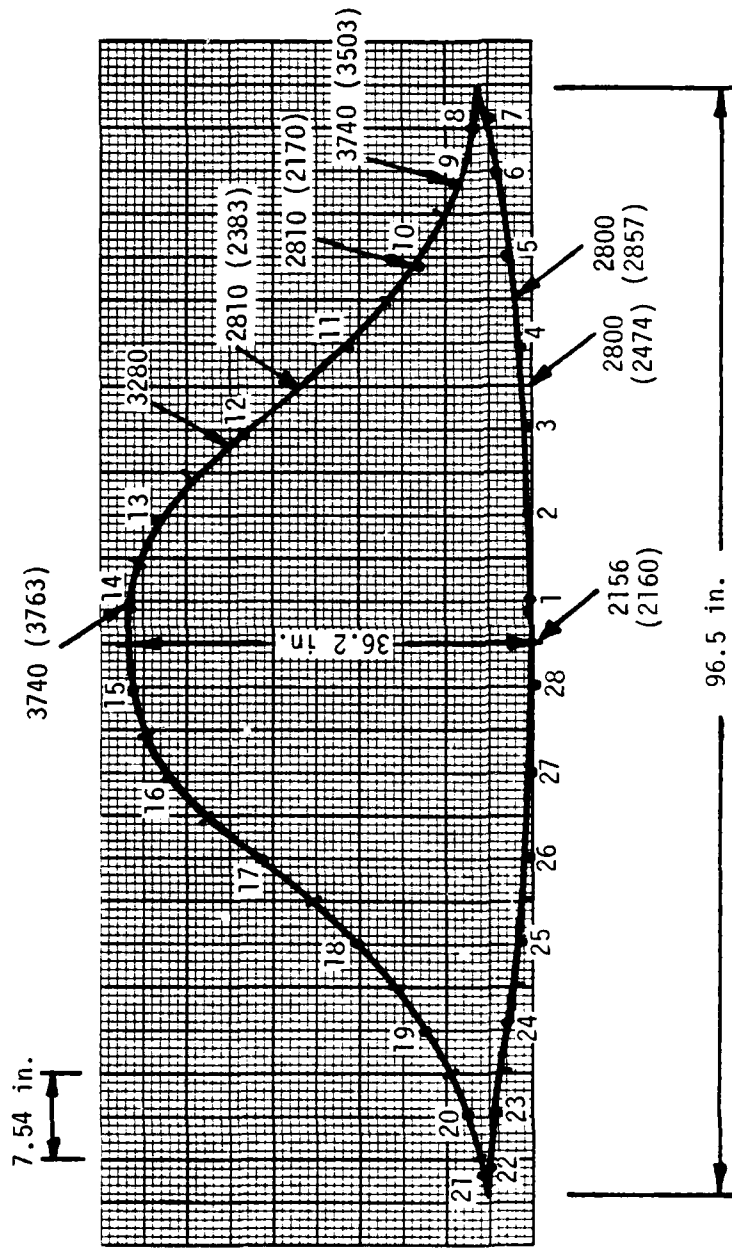


Figure 6-1. Free Space Longitudinal Current Distribution on Conducting Cylinder Contour, $I_{total} = 20 \text{ kA}$

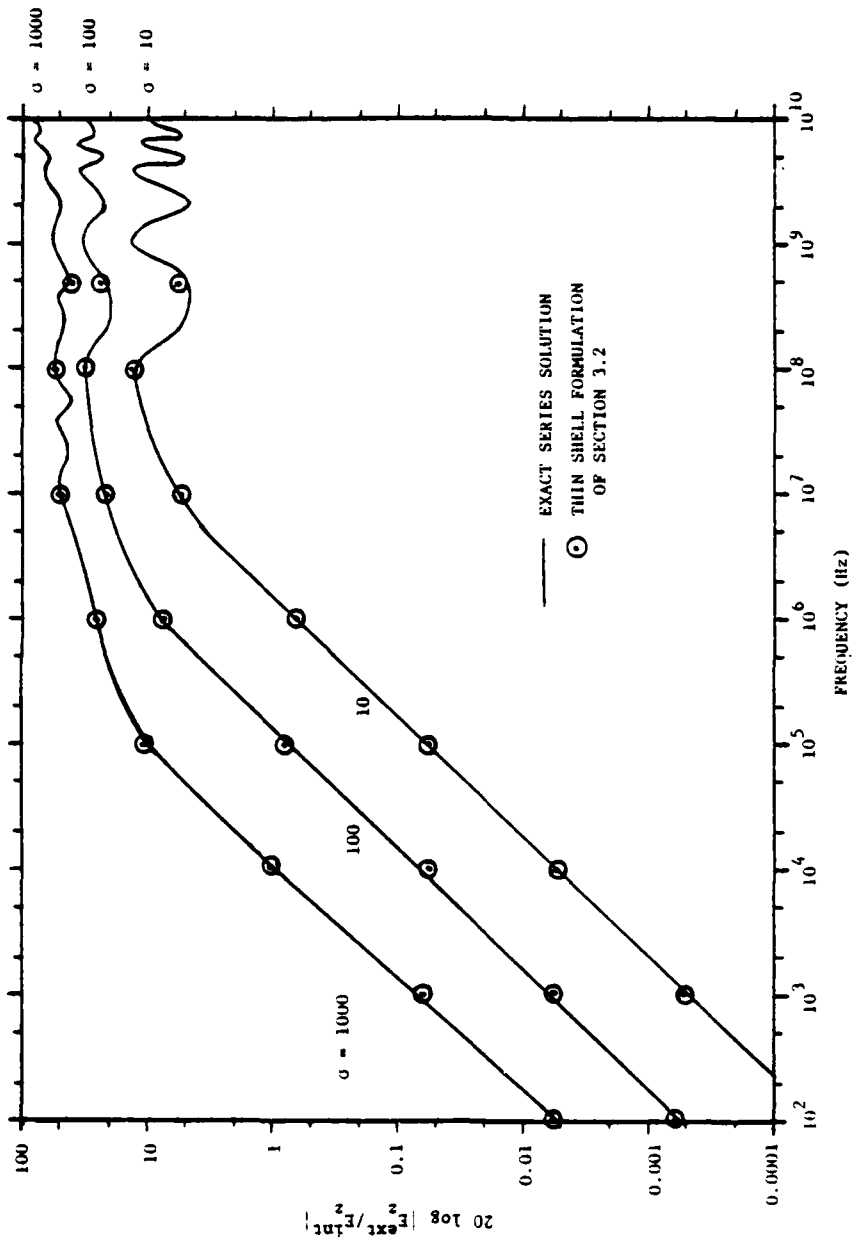


Figure 6-2. Electric Shielding Effectiveness (TM Case) at Center of Lossy Circular Shell, Radius = 0.5m, Thickness = 1mm

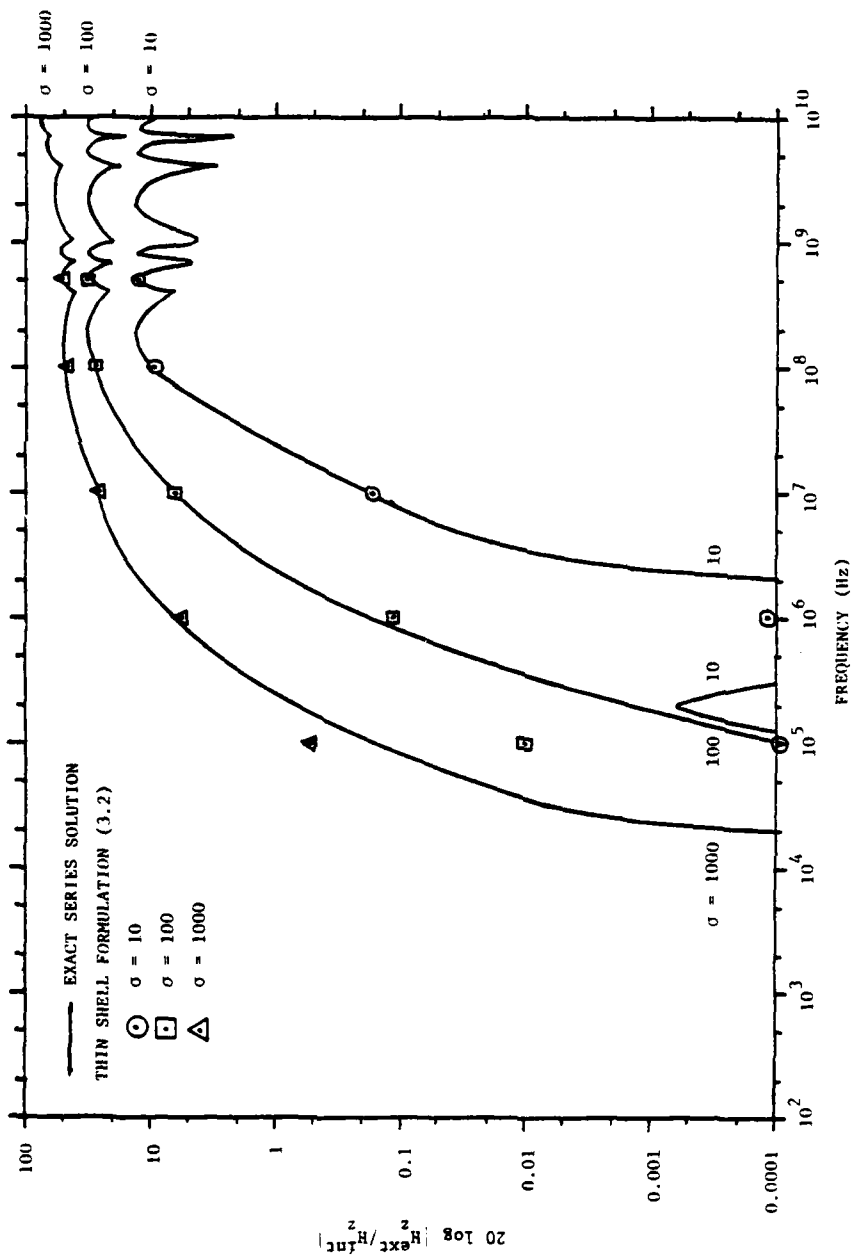
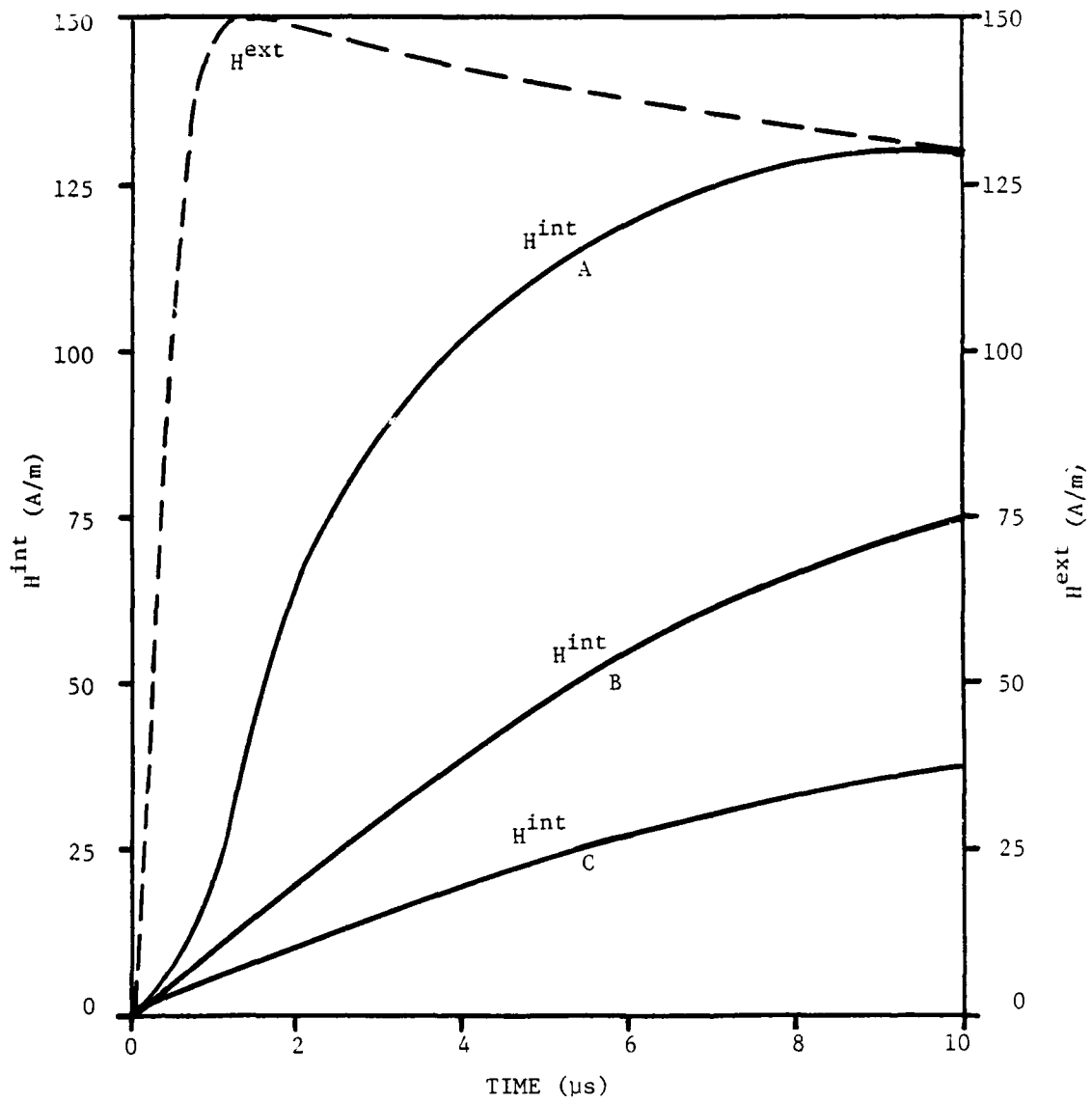


Figure 6-3. Magnetic Shielding Effectiveness (TE Case) At Center of Lossy Circular Shell, Radius = 0.5m, Thickness = 1mm



SHELL	RADIUS (m)	THICKNESS (ply)	σ
A	0.5	8	10^4
B	1.0	8	2×10^4
C	1.0	20	2×10^4

Figure 6-4. External and Internal NSL Magnetic Field for Circular Shell

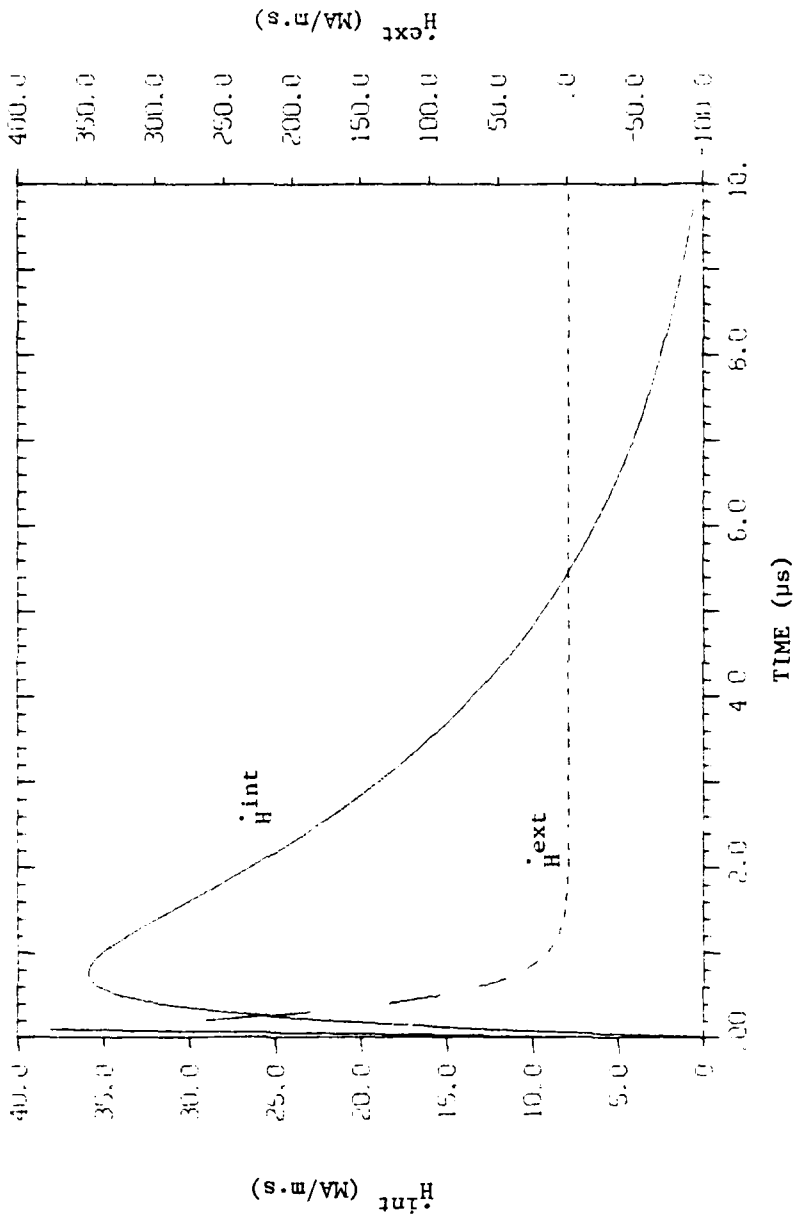


Figure 6-5. Time Derivatives of Internal and External NSL Magnetic Fields for Cylindrical Shell A of Figure 6-4

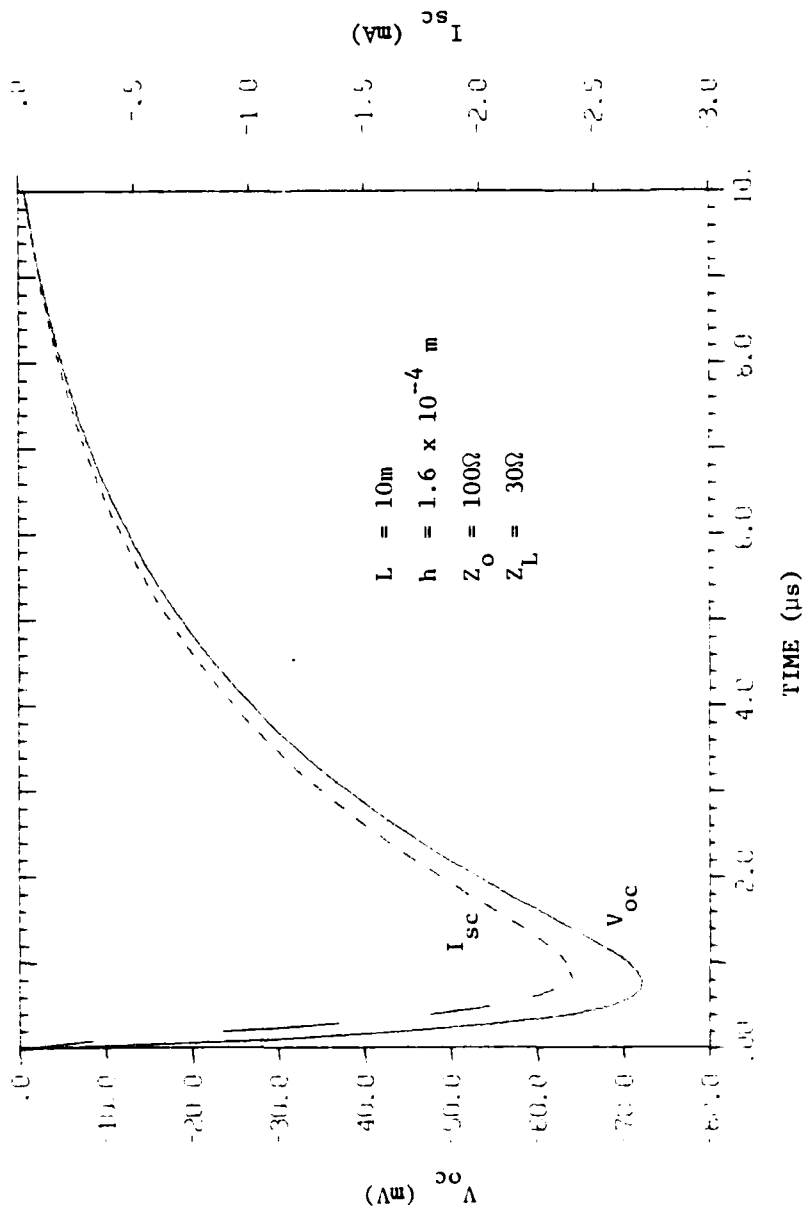


Figure 6-6. Open-Circuit Voltage and Short-Circuit Current Induced on Transmission Line Inside Shell of Figure 6-5

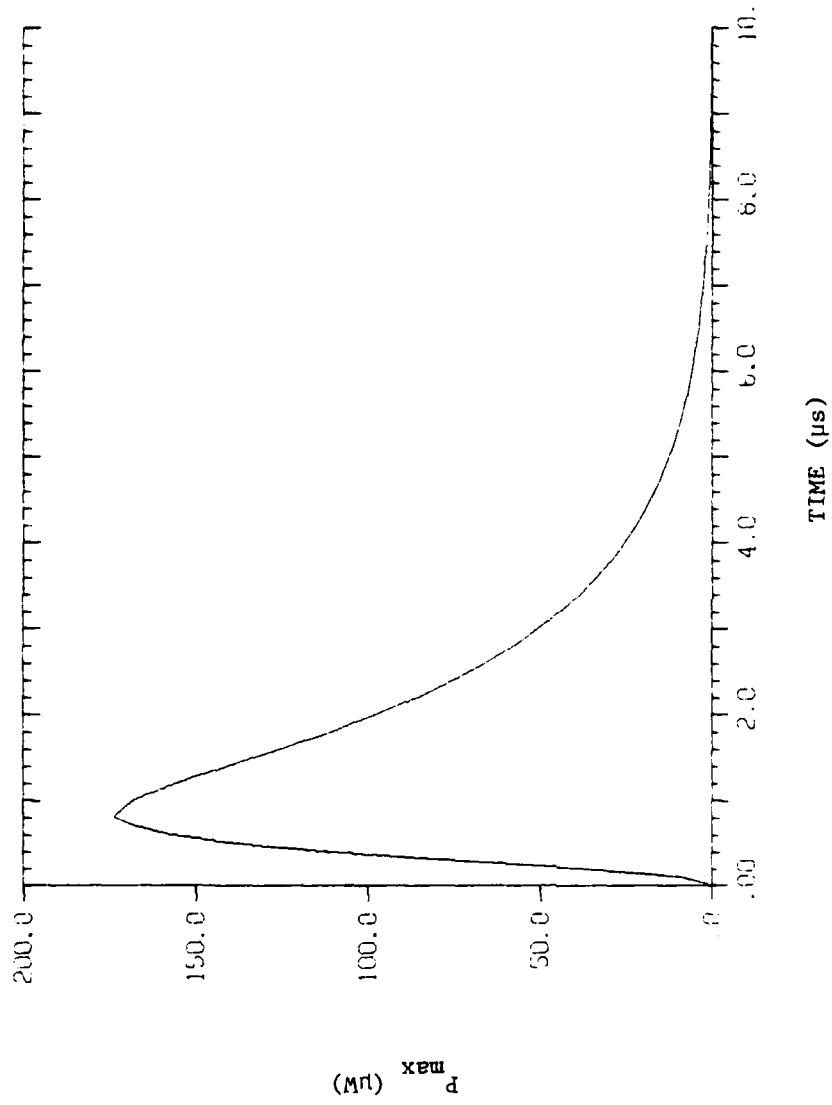
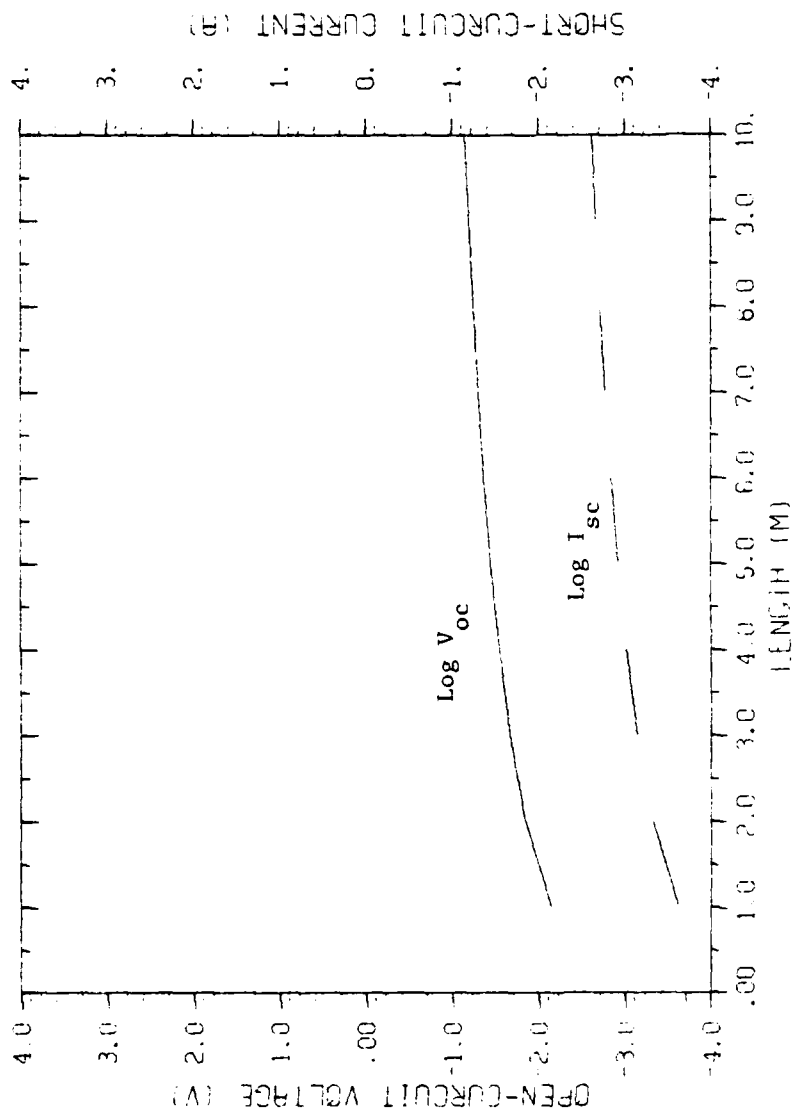
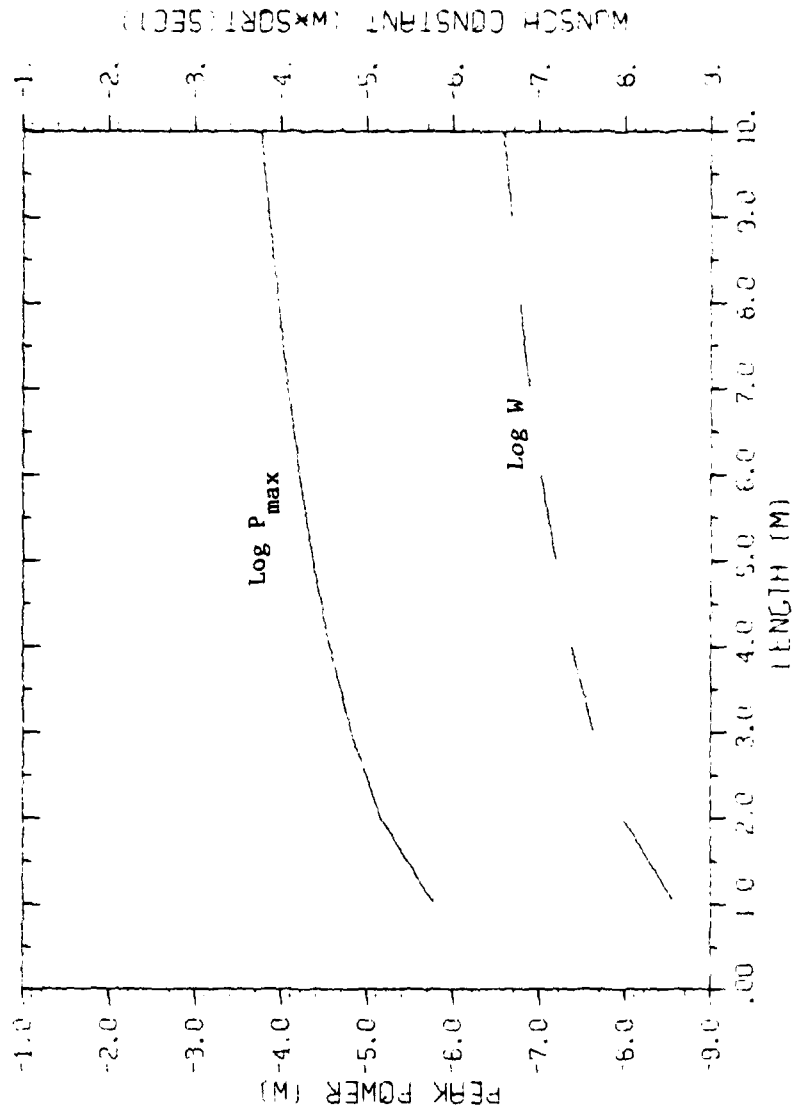


Figure 6-7. Upper Bound on Induced Power Available in Transmission Line of Figure 6-6



$h = 1.6 \times 10^{-4} \text{ m}$
 $Z_o = 100\Omega$
 $Z_L = 30\Omega$

Figure 6-8. Log of V_{oc} and I_{sc} Versus Transmission Line Length for Shell A of Figure 6-4

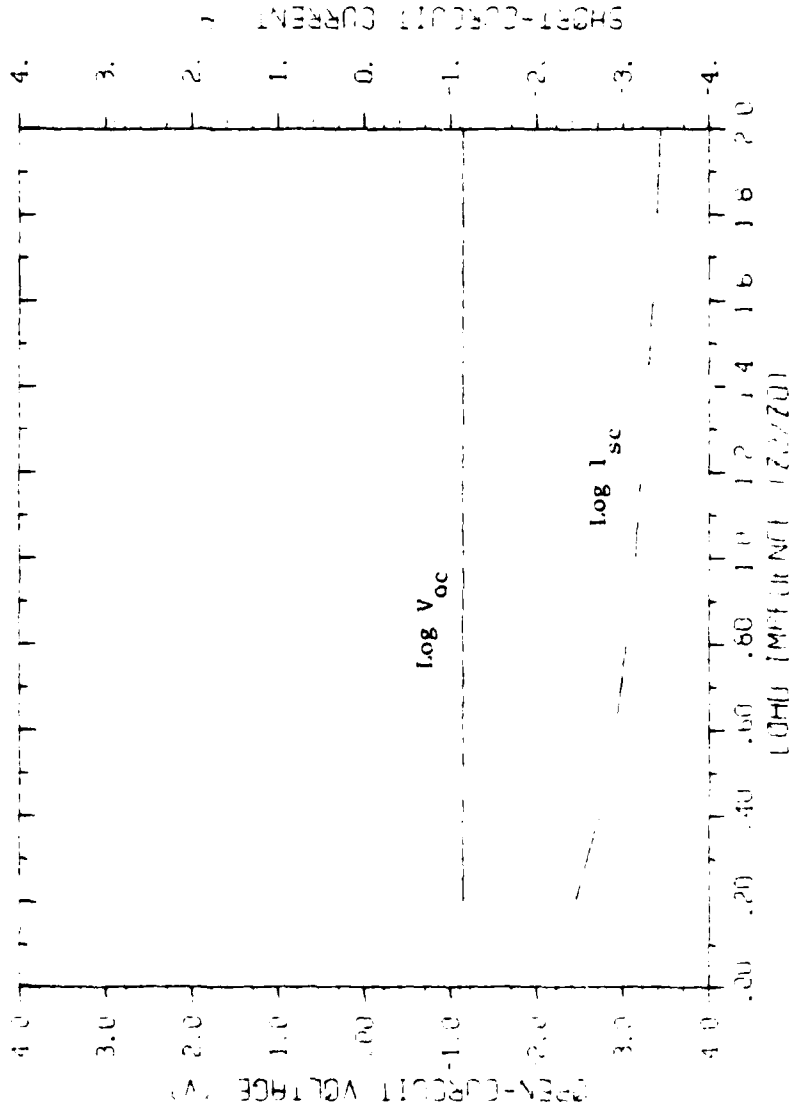


$$h = 1.6 \times 10^{-4} \text{ m}$$

$$Z_0 = 100\Omega$$

$$Z_L = 30\Omega$$

Figure 6-9. Log of P_{max} and Wunsch Constant Versus Transmission Line Length for Shell A of Figure 6-4

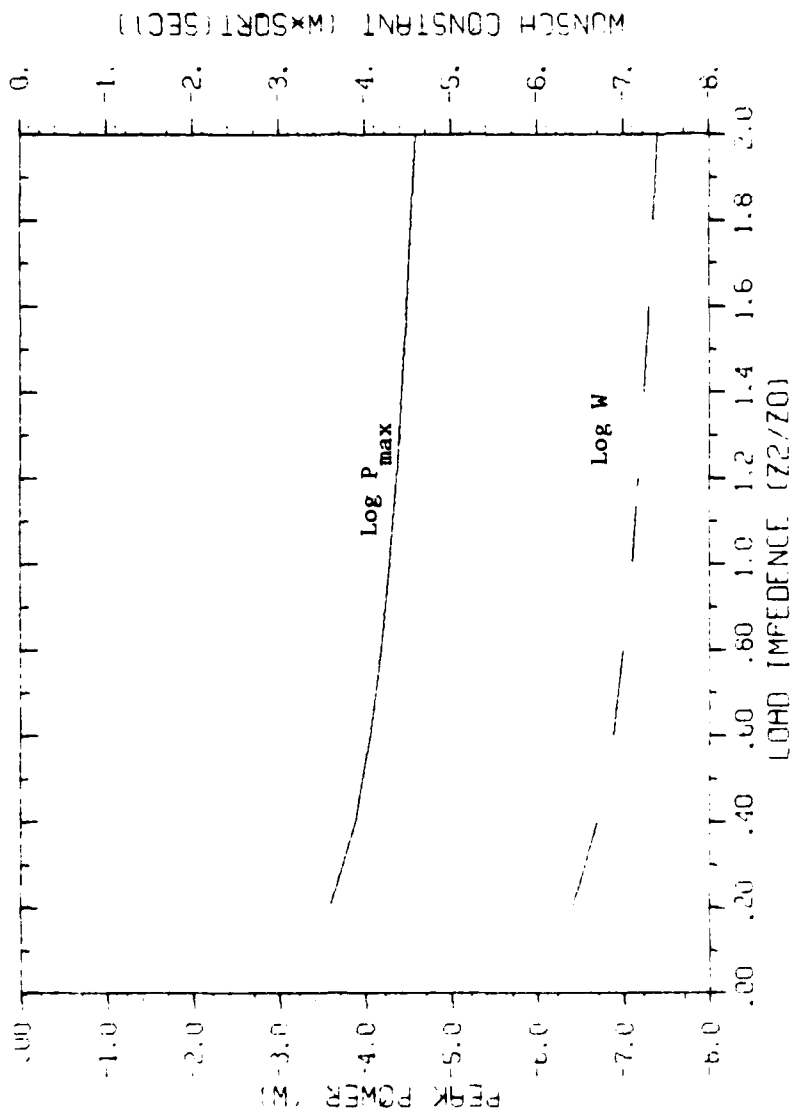


$$h = 1.6 \times 10^{-4} \text{ m}$$

$$L = 10 \text{ m}$$

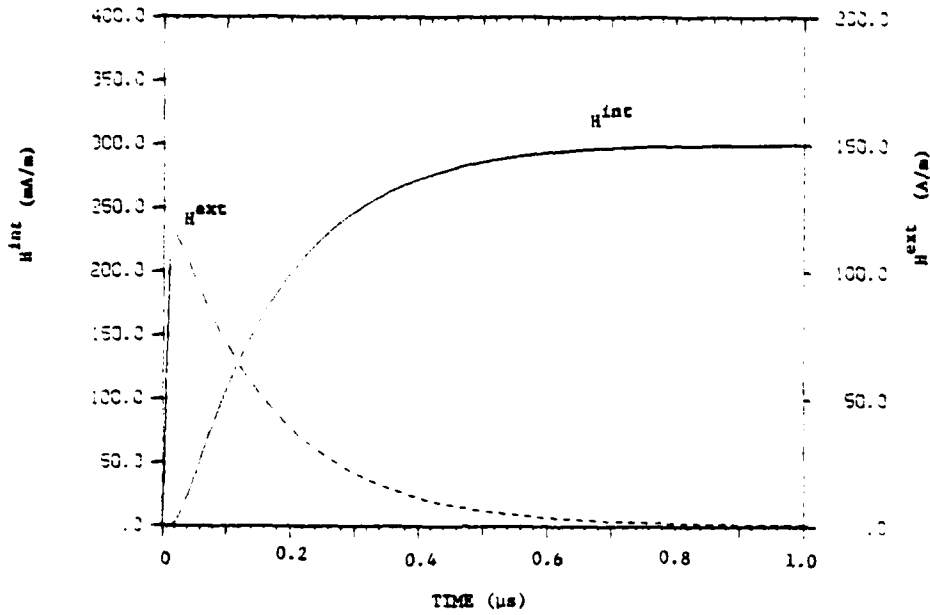
$$Z_o = 100 \Omega$$

Figure 6-10. Log of V_{oc} and I_{sc} Versus Normalized Load Impedance for Shell A of Figure 6-4

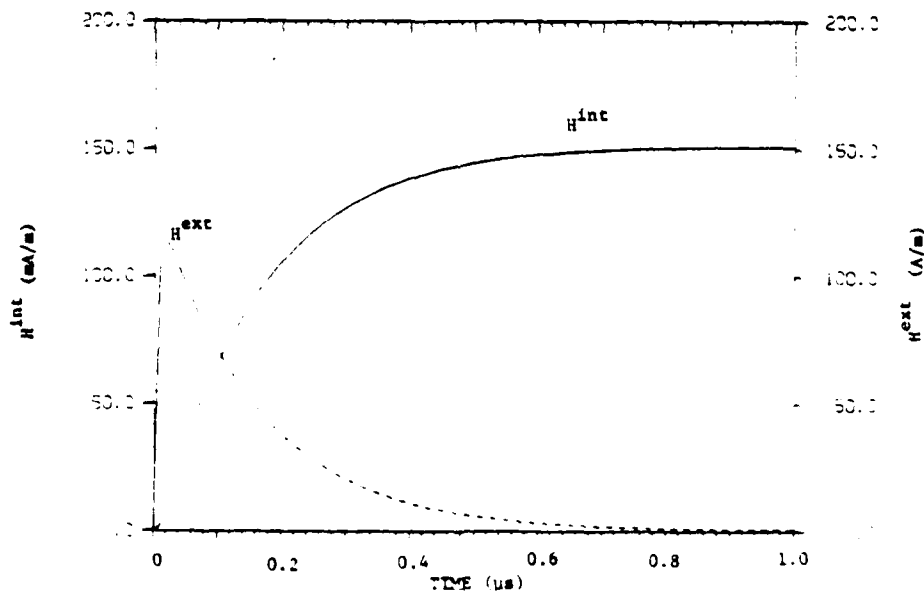


$h = 1.6 \times 10^{-4} \text{ m}$
 $L = 10 \text{ m}$
 $Z_0 = 100 \Omega$

Figure 6-11. Log of P_{max} and Wunsch Constant Versus Normalized Load Impedance for Shell A of Figure 6-4

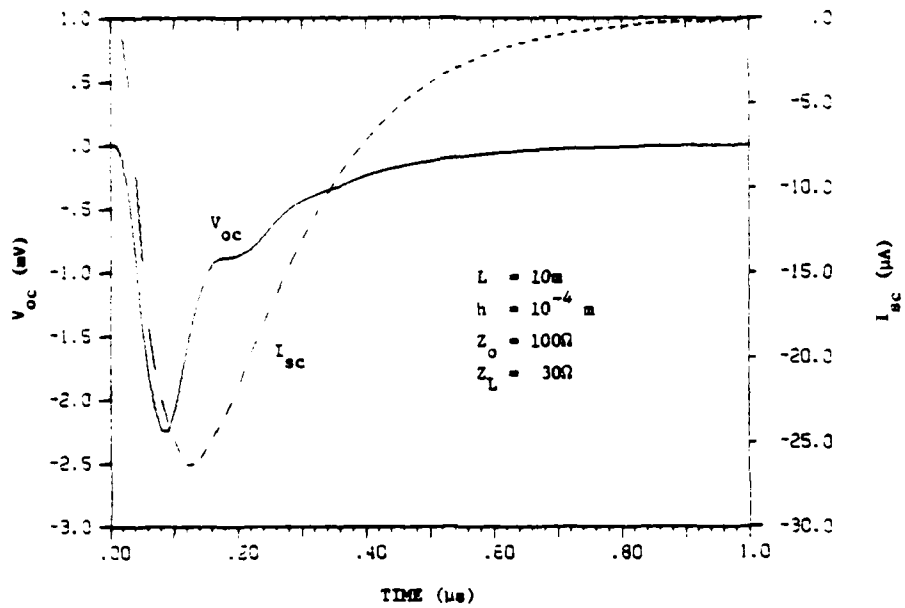


(a) Radius = 1m, Thickness = 8 Ply, $\sigma = 10^5$

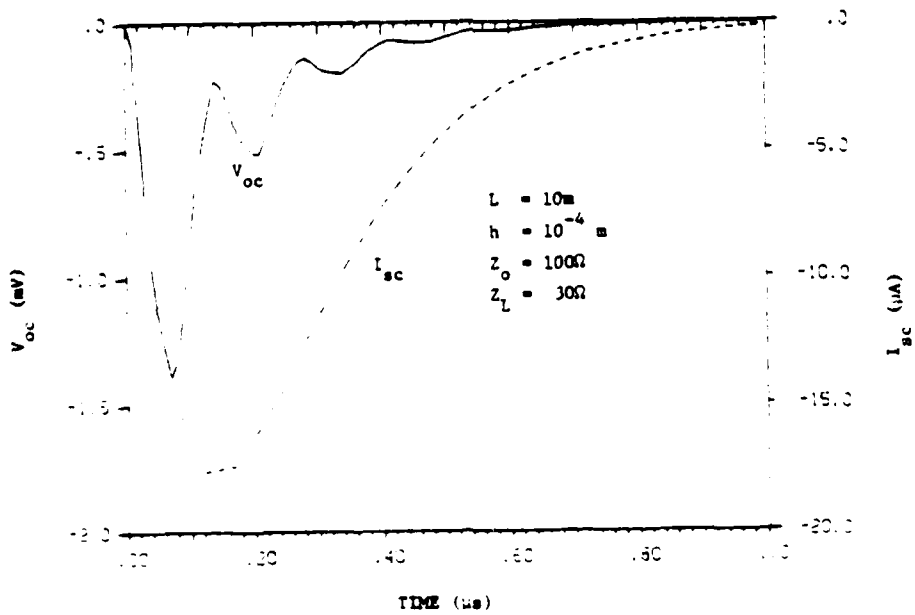


(b) Radius = 10m, Thickness = 8 Ply, $\sigma = 2 \times 10^4$

Figure 6-12. External and Internal NEMP Magnetic Field for Circular Shell

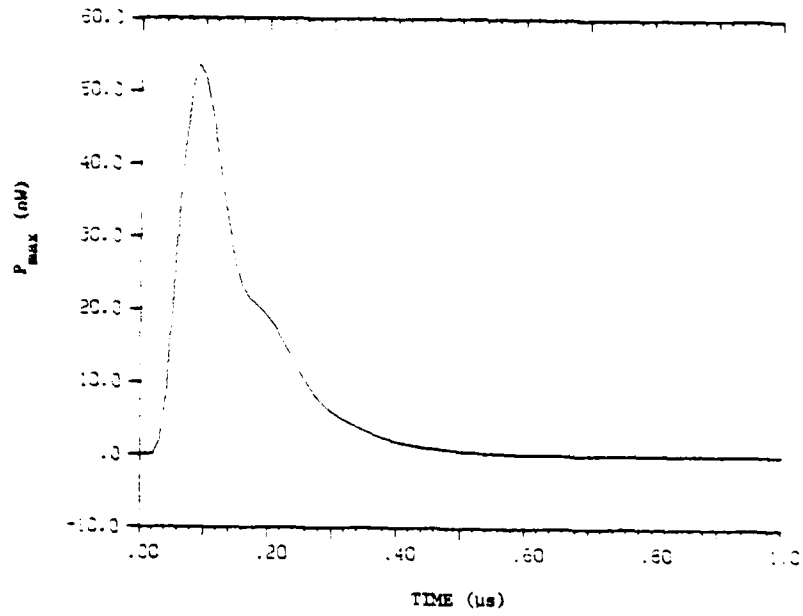


(a) Radius = 1m, Thickness = 8 Ply, $\sigma = 10^5$

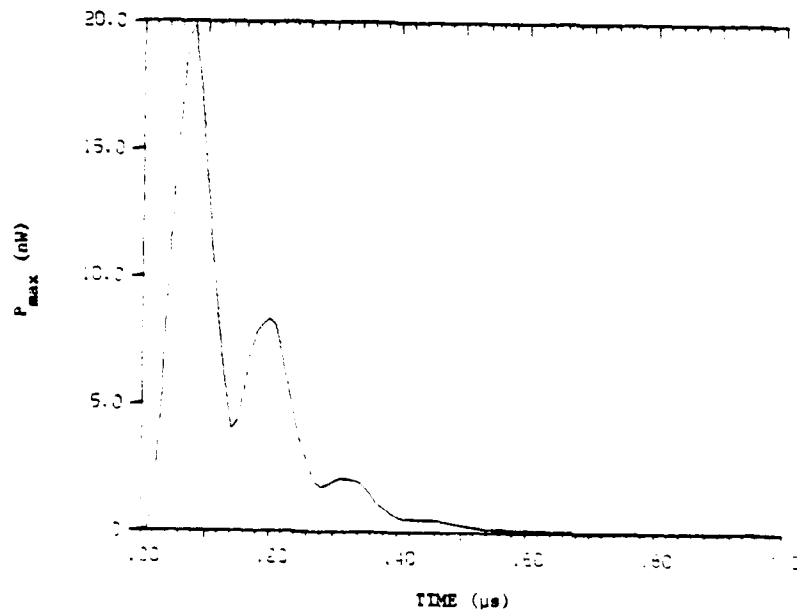


(b) Radius = 10m, Thickness = 8 Ply, $\sigma = 2 \times 10^4$

Figure 6-13. Open-Circuit Voltage and Short-Circuit Current Induced on Transmission Lines Inside Circular Shells of Figure 6-12



(a) Radius = 1m, Thickness = 8 Ply, $J = 10^4$



(b) Radius = 10m, Thickness = 8 Ply, $J = 2 \times 10^4$

Figure 6-14. Upper Bounds on Induced Power Available in Transmission Line Cases of Figure 6-13

6.2 REFERENCES

- [1] R.F. Wallenberg, "Two-Dimensional Scattering and Radiation from Perfectly Conducting Cylinders of Arbitrary Shapes", Ph.D. Dissertation, Syracuse University, Syracuse, NY, Technical Report 68-2, March 1968.
- [2] D.T. Auckland and R.F. Harrington, "Moment Solution for Radiation and Scattering from Conducting Cylinders, TM Case", Syracuse University Technical Report TR 75-8, July 1975.
- [3] J.H. Richmond, "An Integral-Equation Solution for TE Radiation and Scattering from Conducting Cylinders", Ohio State University, Interaction Note 201, April 1973.
- [4] B.J. Wallace, et al., "Composite Forward Fuselage Systems Integration", Vol. II, General Dynamics, September 1978. (Figure 27.)
- [5] "Advanced Composite Aircraft Electromagnetic Design and Synthesis", Interim Report prepared by Syracuse Research Corporation under Contract N00014-78-C-0673 sponsored by Office of Naval Research and Naval Air Systems Command, SRC TR 79-490, April 1980.

APPENDIX A

PROGRAMS FOR PERFECTLY CONDUCTING CYLINDERS OF ARBITRARY CROSS SECTION

The purpose of this appendix is to define the necessary data cards required by the E-field and combined-field programs. The main program segments are listed in Subsections A.1 and A.2. A program to calculate the exact series solution is included in Subsection A.3. The function subprograms and matrix element subroutines are not explained in detail.

The first thing one must do is approximate the contour C of the cylinder by a finite number of straight line segments. Best results are usually achieved when $\Delta \leq 0.1\lambda$ which puts a limit on the electrical size of the objects considered since matrix methods are being used. An example of approximating C is given in Fig. 2-2. Note that the contour need not be closed for the E-field formulation but must be closed for the combined-field formulation. The excitation is such that the incident magnetic field, \underline{H}^i , is equal to unity at the origin. This is done for both polarizations.

Data is read from data cards in the main program according to the format statements:

```
100  FORMAT(6I5)
101  FORMAT(2E20.7)
102  FORMAT(6E11.4)
```

The data cards appear in the sequence shown in Table A-1 and are defined as follows:

NGQ	=	Order of Gaussian quadrature formula used to approximate integrals
A(i), T(i) for i = 1,2,..., NGQ	=	Weights and nodes, respectively, of Gaussian quadrature formula (divided by 2)
ITM = integer option	=	1 for TM case = 0 bypass TM case

ITE = integer option = 1 for TE case
 = 0 bypass TE case

ISC = integer option = 1 for normalized scattered field
 pattern to be computed

NX = Number of angles at which plane
 wave is incident

NP = Number of points at which scattered
 far field is computed

PHIO = First angle at which scattered far
 field is computed

DPHI = Increment, in degrees, at which far
 field pattern is computed

PHII (i) = $i = 1, 2, \dots, NX$ = Angle of plane
 wave incidence measured in degrees
 counter-clockwise from x-axis

AMU = Permeability of material in which
 cylinder is imbedded

EPS = Permittivity of material in which
 cylinder is imbedded

BETA = Used only for combined-field
 program

(x_i, y_i) for
 $i = 1, 2, \dots, NC+1$ = x,y coordinates of end points of
 straight line segments

NFR = Number of frequencies of incident
 plane wave to be considered

FMC = Frequency in MHz (read NFR times)

The three programs were run for a cylinder of circular cross section with a
 radius of 0.3828m at 300 MHz. The results follow each program listing.

Table A-1. Input Data Card Sequence

Format Number	Data Punched on Card
100	NGQ
101	A(1), T(1)
⋮	⋮ ⋮
101	A(NGQ), T(NGQ)
100	ITM, ITE, ISC, NX, NP
102	PHIO, DPHI
102	PHII (1)
⋮	⋮
102	PHI (NX)
102	AMU, EPS, BETA (only for combined-field program)
100	NC
102	x_1 y_1
102	x_2 y_2
⋮	⋮ ⋮
102	x_{NC+1} y_{NC+1}
100	NFR
102	FMC (NFR times)

The various subroutines and function subprograms needed by each program will not be described in detail. Instead, they are shown in Table A-2 corresponding to the computation for which they are used. The variables which are stored in common blocks are defined in Table A-3.

Table A-2. Subroutines Corresponding to Computation

Equation Number in Section 2	Computation	Subroutine
pp 2-5 to 2-7	x-y components of \hat{t}_m, γ_m, R_m	CDATA for E-field CDATACF for combined- field
(22)	elements of $[Z^e]$	ZMNE
(26)	elements of $[Z^h]$	SZH
(27)	elements of \vec{V}^{ie}	TMX
(28)	elements of \vec{V}^{ih}	TEX
(33)	elements of $[T^e]$	TMNE
(36), (37)	elements of $[T^h]$	STH
(46)	$\beta \vec{V}^{ie} + \vec{I}^{ie}$	TMXCF (for combined-field)
(47)	$\beta \vec{V}^{ih} + \vec{I}^{ih}$	TEXCF (for combined-field)
(50) (54)	$\sqrt{\sigma/\lambda}$	TMS for TM case TES for TE case
--	$H_0^{(2)}(x)$	HANK02(X)
--	$H_1^{(2)}(x)$	HANK12(X)
(23)	$\alpha(z)$	ALPHA (z)
--	Solve $A\vec{x} = \vec{b}$ for \vec{x}	DECOMP and SOLVE
--	Solve $A\vec{x} = \vec{b}$ for \vec{x} when A is symmetric	GELS
	J_n, Y_n	BES for exact series solution

Table A-3. Common Block Variables

Block	Variable	Meaning
GQI	NGQ	Order of G-Q integration
	A	Weights/2
	T	Nodes/2
CUV	ULX	$\hat{t}_m \cdot \hat{x}$
	ULY	$\hat{t}_m \cdot \hat{y}$
	NC	NC
C	RCX	$R_m \cdot \hat{x}$
	RCY	$R_m \cdot \hat{y}$
	DC	Δ_m
CK	RKX	$k \cdot RCX$
	RKY	$k \cdot RCY$
	DK	$k \cdot DC$

A.1 E-FIELD PROGRAM

```

1.  C-----MAIN PROGRAM FOR COMPUTING INDUCED ELECTRIC CURRENTS
2.  C      ON TWO-DIMENSIONAL CONDUCTING SHAPES.
3.  C      USES E-FIELD INTEGRAL EQUATION
4.  DIMENSION PHII(10)
5.  COMPLEX Z(1000),VM(500)
6.  COMPLEX ZMNE,SZH
7.  COMMON /CUV/ULX(60),ULY(60),NC/C/RCX(40),RCY(40),DC(40)
8.  COMMON /GQI/A(10),T(10),NGQ
9.  COMMON /CK/RKX(60),RKY(60),DK(60)
10. DATA PI/3.141593/
11. C-----READ IN AND PRINT OUT INPUT DATA
12. 100  FORMAT(6I5)
13. 101  FORMAT(2E20.7)
14. 102  FORMAT(6E11.4)
15. READ(105,100) NGQ
16. READ(105,101)(A(I),T(I),I=1,NGQ)
17.  OUTPUT,NGQ
18. READ(105,100) ITM,ITE,ISC,NX,NP
19.  OUTPUT,ITM,ITE,ISC,NX,NP
20. READ(105,102) PHIO,DPHI
21.  OUTPUT,PHIO,DPHI
22. DO 4 I=1,NX
23. READ(105,102) PHII(I)
24.  OUTPUT,I,PHII(I)
25. 4 CONTINUE
26. READ(105,102) AMU,EPS
27.  OUTPUT,AMU,EPS
28. CALL CDATA(INC)
29. READ(105,100) NFR
30. DO 50 INF=1,NFR
31. READ(105,102) FMC
32. WRITE(108,300) FMC
33. AK=2.*PI*FMC*SQRT(AMU*EPS)*1.E 6
34. DO 5 I=1,NC
35. RKX(I)=RCX(I)*AK
36. RKY(I)=RCY(I)*AK
37. DK(I)=DC(I)*AK
38. 5 CONTINUE
39. IF(ITM.NE.1) GO TO 30
40. C-----FORM UPPER RT. TRIANGLE OF TM Z MATRIX.
41. K=1
42. DO 1 IN=1,NC
43. DO 1 IM=1,IN
44. Z(K)=ZMNE(IM,IN)
45. K=K+1
46. 1 CONTINUE
47. C-----FORM TM EXCITATION VECTORS.
48. CALL TMX(VM,PHII,NX)

```

```

49. C-----SOLVE FOR NORMALIZED TM ELECTRIC CURRENTS.
50.   MR=NC*(NC+1)/2
51.   CALL GELS(VM,Z,NC,NX,MR)
52.   K=1
53.   DO 2 I=1,NX
54.     WRITE(108,200) PHII(I)
55.     WRITE(108,201)
56.     DO 3 J=1,NC
57.       VMM=CABS(VM(K))
58.       WRITE(108,202) J,VM(K),VMM
59.       K=K+1
60.   3   CONTINUE
61.   2   CONTINUE
62.   IF(ISC.EQ.1) CALL TMS(VM,NX,PHII,PHI0,DPHI,NP)
63. 200  FORMAT('0',15X,'TM CURRENTS FOR PHI #',E11.4,3X,'DEGREES')
64. 201  FORMAT(' ',6X,'PULSE NO.',11X,'REAL',11X,'IMAG',11X,'MAG.')
65. 202  FORMAT(' ',15,5X,3E15.6)
66. 30   IF(ITE.NE.1) GO TO 60
67. C-----FORM UPPER RT. TRIANGLE OF TE Z MATRIX.
68.   K=1
69.   IB=1+IDC
70.   DO 31 IN=IB,NC
71.     DO 31 IM=IB,IN
72.       Z(K)=SZH(IM-1,IN-1,1,1)+SZH(IM-1,IN,1,-1)+
73.       1SZH(IM,IN-1,-1,1)+SZH(IM,IN,-1,-1)
74.       K=K+1
75.   31  CONTINUE
76. C-----FORM TE EXCITATION VECTORS.
77.   CALL TEX(VM,PHII,NX,IDC)
78. C-----SOLVE FOR NORMALIZED TE CURRENTS.
79.   NF=NC-IB+1
80.   MR=NF*(NF+1)/2
81.   CALL GELS(VM,Z,NF,NX,MR)
82.   K=1
83.   DO 32 I=1,NX
84.     WRITE(108,300) PHII(I)
85.     WRITE(108,301)
86.     DO 33 J=IB,NC
87.       VMM=CABS(VM(K))
88.       WRITE(108,202) J,VM(K),VMM
89.       K=K+1
90.   33  CONTINUE
91.   32  CONTINUE
92.   IF(ISC.EQ.1) CALL TES(VM,NX,PHII,PHI0,DPHI,NP,IDC)
93.   60  CONTINUE
94.   50  CONTINUE
95. 300  FORMAT('0',15X,'TE CURRENTS FOR PHI #',E11.4,3X,'DEGREES')
96. 301  FORMAT(' ',3X,'TRIANGLE NO.',12X,'REAL',11X,'IMAG',11X,'MAG.')
97. 302  FORMAT('1',FREQUENCY OF PLANE WAVE #',E15.7,3X,'MHZ')
98.   STOP
99.   END

```

Sample output data is:

RUN
NGQ = 4
ITM = 1
ITE = 1
ISC = 1
NX = 1
NP = 4
PHIO = .000000
UPHI = 90.0000
I = 1
PHII(I) = .000000
AMU = 1.255000E-06
EPS = 8.850000E-12
-NO. OF STRAIGHT LINE SEGMENTS APPROXIMATING C = 24

ULX	ULY	RCX	RCY	DC
.1301E 00	.9915E 00	.3763E 00	.4955E-01	.9995E-01
.3833E 00	.9236E 00	.3506E 00	.1452E 00	.9993E-01
.6085E 00	.7936E 00	.3011E 00	.2310E 00	.9993E-01
.7936E 00	.6085E 00	.2310E 00	.3011E 00	.9993E-01
.9236E 00	.3833E 00	.1452E 00	.3506E 00	.9993E-01
.9915E 00	.1301E 00	.4955E-01	.3763E 00	.9995E-01
.9915E 00	.1301E 00	.4955E-01	.3763E 00	.9995E-01
.9236E 00	.3833E 00	.1452E 00	.3506E 00	.9993E-01
.7936E 00	.6085E 00	.2310E 00	.3011E 00	.9993E-01
.6085E 00	.7936E 00	.3011E 00	.2310E 00	.9993E-01
.3833E 00	.9236E 00	.3506E 00	.1452E 00	.9993E-01
.1301E 00	.9915E 00	.3763E 00	.4955E-01	.9995E-01
.1301E 00	.9915E 00	.3763E 00	.4955E-01	.9995E-01
.3833E 00	.9236E 00	.3506E 00	.1452E 00	.9993E-01
.6085E 00	.7936E 00	.3011E 00	.2310E 00	.9993E-01
.7936E 00	.6085E 00	.2310E 00	.3011E 00	.9993E-01
.9236E 00	.3833E 00	.1452E 00	.3506E 00	.9993E-01
.9915E 00	.1301E 00	.4955E-01	.3763E 00	.9995E-01
.9915E 00	.1301E 00	.4955E-01	.3763E 00	.9995E-01
.9236E 00	.3833E 00	.1452E 00	.3506E 00	.9993E-01
.7936E 00	.6085E 00	.2310E 00	.3011E 00	.9993E-01
.6085E 00	.7936E 00	.3011E 00	.2310E 00	.9993E-01
.3833E 00	.9236E 00	.3506E 00	.1452E 00	.9993E-01
.1301E 00	.9915E 00	.3763E 00	.4955E-01	.9995E-01

-CLOSED CONTOUR, IDC = 0

FREQUENCY OF PLANE WAVE * 3000000E 03 MHZ

PULSE NO.	TM CURRENTS FOR PHI * .0000E 00 DEGREES		
	REAL	IMAG	MAG.
1	.125255E 01	.167993E 01	.209549E 01
2	.882587E 00	.178334E 01	.198979E 01
3	.188352E 00	.178166E 01	.179159E 01
4	.604287E 00	.140326E 01	.152784E 01
5	.107335E 01	.608134E 00	.123366E 01
6	.916432E 00	-.225217E 00	.943701E 00
7	.323787E 00	-.598796E 00	.680731E 00
8	.178457E 00	-.426260E 00	.462109E 00
9	.290834E 00	-.761568E-01	.300640E 00
10	.142750E 00	.102149E 00	.175533E 00
11	.157029E-01	.764418E-01	.780380E-01
12	.860298E-01	.201291E-02	.860533E-01
13	.860316E-01	.201503E-02	.860552E-01
14	.157045E-01	.764405E-01	.780374E-01
15	.142748E 00	.102147E 00	.175531E 00
16	.290836E 00	-.761544E-01	.300641E 00
17	.178457E 00	-.426262E 00	.462110E 00
18	.323791E 00	-.598795E 00	.680732E 00
19	.916426E 00	-.225217E 00	.943694E 00
20	.107337E 01	.608135E 00	.123367E 01
21	.604283E 00	.140325E 01	.152783E 01
22	.188351E 00	.178168E 01	.179161E 01
23	.882588E 00	.178333E 01	.198978E 01
24	.125255E 01	.167994E 01	.209549E 01

TM SCATTERED FIELD PATTERN FOR PHI = .0000E 00

PHI	SQRT(S/L)
.0000E 00	.1132E 01
.9000E 02	.1089E 01
.1800E 03	.2600E 01
.2700E 03	.1089E 01

TRIANGLE NO.	TE CURRENTS FOR PHI = .0000E 00	DEGREES
	REAL	IMAG
1	.154673E 01	.101682E 01
2	.145044E 01	.114043E 01
3	.112359E 01	.144623E 01
4	.508782E 00	.172797E 01
5	.319852E 00	.167835E 01
6	.105135E 01	.108613E 01
7	.128557E 01	.102806E 00
8	.900259E 00	-.765437E 00
9	.220425E 00	-.105381E 01
10	.278295E 00	-.713143E 00
11	.387825E 00	-.694841E -01
12	.260197E 00	.483124E 00
13	.174323E 00	.693457E 00
14	.260201E 00	.483125E 00
15	.387827E 00	-.694811E -01
16	.278298E 00	-.713135E 00
17	.220427E 00	-.105380E 01
18	.900258E 00	-.765431E 00
19	.128557E 01	.102808E 00
20	.105135E 01	.108612E 01
21	.319854E 00	.167836E 01
22	.508785E 00	.172798E 01
23	.112359E 01	.144625E 01
24	.145045E 01	.114044E 01

TE SCATTERED FIELD PATTERN FOR PHI = .0000E 00

PHI	SQRT(S/L)
.0000E 00	.1026E 01
.9000E 02	.6614E 00
.1800E 03	.1476E 01
.2700E 03	.6614E 00

STEP 0

A.2 COMBINED-FIELD PROGRAM

```

1.  C-----COMBINED FIELD FORMULATION FOR COMPUTING PLANE WAVE
2.  C      SCATTERING ON PERFECTLY CONDUCTING CYLINDERS OF
3.  C      ARBITRARY SHAPE.
4.  DIMENSION PHI(10),IPS(50)
5.  COMPLEX Z(1000),VM(500),DUM(500),XC(50),CUR(50)
6.  COMPLEX TMNE,ZMNE,STM,SZM
7.  COMMON /CUV/ILX(60),JLY(60),NC/C/RCX(40),RCY(40),DC(60)
8.  COMMON /CK/RKX(60),RKY(60),DK(60)
9.  COMMON /GQI/A(17),T(10),NGQ
10. DATA PI/3.141593/
11. C-----READ IN AND PRINT OUT INPUT DATA
12. 100 FORMAT(6I5)
13. 101 FORMAT(2E20.7)
14. 102 FORMAT(6E11.4)
15. READ(105,100) NGQ
16. READ(105,101)(A(I),T(I),I=1,NGQ)
17. OUTPUT,NGQ
18. READ(105,100) ITM,ITE,ISC,NX,NP
19. OUTPUT,ITM,ITE,ISC,NX,NP
20. READ(105,102) PHIO,DPHI
21. OUTPUT,PHIO,DPHI
22. DO 3 I=1,NX
23. READ(105,102) PHII(I)
24. OUTPUT,I,PHII(I)
25. 3 CONTINUE
26. READ(105,102) AMU,EPS,BETA
27. OUTPUT,AMU,EPS,BETA
28. CALL COATACF
29. READ(105,100) NFR
30. OUTPUT,NFR
31. DO 50 INF=1,NFR
32. READ(105,102) FMC
33. WRITE(108,300) FMC
34. AK=2.*PI*FMC*SQRT(AMU*EPS)*1.E 6
35. OUTPUT,AK
36. DO 7 I=1,NC
37. RKX(I)=RCX(I)*AK
38. RKY(I)=RCY(I)*AK
39. DK(I)=DC(I)*AK
40. 7 CONTINUE
41. IF(ITM.NE.1) GO TO 30
42. C-----FORM TM COMBINED FIELD MATRIX
43. K=1
44. DO 1 IN=1,NC
45. L=(IN-1)*NC+1
46. DO 1 IM=1,IN
47. DUM(K)=BETA*ZMNE(IM,IN)
48. Z(L)=TMNE(IM,IN)+DUM(K)
49. K=K+1

```

```

50.      L=L+1
51.      1  CONTINUE
52.      DO 2 IM=2,NC
53.      IM1=IM-1
54.      L=IM*IM1/2+1
55.      DO 2 IN=1,IM1
56.      Z(IM+NC*(IN-1))=TMNE(IM,IN)+DUM(L)
57.      L=L+1
58.      2  CONTINUE
59.      CALL TMXCF(VM,PHI,IX,NX,BETA)
60.      CALL DECOMP(NC,IPS,Z)
61.      C-----SOLVE FOR NORMALIZED TM ELECTRIC CURRENTS.
62.      L=1
63.      K=1
64.      DO 4 IX=1,NX
65.      WRITE(108,200) PHI(IX)
66.      WRITE(108,201)
67.      DO 5 I=1,NC
68.      XC(I)=VM(K)
69.      K=K+1
70.      5  CONTINUE
71.      CALL SOLVE(NC,IPS,Z,XC,CUR)
72.      DO 6 I=1,NC
73.      CM=CABS(CUR(I))
74.      VM(L)=CUR(I)
75.      WRITE(108,202) I,CUR(I),CM
76.      L=L+1
77.      6  CONTINUE
78.      4  CONTINUE
79.      IF(ISC.EQ.1) CALL TMS(VM,NX,PHI,PHI0,DPHI,DP0)
80.      200  FORMAT('0',1X,'TM CURRENTS FOR PHI =',F11.4)
81.      201  FORMAT(' ',1X,'PULSE NO.',1X,'REAL',1X,'IMAG',1X,'MAG. ')
82.      202  FORMAT(' ',1X,15,5X,3E15.6)
83.      30  IF(ITE.NE.1) GO TO 60
84.      C-----FORM UPPER RT. TRIANGLE OF TE Z MATRIX.
85.      K=1
86.      DO 31 IN=1,NC
87.      L=(IN-1)*NC+1
88.      DO 31 IM=1,IN
89.      DUM(K)=BETA*(SZH(IM-1,IN-1,1,1)+SZH(IM-1,IN,1,-1)
90.      1+SZH(IM,IN-1,-1,1)+SZH(IM,IN,-1,-1))
91.      Z(L)=DUM(K)*STH(IM-1,IN-1,1,1)*STH(IM-1,IN,1,-1)
92.      1+STH(IM,IN-1,-1,1)+STH(IM,IN,-1,-1)
93.      K=K+1
94.      L=L+1
95.      31  CONTINUE
96.      DO 32 IM=2,NC
97.      IM1=IM-1
98.      L=IM*IM1/2+1
99.      DO 32 IN=1,IM1

```

```

100.      Z(IM,NC*(IN-1))=DUM(L)+STH(IM-1,IN-1,1,1)+STH(IM-1,IN,1,-1)
101.      1+STH(IM,IN-1,-1,1)+STH(IM,IN,-1,-1)
102.      L=L+1
103.      32  CONTINUE
104.      C-----FORM TE EXCITATION VECTORS.
105.      CALL TEXCF(VM,PHII,NX,BETA)
106.      CALL DECOMP(NC,IPS,Z)
107.      C-----SOLVE FOR NORMALIZED TE CURRENTS.
108.      K=1
109.      L=1
110.      DO 34 IX=1,NX
111.      WRITE(108,300) PHII(IX)
112.      WRITE(108,301)
113.      DO 35 I=1,NC
114.      XC(I)=VM(K)
115.      K=K+1
116.      35  CONTINUE
117.      CALL SOLVE(NC,IPS,Z,XC,CUR)
118.      DO 36 I=1,NC
119.      CM=CABS(CUR(I))
120.      VM(L)=CUR(I)
121.      WRITE(108,202) I,CUR(I),CM
122.      L=L+1
123.      36  CONTINUE
124.      34  CONTINUE
125.      IF(ISC.EQ.1) CALL TES(VM,NX,PHII,PHIS,DPHI,NP,DI)
126.      60  CONTINUE
127.      50  CONTINUE
128.      300 FORMAT('0',15X,'TE CURRENTS FOR PHI =',E11.4)
129.      301 FORMAT(' ',3X,'TRIANGLE NO.',12X,'REAL',11X,'IMAG',11X,'MAG. ')
130.      302 FORMAT('1',15X,'FREQUENCY OF INCIDENT PLANE WAVE =',F15.7,3X,'MHz')
131.      STOP
132.      END

```

Sample output is given by:

RUN
NGQ = 4
ITM = 1
ITE = 1
ISC = 1
NX = 1
NP = 4
PHIO = .000000
UPHI = 90.0000
I = 1
PHII(1) = .000000
AMU = 1.255000E-06
EPS = 2.350000E-12
BETA = 10.0000

NO. OF PRINTS SPECIFYING CANTOR = 24

ULX		JLY		RCX		RCY		DC	
.1301E	00	.9915E	00	.3763E	00	.4955E	01	.9995E	01
.3833E	00	.9236E	00	.3506E	00	.1452E	00	.9993E	01
.6085E	00	.7936E	00	.3011E	00	.2310E	00	.9993E	01
.7936E	00	.6085E	00	.2310E	00	.3011E	00	.9993E	01
.9236E	00	.3833E	00	.1452E	00	.3506E	00	.9993E	01
.9915E	00	.1301E	00	.4955E	01	.3763E	00	.9995E	01
.9915E	00	.1301E	00	.4955E	01	.3763E	00	.9995E	01
.9236E	00	.3833E	00	.1452E	00	.3506E	00	.9993E	01
.7936E	00	.6085E	00	.2310E	00	.3011E	00	.9993E	01
.6085E	00	.7936E	00	.3011E	00	.2310E	00	.9993E	01
.3833E	00	.9236E	00	.3506E	00	.1452E	00	.9993E	01
.1301E	00	.9915E	00	.3763E	00	.4955E	01	.9995E	01
.1301E	00	.9915E	00	.3763E	00	.4955E	01	.9995E	01
.3833E	00	.9236E	00	.3506E	00	.1452E	00	.9993E	01
.6085E	00	.7936E	00	.3011E	00	.2310E	00	.9993E	01
.7936E	00	.6085E	00	.2310E	00	.3011E	00	.9993E	01
.9236E	00	.3833E	00	.1452E	00	.3506E	00	.9993E	01
.9915E	00	.1301E	00	.4955E	01	.3763E	00	.9995E	01
.9915E	00	.1301E	00	.4955E	01	.3763E	00	.9995E	01
.9236E	00	.3833E	00	.1452E	00	.3506E	00	.9993E	01
.7936E	00	.6085E	00	.2310E	00	.3011E	00	.9993E	01
.6085E	00	.7936E	00	.3011E	00	.2310E	00	.9993E	01
.3833E	00	.9236E	00	.3506E	00	.1452E	00	.9993E	01
.1301E	00	.9915E	00	.3763E	00	.4955E	01	.9995E	01

VER = 1

FREQUENCY OF INCIDENT PLANE WAVE = .3000000E 03 M.17
 AK = 6.28195

PULSE NO.	TM CURRENTS FOR PHI = .0000E 00		MAG.
	REAL	IMAG	
1	.124978E 01	.168728E 01	.209973E 01
2	.881834E 00	.178897E 01	.199451E 01
3	.191649E 00	.178697E 01	.179715E 01
4	.597827E 00	.141196E 01	.153330E 01
5	.106931E 01	.622016E 00	.123706E 01
6	.918747E 00	-.211561E 00	.942790E 00
7	.328355E 00	-.591191E 00	.676257E 00
8	.178453E 00	-.422296E 00	.458453E 00
9	.295127E 00	-.696707E -01	.303239E 00
10	.146421E 00	.112055E 00	.184378E 00
11	.147271E -01	.863757E -01	.876221E -01
12	.865843E -01	.103815E -01	.872044E -01
13	.865862E -01	.103792E -01	.872061E -01
14	.147265E -01	.863774E -01	.876237E -01
15	.146420E 00	.112054E 00	.184377E 00
16	.295128E 00	-.696698E -01	.303240E 00
17	.178457E 00	-.422298E 00	.458456E 00
18	.328356E 00	-.591193E 00	.676260E 00
19	.918746E 00	-.211559E 00	.942789E 00
20	.106931E 01	.622011E 00	.123706E 01
21	.597828E 00	.141194E 01	.153331E 01
22	.191636E 00	.178690E 01	.179715E 01
23	.881826E 00	.178897E 01	.199450E 01
24	.124979E 01	.168729E 01	.209974E 01

TM SCATTERED FIELD PATTERN FOR PHI = .0000E 00

PHI	SQRT(S/L)
.0000E 00	.1131E 01
.9000E 02	.1088E 01
.1800E 03	.2601E 01
.2700E 03	.1088E 01

TE CURRENTS FOR PHI = .0000E 00

TRIANGLE NO.	REAL	IMAG	MAG.
1	.154648E 01	.101488E 01	.185101E 01
2	.145042E 01	.114052E 01	.184512E 01
3	.112366E 01	.144641E 01	.183158E 01
4	.508975E 00	.172835E 01	.180174E 01
5	.319650E 00	.167909E 01	.170924E 01
6	.105141E 01	.108711E 01	.151237E 01
7	.128678E 01	.103640E 00	.129025E 01
8	.901037E 00	.765204E 00	.118212E 01
9	.220995E 00	.105425E 01	.107717E 01
10	.278288E 00	.713866E 00	.766195E 00
11	.388414E 00	.700233E 01	.384675E 00
12	.261154E 00	.482941E 00	.549029E 00
13	.175455E 00	.693445E 00	.715298E 00
14	.261152E 00	.482944E 00	.549032E 00
15	.388409E 00	.700145E 01	.384669E 00
16	.278284E 00	.713856E 00	.766184E 00
17	.220999E 00	.105424E 01	.107716E 01
18	.901039E 00	.765197E 00	.118212E 01
19	.128679E 01	.103644E 00	.129025E 01
20	.105141E 01	.108710E 01	.151237E 01
21	.319647E 00	.167908E 01	.170924E 01
22	.508978E 00	.172835E 01	.180173E 01
23	.112366E 01	.144640E 01	.183158E 01
24	.145043E 01	.114051E 01	.184513E 01

TE SCATTERED FIELD PATTERN FOR PHI = .0000E 00

PHI	SQRT(S/L)
.0000E 00	.1026E 01
.9000E 02	.6618E 00
.1800E 03	.1475E 01
.2700E 03	.6618E 00

STEP 0

A.3 EXACT SERIES PROGRAM

```

1.  C-----PROGRAM TO COMPUTE ELECTRIC CURRENTS INDUCED ON
2.  C     PERFECTLY CONDUCTING CIRCULAR CYLINDERS USING
3.  C     THE INFINITE SERIES SOLUTION.  THE NORMALIZED
4.  C     SCATTERED FIELD PATTERN IS ALSO COMPUTED.
5.  C     COMPLEX A(50),B(50),C(50),D(50)
6.  C     DIMENSION CPM1(50),CPM2(50)
7.  C     DIMENSION BJ(100),BY(100)
8.  C     COMPLEX AO,BO,CO,DO,HM1,HP, HJZ,JP,STE,STMU,UN
9.  C     COMMON YO(33),PI2,PI4,PI7
10. C     REAL JZM,JP
11. C     DATA J/(2.71),PI/3.141593/
12. 100  FORMAT(5E14.7)
13. 101  FORMAT(5I5)
14. 102  FORMAT(4E11.4)
15. 103  READ(105,100)(YO(I),I=1,33)
16. 104  PI2=2./PI
17. 105  PI4=PI/4.
18. 106  PI7=.75*PI
19. C-----NB = NB, # OF BESSEL FUNCTIONS TAKEN
20. C     READ(105,101) NB,NC,NI
21. C     OUTPUT,NB,NC,NI
22. C     READ(105,102) AR,PHO,DPHI
23. C     OUTPUT,AR,PHO,DPHI
24. C     AK=AR*2./PI
25. C     F1=2./PI*AK
26. C     F2=SQRT(2./PI)
27. C     CALL BES(NB+1,AK,BJ,BY)
28. C     HM1=BJ(1)/U*BY(1)
29. C     AO=1./HM1
30. C     BO=BJ(1)/HM1
31. C     CO=BJ(2)/U*BY(2)
32. C     DO=1./HP
33. C     DO=BJ(2)/HP
34. C     UN=U
35. C     MIN=1
36. C     DO 1 I=1,NB
37. C     HM1=BJ(I+1)/U*BY(I+1)
38. C     A(I)=UN/HM1
39. C     B(I)=MIN*BJ(I+1)/HM1
40. C     HP=HM1/IAK
41. C     C(I)=UN/HP
42. C     D(I)=MIN*(BJ(I)-I*BJ(I+1)/AK)/HP
43. C     HM1=H
44. C     JN=U*UN
45. C     MIN=MIN
46. 1    CONTINUE
47. C     WRITE(108,100) AO,BO
48. C     WRITE(108,100) CO,DO
49. C     DO 10 I=1,NB
50. C     WRITE(108,201) I,A(I),B(I)
51. C     WRITE(108,201) I,C(I),D(I)
52. 10   CONTINUE
53. C-----COMPUTE THE CURRENTS.
54. C     WRITE(108,200)
55. C     JPM=2.*PI/NC
56. C     PH=DPHI/2.
57. C     DO 3 I=1,NC
58. C     JZ=AO
59. C     DO * J=1,NB

```

```

60.      JZ=JZ+2.*A(J)*COS(PH*J)
61.      *
62.      CONTINUE
63.      PH=PH+DPH
64.      JZ=F1*JZ
65.      JZM=CABS(JZ)
66.      WRITE(108,201) I,JZ,JZM
67.      3
68.      C-----COMPUTE TE CURRENTS.
69.      WRITE(108,202)
70.      PH=0.
71.      DO 5 I=1,NC
72.      JP=CO
73.      DO 6 J=1,NB
74.      JP=JP+2.*C(J)*COS(PH*J)
75.      6
76.      PH=PH+DPH
77.      JPM=CABS(JP)
78.      WRITE(108,201) I,JP,JPM
79.      8
80.      C-----COMPUTE TM AND TE NORMALIZED SCATTERED FIELD PATTERNS
81.      WRITE(108,203)
82.      WRITE(108,204)
83.      PH=PH0*PI/180.
84.      DP=DPH*PI/180.
85.      DO 7 I=1,NI
86.      STM=80
87.      STE=00
88.      DO 8 J=1,NB
89.      CP=COS(J*PH)
90.      STM=STM+2.*3(J)*CP
91.      STE=STE+2.*0(J)*CP
92.      8
93.      SE=F2*CABS(STE)
94.      SM=F2*CABS(STM)
95.      WRITE(108,204) PH0,SM,SE
96.      PH0=PH0+DPH
97.      PH=PH+DP
98.      7
99.      CONTINUE
100.     200 FORMAT('11',1TM CURRENTS...')
101.     201 FORMAT('11',1(0,4E15.6))
102.     202 FORMAT('101',1TE CURRENTS...')
103.     203 FORMAT('11',1 TM AND TE NORMALIZED SCATTERED FIELD PATTERNS')
104.     204 FORMAT('11',3E11.4)
105.     205 FORMAT('101',3Y,1PW1,1EX,1TM,1EX,1TE')
106.     STOP
107.     END

```

Sample output is given by:

RUN

NB = 10

NC = 24

NI = 36

AR = .382800

RHO = .000000

DPHI = 10.0000

.7560842E-03	.1961226E 01	.1486227E-06	-.3855161E-02	
.1853659E 01	-.3675514E 00	.9621708E 00	.1907837E 00	
1	-.367551E 00	.185366E 01	-.962171E 00	-.190783E 00
1	-.176372E 01	-.815625E 00	-.176180E 00	.380973E 00
2	-.117822E 01	.115772E 01	.508775E 00	-.499923E 00
2	-.685802E 00	-.195346E 01	.109727E 00	.312549E 00
3	-.116608E 01	-.287091E 00	-.571510E-01	.232131E 00
3	.155797E 01	-.489399E 00	-.898130E-01	-.285914E 00
4	.254945E-01	-.626816E 00	.165156E-02	-.406059E-01
4	.269038E-01	.542070E 00	.245724E-02	.495096E-01
5	.222761E 00	.813862E-03	-.133480E-04	.365347E-02
5	-.129210E 00	.512326E-03	-.157216E-04	-.396501E-02
6	-.116936E-04	.585782E-01	.398494E-07	-.199623E-03
6	-.544304E-05	-.262491E-01	.429988E-07	.207362E-03
7	-.123943E-01	-.923732E-07	-.555454E-10	.745288E-05
7	.459257E-02	-.349651E-07	-.579638E-10	-.761340E-05
8	.450554E-09	-.220967E-02	.415758E-13	-.203901E-06
8	.145061E-09	.701962E-03	.427046E-13	.206651E-06
9	.341316E-03	.146022E-11	-.183030E-16	.427820E-08
9	-.951423E-04	.410734E-12	-.136369E-16	-.431704E-08
10	-.331304E-14	.465686E-04	.506134E-20	-.711431E-10
10	-.829195E-15	-.116807E-04	.512673E-20	.716012E-10

TM CURRENTS...

1	-.126455E 01	.167788E 01	.210104E 01
2	-.896445E 00	.177994E 01	.199294E 01
3	-.207342E 00	.177882E 01	.179087E 01
4	.579420E 00	.140687E 01	.152152E 01
5	.104805E 01	.625184E 00	.122036E 01
6	.901943E 00	-.196249E 00	.923046E 00
7	.725969E 00	.569256E 00	.655979E 00
8	-.166396E 00	.407463E 00	.440129E 00
9	-.280348E 00	.685472E-01	.288607E 00
10	-.139286E 00	.106374E 00	.175260E 00
11	.139867E-01	.834404E-01	.846044E-01
12	.825951E-01	.122661E-01	.835009E-01
13	.825952E-01	.122641E-01	.835007E-01
14	.139904E-01	.834385E-01	.846033E-01
15	-.139280E 00	.106376E 00	.175256E 00
16	-.280346E 00	.685377E-01	.288602E 00
17	-.166407E 00	.407451E 00	.440122E 00
18	.725948E 00	.569257E 00	.655979E 00
19	.901928E 00	-.196271E 00	.923036E 00
20	.104806E 01	.625153E 00	.122035E 01
21	.579447E 00	.140685E 01	.152151E 01
22	-.207312E 00	.177882E 01	.179086E 01
23	-.896417E 00	.177994E 01	.199293E 01
24	-.126454E 01	.167788E 01	.210104E 01

TE CURRENTS...

1	.154852E 01	.101437E 01	.185118E 01
2	.144972E 01	.113488E 01	.134109E 01
3	.111826E 01	.143071E 01	.131588E 01
4	.506173E 00	.169820E 01	.177203E 01
5	-.305532E 00	.164074E 01	.166894E 01
6	-.101326E 01	.106239E 01	.146812E 01
7	-.123804E 01	.113352E 00	.124322E 01
8	-.869856E 00	.724165E 00	.113184E 01
9	-.218888E 00	.100826E 01	.103175E 01
10	.261561E 00	.688452E 00	.736465E 00
11	.369950E 00	.721736E-01	.376924E 00
12	.249369E 00	-.460950E 00	.524080E 00
13	.167391E 00	.664501E 00	.685260E 00
14	.249365E 00	-.460963E 00	.524090E 00
15	.369948E 00	.721528E-01	.376918E 00
16	.261571E 00	.688433E 00	.736451E 00
17	-.218865E 00	.100826E 01	.103174E 01
18	-.869833E 00	.724185E 00	.113184E 01
19	-.123804E 01	.113319E 00	.124321E 01
20	-.101328E 01	.106236E 01	.146811E 01
21	-.305561E 00	.164073E 01	.166894E 01
22	.506146E 00	.169821E 01	.177203E 01
23	.111824E 01	.143074E 01	.131589E 01
24	.144971E 01	.113489E 01	.134110E 01

TM AND TE NORMALIZED SCATTERED FIELD PATTERNS

PHI		TM		TE	
•0000E	00	•1134E	01	•1020E	01
•1000E	02	•1133E	01	•1030E	01
•2000E	02	•1129E	01	•1057E	01
•3000E	02	•1122E	01	•1082E	01
•4000E	02	•1112E	01	•1082E	01
•5000E	02	•1099E	01	•1033E	01
•6000E	02	•1087E	01	•9214E	00
•7000E	02	•1083E	01	•7639E	00
•8000E	02	•1087E	01	•6332E	00
•9000E	02	•1092E	01	•6539E	00
•1000E	03	•1078E	01	•8261E	00
•1100E	03	•1034E	01	•1014E	01
•1200E	03	•9878E	00	•1120E	01
•1300E	03	•1048E	01	•1122E	01
•1400E	03	•1315E	01	•1080E	01
•1500E	03	•1737E	01	•1110E	01
•1600E	03	•2174E	01	•1255E	01
•1700E	03	•2496E	01	•1421E	01
•1800E	03	•2614E	01	•1491E	01
•1900E	03	•2496E	01	•1421E	01
•2000E	03	•2174E	01	•1255E	01
•2100E	03	•1737E	01	•1110E	01
•2200E	03	•1315E	01	•1080E	01
•2300E	03	•1048E	01	•1122E	01
•2400E	03	•9878E	00	•1120E	01
•2500E	03	•1034E	01	•1014E	01
•2600E	03	•1078E	01	•8261E	00
•2700E	03	•1092E	01	•6539E	00
•2800E	03	•1087E	01	•6332E	00
•2900E	03	•1083E	01	•7639E	00
•3000E	03	•1087E	01	•9214E	00
•3100E	03	•1099E	01	•1033E	01
•3200E	03	•1112E	01	•1082E	01
•3300E	03	•1122E	01	•1082E	01
•3400E	03	•1129E	01	•1057E	01
•3500E	03	•1133E	01	•1030E	01

ST8P 0

A.4 PROGRAM TO COMPUTE CURRENT DISTRIBUTION DUE TO IMPRESSED LONGITUDINAL CURRENT

A computer program is presented here for the special excitation considered in Subsection 2.8. Subroutine CDATA is used to specify the contour C as was done in the E-field program. The data cards needed for this are exactly the same. The total axial current I_z is stored in the FORTRAN variable ZI. DO loop 1 forms the matrix given by Equation (105) of Section 2. The system of linear equations is solved by RDECOMP and RSOLVE.

The example given here is for the cross section of a fuselage station as shown in Fig. 6-1. A total of 28 subsections were used to approximate the contour. The subsection number and the total current flowing axially on that subsection is printed out.

```

1. C-----PROGRAM FOR COMPUTING CURRENT DISTRIBUTION ON
2. C   PERFECTLY CONDUCTING CYLINDRICAL SHELL CARRYING
3. C   TOTAL LONGITUDINAL CURRENT ZI.
4.     COMMON /CUV/ULX(60),ULY(60),NC/C/RCX(60),RCY(60),DC(60)
5.     DIMENSION CM(2500),VK(50),ALPH(50),IPS(50)
6.     100  FORMAT(6I5)
7.     101  FORMAT(2E20.7)
8.     102  FORMAT(6E11.4)
9.     103  FORMAT(I10,2F15.7)
10.    104  FORMAT(2I5,E15.7,2I5,E15.7)
11.     CF=.222158
12.     READ(105,102) ZI
13.     OUTPUT,ZI
14.     CALL CDATA(IDC)
15.     DO 10 I=1,NC
16.     RCX(I)=RCX(I)*CF
17.     RCY(I)=RCY(I)*CF
18.     DC(I)=DC(I)*CF
19.     10   CONTINUE
20.     K=1
21.     DO 1 J=1,NC
22.     D2=DC(J)/2.
23.     UX=D2*ULX(J)
24.     JY=D2*ULY(J)

```

```

25.      DO 1 I=1,NC
26.      IF(I.EQ.J) GO TO 7
27.      RX=RCX(I)-RCX(J)
28.      RY=RCY(I)-RCY(J)
29.      RU=(RX-UX)**2+(RY-UY)**2
30.      RL=(RX+UX)**2+(RY+UY)**2
31.      DTJ=ULX(J)*RX+ULY(J)*RY
32.      DNJ=ABS(ULY(J)*RX-ULX(J)*RY)
33.      TH1=ATAN(D2=DTJ, DNJ)
34.      TH2=ATAN(-D2=DTJ, DNJ)
35.      CM(K)=D2*(ALOG(RU*RL)/2.-2.)-DTJ*ALOG(RJ/RL)/2.
36.      1+DNJ*(TH1-TH2)
37.      K=K+1
38.      GO TO 8
39.      7  CM(K)=DC(J)*(ALOG(D2)-1.)
40.      K=K+1
41.      2  CONTINUE
42.      1  CONTINUE
43.      DO 3 I=1,NC
44.      VK(I)=10.
45.      3  CONTINUE
46.      CALL RDECOMP(NC,IPS,CM)
47.      CALL RSOLVE(NC,IPS,CM,VK,ALPH)
48.      S1=0.
49.      S=0.
50.      DO 4 I=1,NC
51.      S=S+ALPH(I)*DC(I)
52.      S1=S1+DC(I)
53.      4  CONTINUE
54.      OUTPUT,S
55.      OUTPUT,S1
56.      C=S/ZI
57.      DO 5 I=1,NC
58.      ALPH(I)=ALPH(I)/C
59.      WRITE(102,103) I,ALPH(I)
60.      5  CONTINUE
61.      SC=0.
62.      DO 6 I=1,NC
63.      SC=SC+ALPH(I)*DC(I)
64.      6  CONTINUE
65.      OUTPUT,SC
66.      STOP
67.      END

```

Sample output is given by:

RUN
 ZI = 20000.0
 -NB. SF STRAIGHT LINE SEGMENTS APPROXIMATING C = 28

ULX	ULY	RCX	RCY	DC
.0000E 00	.0000E 00			
-.1000E 01	.0000E 00			
-.1000E 01	.0000E 00	-.5000E 00	.0000E 00	.1000E 01
-.2000E 01	.5000E -01			
-.9988E 00	.4994E -01	-.1500E 01	.2500E -01	.1001E 01
-.3000E 01	.1000E 00			
-.9988E 00	.4994E -01	-.2500E 01	.7500E -01	.1001E 01
-.4000E 01	.2000E 00			
-.9950E 00	.9950E -01	-.3500E 01	.1500E 00	.1005E 01
-.5000E 01	.3500E 00			
-.9889E 00	.1483E 00	-.4500E 01	.2750E 00	.1011E 01
-.6000E 01	.4500E 00			
-.9950E 00	.9950E -01	-.5500E 01	.4000E 00	.1005E 01
-.6300E 01	.5000E 00			
-.9864E 00	.1644E 00	-.6150E 01	.4750E 00	.3041E 00
-.6000E 01	.6000E 00			
.9487E 00	.3162E 00	-.6150E 01	.5500E 00	.3162E 00
-.5000E 01	.1000E 01			
.9285E 00	.3714E 00	-.5500E 01	.8000E 00	.1077E 01
-.4000E 01	.1600E 01			
.8575E 00	.5145E 00	-.4500E 01	.1300E 01	.1166E 01
-.3000E 01	.2700E 01			
.6727E 00	.7399E 00	-.3500E 01	.2150E 01	.1487E 01
-.2000E 01	.4000E 01			
.6097E 00	.7926E 00	-.2500E 01	.3350E 01	.1640E 01
-.1000E 01	.4600E 01			
.8575E 00	.5145E 00	-.1500E 01	.4300E 01	.1166E 01
.0000E 00	.4750E 01			
.9889E 00	.1483E 00	-.5000E 00	.4675E 01	.1011E 01
.1000E 01	.4600E 01			
.9889E 00	-.1483E 00	.5000E 00	.4675E 01	.1011E 01
.2000E 01	.4000E 01			
.8575E 00	-.5145E 00	.1500E 01	.4300E 01	.1166E 01
.3000E 01	.2700E 01			
.6097E 00	-.7926E 00	.2500E 01	.3350E 01	.1640E 01
.4000E 01	.1600E 01			
.6727E 00	-.7399E 00	.3500E 01	.2150E 01	.1487E 01
.5000E 01	.1000E 01			
.8575E 00	-.5145E 00	.4500E 01	.1300E 01	.1166E 01
.6000E 01	.6000E 00			
.9285E 00	-.3714E 00	.5500E 01	.8000E 00	.1077E 01
.6300E 01	.5000E 00			

.9437E 00	-.3162E 00	.6150E 01	.5500E 00	.3162E 00
.6000E 01	.4500E 00			
-.9864E 00	-.1644E 00	.6150E 01	.4750E 00	.3041E 00
.5000E 01	.3500E 00			
-.9950E 00	-.9950E-01	.5500E 01	.4000E 00	.1005E 01
.4000E 01	.2000E 00			
-.9839E 00	-.1483E 00	.4500E 01	.2750E 00	.1011E 01
.3000E 01	.1000E 00			
-.9950E 00	-.9950E-01	.3500E 01	.1500E 00	.1005E 01
.2000E 01	.5000E-01			
-.9938E 00	-.4994E-01	.2500E 01	.7500E-01	.1001E 01
.1000E 01	.0000E 00			
-.9938E 00	-.4994E-01	.1500E 01	.2500E-01	.1001E 01
.0000E 00	.0000E 00			
-.1000E 01	.0000E 00	.5000E 00	.0000E 00	.1000E 01

-CLOSED CONTOUR, IDC = 0

S = 68.7375

S1 = 6.30543

1	.2200409E 04
2	.2247948E 04
3	.2354470E 04
4	.2594063E 04
5	.2857402E 04
6	.4112020E 04
7	.1157018E 05
8	.1033439E 05
9	.3502833E 04
10	.2170148E 04
11	.2087022E 04
12	.2678784E 04
13	.3587517E 04
14	.3763301E 04
15	.3763308E 04
16	.3587514E 04
17	.2678781E 04
18	.2087030E 04
19	.2170130E 04
20	.3502849E 04
21	.1033443E 05
22	.1157015E 05
23	.4112012E 04
24	.2857416E 04
25	.2594052E 04
26	.2354471E 04
27	.2247945E 04
28	.2200424E 04

SC = 20000.0

STOP 0

APPENDIX B

PROGRAMS FOR THIN SHELLS OF ARBITRARY CROSS SECTION AND FINITE CONDUCTIVITY

Two computer programs are presented here for the determination of the field interior to electrically thin, lossy shells. The formulations used are the impedance sheet approximation derived in Section 3 and the exact series solution of Section 4. The required data cards are described and a sample of the program output is given.

B.1 IMPEDANCE SHEET APPROXIMATION PROGRAM

The input data card sequence needed for this program is almost exactly the same as that used in the E-field program of Appendix A. In fact, Table A-1 may be used here where the card containing AMU and EPS is replaced by the card sequence:

ST = shell thickness in meters
SEPS = normalized (to free space) permittivity of shell material
SIG = conductivity of shell material in mhos/meter
VCO = velocity of light in medium outside and inside shell
NMP = number of near-field measurement points inside shell at which shielding effectiveness calculations are to be made
XM(i) = X-Y coordinates of interior field measurement points in meters, $i = 1, 2, \dots, NMP$
YM(i)

Also, FHZ is the frequency of the incident plane wave in hertz.

The main program is much the same as in the E-field case. The two polarizations are handled separately and the upper right triangle of the E-field impedance matrix is created first. To this an impedance load is added using Equation (9) or (11) of Section 3. The E-field excitation vector

is then formed and the resulting system of equations is solved. The interior field due to the equivalent polarization current alone is computed by sub-routines QNFMS for the TM case or PNFMS for the TE case. These computations are defined by Equations (50) and (52) of Section 3, respectively. To find the total interior field, then, the incident field must be added to these "scattered" fields at each interior point. The shielding effectiveness calculation may then be done according to Equation (1) of Section 3.

```

1. C-----THIN SHELL PROGRAM !
2. C     MAIN PROGRAM FOR COMPUTING EQUIVALENT POLARIZATION
3. C     CURRENT FOR A THIN SHELL USING THE FULL FIELD FORMULATION.
4. C     COMMON /COV/ LX(60),LY(60),NC/3/RCX(60),RCY(60),DC(60)
5. C     COMMON /MS/XM(100),YM(100),XMK(100),YMK(100),NMP
6. C     COMMON /CK/RKX(60),RKY(60),CK(60)
7. C     COMMON /GGI/A(10),T(10),NGG
8. C     DIMENSION PHII(10)
9. C     COMPLEX Z(1000),VM(500),CU(50),EZI(50)
10. C     COMPLEX U,ZMNE,SZM,CSGRT,BETA,CEXP,EZC,-ZC
11. DATA PI/3.141593/,U/(0.71.)/
12. 100  FORMAT(6I5)
13. 101  FORMAT(2E20.7)
14. 102  FORMAT(6E11.4)
15. 103  FORMAT(5E15.6)
16. READ(105,100) NGG
17. READ(105,101) (A(I),T(I),I=1,NGG)
18. OUTPUT,NGG
19. READ(105,100) ITM,ITE,ISC,NX,NP
20. OUTPUT,ITM,ITE,ISC,NX,NP
21. READ(105,102) PHIC,OPHI
22. OUTPUT,PHIC,OPHI
23. DO 4 I=1,NX
24. READ(105,102) PHII(I)
25. OUTPUT,I,PHII(I)
26. 4   CONTINUE
27. READ(105,102) ST,SEPS,SIG,VCO
28. OUTPUT,ST,SEPS,SIG,VCO
29. READ(105,100) NMP
30. OUTPUT,NMP
31. DO 6 I=1,NMP
32. READ(105,102) XM(I),YM(I)
33. 6   CONTINUE
34. CALL CDATA(100)
35. READ(105,100) NFR
36. DO 50 I=1,NFR
37. READ(105,102) FHZ
38. WRITE(108,300) FHZ
39. WF=2.*PI*FHZ
40. AKO=WF/VCO
41. STK=AKO*ST
42. AMUO=4.*PI*1.E-07
43. EPSO=1./(AMUO*VCO*VCO)
44. BETA=STK*(U*(SEPS-1.)+SIG/(WF*EPSO))
45. OUTPUT,AMUO,EPSO,WF
46. DO 5 I=1,NC
47. RKX(I)=RCX(I)*AKO
48. RKY(I)=RCY(I)*AKO

```

```

49.      OK(I)=OZ(I)*AKO
50.      CONTINUE
51.      DO 7 I=1,NMP
52.      XK(I)=KM(I)*AKO
53.      YK(I)=YM(I)*AKO
54.      7 CONTINUE
55.      K=1
56.      DO 8 I=1,NX
57.      CS=COS(PHII(I)*PI/180.)
58.      SN=SIN(PHII(I)*PI/180.)
59.      DO 8 J=1,NMP
60.      EZ(I,K)=CEXP( *(XK(J)*CS+YK(J)*SN))
61.      K=K+1
62.      8 CONTINUE
63.      IF(I*NM.EQ.1) GO TO 30
64.      C-----FORM UPPER RT. TRIANGLE OF TM Z MATRIX.
65.      K=1
66.      DO 1 IN=1,NC
67.      DO 1 IM=1,IN
68.      Z(K)=ZMNE(IM,IN)
69.      K=K+1
70.      1 CONTINUE
71.      C-----ADD LOAD IMPEDANCE MATRIX
72.      K=1
73.      DO 10 I=1,NC
74.      Z(K)=Z(K)+OK(I)/BETA
75.      K=K+1
76.      10 CONTINUE
77.      C-----FORM TM EXCITATION VECTORS.
78.      CALL TMX(VM,PHII,NX)
79.      C-----SOLVE FOR NORMALIZED TM ELECTRIC CURRENTS.
80.      MR=NC*(NC+1)/2
81.      CALL GELS(VM,Z,NC,NX,MR)
82.      K=1
83.      _X=1
84.      DO 2 I=1,NX
85.      WRITE(108,200) PHII(I)
86.      WRITE(108,201)
87.      DO 3 J=1,NC
88.      VMM=CABS(VM(K))
89.      CU(J)=VM(K)
90.      WRITE(108,202) J,VM(K),VMM
91.      K=K+1
92.      2 CONTINUE
93.      WRITE(108,203)
94.      DO 9 IM=1,NMP
95.      CALL DNEMS(C,EZC,XK(IM),YK(IM))
96.      EZC=EZC+EZ!(C,X)
97.      *OUTPUT,EZC
98.      SE=20.*ALOG10(CABS(EZ!(LX)/P30))
99.      WRITE(108,100) XK(IM),YK(IM),SE

```

```

100.      LX=LX+1
101.      9      CONTINUE
102.      2      CONTINUE
103.      IF(ISC.EQ.1) CALL TMS(VM,NX,PHI1,PHI2,OPHI,NO)
104.      200     FORMAT('0',15X,'TM CURRENTS FOR PHI =',F11.4,3X,'DEGREES')
105.      201     FORMAT(' ',6X,'PULSE NO=',11X,'REAL',11X,'IMAG',11X,'IMAG.1')
106.      202     FORMAT(' ',15,5X,3E15.6)
107.      203     FORMAT('0', 'SHIELDING EFFECTIVENESS FOR TM CASE')
108.      30      IF(ITE.NE.1) GO TO 50
109.      C-----FORM UPPER RT. TRIANGLE OF TE Z MATRIX.
110.          K=1
111.          IB=1+IDC
112.          DO 31 IN=IB,NC
113.          DO 31 IM=IB,IN
114.          Z(K)=SZH(IM=1,IN=1,1,1)+SZH(IM=1,IN=1,-1)+
115.          1SZH(IM,IN=1,-1,1)+SZH(IM,IN=-1,-1)
116.          K=K+1
117.      31      CONTINUE
118.      C-----ADD LEAD IMPEDANCE MATRIX
119.          NU=NC-IDC
120.          IF(IDC.EQ.1) GO TO 34
121.          DL=DK(NC)
122.          DU=DK(1)
123.          GO TO 35
124.      34      DL=DK(1)
125.          DU=DK(2)
126.      35      K=1
127.          DO 36 I=1,NU
128.          Z(K)=Z(K)+(DL+DU)/3./BETA
129.          DL=DU
130.          DU=DK(I+IB)
131.          K=K+I+1
132.      36      CONTINUE
133.          K=2
134.          NU1=NU-1
135.          DO 37 I=1,NU1
136.          Z(K)=Z(K)+DK(I+IDC)/(6.*BETA)
137.          K=K+I+2
138.      37      CONTINUE
139.          IF(IDC.EQ.1) GO TO 38
140.          K=NC*(NC-1)/2+1
141.          Z(K)=Z(K)+DK(NC)/6./BETA
142.      38      CONTINUE
143.      C-----FORM TE EXCITATION VECTORS.
144.          CALL TEX(VM,PHI1,NX,IDC)
145.          DO 40 I=1,NU
146.      40      CONTINUE
147.      C-----SOLVE FOR NORMALIZED TE CURRENTS.
148.          MR=NU*(NU+1)/2
149.          CALL GELS(VM,Z,NU,NX,MR)
150.          LX=1

```

```

151.      K=1
152.      DO 32 I=1,NX
153.      WRITE(108,300) PHII(I)
154.      WRITE(108,301)
155.      DO 33 J=1B,NC
156.      VMM=CABS(VM(K))
157.      CJ(J)=VM(K)
158.      WRITE(108,202) J,VM(K),VMM
159.      K=K+1
160. 33     CONTINUE
161.      WRITE(108,303)
162.      DO 39 IM=1,NMP
163.      CALL PNFMS(CJ,HZC,XMK(IM),YMK(IM))
164.      HZC=HZC+EZI(LX)
165.      OUTPUT,HZC
166.      SE =20.**ALOG10(CABS(EZI(LX)/HZC))
167.      WRITE(108,103) XM(IM),YM(IM),SE
168.      LX=LX+1
169. 39     CONTINUE
170. 32     CONTINUE
171.      IF(ISC.EQ.1) CALL TES(VM,NX,PHII,PHIO,DPHI,NO,IO)
172. 60     CONTINUE
173. 50     CONTINUE
174. 300    FORMAT('0',15X,'TE CURRENTS FOR PHI =',F11.4,'X, (DEGREES)')
175. 301    FORMAT(' ',3X,'TRIANGLE NO.',12X,'RFAL',11X,'IMAG',11X,'IMAG.1')
176. 302    FORMAT('1',15X,'FREQUENCY OF PLANE WAVE =',F15.7,'X, (HZ)')
177. 303    FORMAT('0',15X,'SHIELDING EFFECTIVENESS FOR TE CASE')
178.      STOP
179.      END

```

Sample output is given by:

```

RUN
  NGG = 4
  ITM = 1
  ITE = 1
  ISC = 0
  NX = 1
  NP = 1
  PHIC = .000000
  DPHI = 5.000000
  I = 1
  PHII(I) = .000000
  ST = 9.999999E-04
  SEPS = 1.000000
  SIG = 10000.0
  VCO = 3.000000E 08
  NMP = 1
  -NO. OF STRAIGHT LINE SEGMENTS APPROXIMATING C = 16

      ULX      ULY      RCX      RCY      DC
    .5000E 00   .0000E 00
    .4620E 00  -.1910E 00
   -.1951E 00  -.9808E 00   .4810E 00  -.9550E-01   .1947E 00
    .3540E 00  -.3540E 00
   -.5523E 00  -.8336E 00   .4080E 00  -.2725E 00   .1955E 00
    .1910E 00  -.4620E 00
   -.8336E 00  -.5523E 00   .2725E 00  -.4080E 00   .1955E 00
    .0000E 00  -.5000E 00
   .9808E 00  -.1951E 00   .9550E-01  -.4810E 00   .1947E 00
   .1910E 00  -.4620E 00
   .9808E 00   .1951E 00  -.9550E-01  -.4810E 00   .1947E 00
   -.3540E 00  -.3540E 00
   .8336E 00   .5523E 00  -.2725E 00  -.4080E 00   .1955E 00
   .4620E 00  -.1910E 00
   .5523E 00   .8336E 00  -.4080E 00  -.2725E 00   .1955E 00
   -.5000E 00   .0000E 00
   .1951E 00   .9808E 00  -.4810E 00  -.9550E-01   .1947E 00
   .4620E 00   .1910E 00
   .1951E 00   .9808E 00  -.4810E 00   .9550E-01   .1947E 00
   -.3540E 00   .3540E 00
   .5523E 00   .8336E 00  -.4080E 00   .2725E 00   .1955E 00
   -.1910E 00   .4620E 00
   .8336E 00   .5523E 00  -.2725E 00   .4080E 00   .1955E 00
    .0000E 00   .5000E 00
   .9808E 00   .1951E 00  -.9550E-01   .4810E 00   .1947E 00
   .1910E 00   .4620E 00
   .9808E 00  -.1951E 00   .9550E-01   .4810E 00   .1947E 00
   .3540E 00   .3540E 00
   .8336E 00  -.5523E 00   .2725E 00   .4080E 00   .1955E 00
   .4620E 00   .1910E 00
   .5523E 00  -.8336E 00   .4080E 00   .2725E 00   .1955E 00
   .5000E 00   .0000E 00
   .1951E 00  -.9808E 00   .4810E 00   .9550E-01   .1947E 00
  -CLOSED CURVATURE, IDC = 0

```

FREQUENCY OF PLANE WAVE = .1000000E 08 HZ
 AMUO = 1.256637E-06
 EPSO = 8.841948E-12
 WF = 6.283186E 07

TM CURRENTS FOR PHI = .0000F 00 DEGREES

PULSE NO.	REAL	IMAG	MAG.
1	.378525E 01	-.269116E 01	.464440E 01
2	.350129E 01	-.275624E 01	.445599E 01
3	.295902E 01	-.284401E 01	.410416E 01
4	.224299E 01	-.290525E 01	.367035E 01
5	.147549E 01	-.291541E 01	.326761E 01
6	.765252E 00	-.287334E 01	.297350E 01
7	.221265E 00	-.280014E 01	.280887E 01
8	-.706900E-01	-.274259E 01	.274350E 01
9	-.706981E-01	-.274259E 01	.274350E 01
10	.221276E 00	-.280009E 01	.280882E 01
11	.765254E 00	-.287334E 01	.297350E 01
12	.147568E 01	-.291541E 01	.326760E 01
13	.224300E 01	-.290525E 01	.367036E 01
14	.295902E 01	-.284402E 01	.410418E 01
15	.350128E 01	-.275626E 01	.445600E 01
16	.378525E 01	-.269118E 01	.464441E 01

SHIELDING EFFECTIVENESS FOR TM CASE
 EZC = (4.007816E-04, -8.124560E-04)
 .000000E 00 .000000E 00 .608581E 02

TE CURRENTS FOR PHI = .0000F 00 DEGREES

TRIANGLE NO.	REAL	IMAG	MAG.
1	.981393E 00	.224932E 00	.100684E 01
2	.982880E 00	.209009E 00	.100486E 01
3	.986463E 00	.163158E 00	.999865E 00
4	.989852E 00	.943096E-01	.994335E 00
5	.990797E 00	.134543E-01	.990889E 00
6	.988479E 00	-.673963E-01	.990774E 00
7	.983917E 00	-.136243E 00	.993304E 00
8	.979551E 00	-.182094E 00	.996333E 00
9	.977791E 00	-.198021E 00	.997641E 00
10	.979552E 00	-.182095E 00	.996334E 00
11	.983916E 00	-.136243E 00	.993304E 00
12	.988479E 00	-.673963E-01	.990774E 00
13	.990799E 00	.134555E-01	.990890E 00
14	.989854E 00	.943103E-01	.994336E 00
15	.986462E 00	.163159E 00	.999864E 00
16	.982880E 00	.209008E 00	.100486E 01

SHIELDING EFFECTIVENESS FOR TE CASE
 HZC = (-4.711151E-04, -5.401962E-03)
 .000000E 00 .000000E 00 .453160E 02
 *STEP = 0

B.2 EXACT-SERIES PROGRAM

The computer program listed here computes the longitudinal component of an interior field at the center of a lossy shell of circular cross section. The formulas of Section 4 are used. The input data is defined by:

A0 = outer radius of shell in meters
A1 = inner radius of shell in meters
EPSB = normalized (to free space) permittivity of shell material
SIG = conductivity of shell material in mhos/meter
FO = initial frequency in hertz
DF = frequency-run increment (hertz)
NF = number of frequencies at which computation is desired

The required Bessel functions are computed by the following subroutines:

$J_0(z), Y_0(z)$ - CBES0
 $J_1(z), Y_1(z)$ - CBES1
 $H_0^{(2)}(x)$ - HANK02
 $H_1^{(2)}(x)$ - HANK12

In the above, z is a complex number and x is a real number. The variables T11, T12, T21, and T22 are computed according to Equation (7) if $|k_b a_0| < RM$. Otherwise, Equation (21) is used. Equations (6) and (9) are thus evaluated for $n = 0$ and the shielding effectiveness according to Equation (1) in Section 3 may be determined.

```

1. C-----PROGRAM TO COMPUTE SHIELDING EFFECTIVENESS AT
2. C   CENTER OF LOSSY CYLINDRICAL SHELL. BOTH
3. C   POLARIZATIONS AT NORMAL INCIDENCE.
4. C   COMPLEX BU00,BU01,BU11,BU10,BY00,BY01,BY10,BY11
5. C   COMPLEX HANK02,HANK12,ETB,KB,H0,H1,STK
6. C   COMPLEX T11,T12,T21,T22,ETR,U,CSQRT
7. C   COMPLEX CCBS,CSIN,C1,C2,C3,DD,A,B,DD,TE,TH
8. C   REAL KO
9. C   DATA U/(0.,1.)/,PI/3.141593/,C/3.E 08/,ET0/377./
10. C   DATA EPS0/8.84194E-12/,RM/3./
11. 100  FORMAT(6E15.7)
12. 101  FORMAT(5I5)
13. 102  FORMAT('0',6X,'FREQ.',8X,'ABS(KBA1)',8X,'KOA1',12X,'TESE',11X
14. C   *,'TMSE')
15. 103  FORMAT(' ',15,4E15.7)
16. C   A1 = INNER RADIUS (IN METERS)
17. C   A0 = OUTER RADIUS (IN METERS)
18. C   KB = WAVENUMBER OF SHELL REGION
19. C   AK = WAVENUMBER OF FREE SPACE
20. C   ETB = RELATIVE IMPEDANCE OF SHELL MATERIAL
21. C   READ(105,100) AO,A1,EPSS,SIG
22. C   OUTPUT,AO,A1,EPSS,SIG
23. C   D=AO-A1
24. C   READ(105,100) FO,DF
25. C   READ(105,101) NF
26. C   OUTPUT,FO,DF,NF
27. C   SIGN=SIG/EPSS
28. C-----PERFORM FREQUENCY RUN
29. C   WRITE(108,102)
30. C   DO 1 IX=1,NF
31. C   FHZ=FO
32. C   WF=2.*PI*FHZ
33. C   KO=WF/C
34. C   KB=CSQRT(EPSS-U*SIGN/WF)*KO
35. C   ETB=KO/KB
36. C   STK=KB*D
37. C   AKO=KO*AO
38. C   AK1=KO*A1
39. C   C1=PI*KB*A1/2.
40. C   C2=2.*U/(PI*AKO)
41. C   C3=SQRT(A1/A0)
42. C   H0=HANK02(AKO)
43. C   H1=HANK12(AKO)
44. C   HOR=REAL(HANK02(AK1))
45. C   HIR=REAL(HANK12(AK1))
46. C   DABS=CABS(KB*A1)
47. C   IF(DABS.GT,RM) GO TO 2
48. C   CALL CBES0(KB*AO,BU00,BY00)
49. C   CALL CBES0(KB*A1,BU01,BY01)

```

```

50.      CALL CBES1(KR*A0,BJ10,BY10)
51.      CALL CBES1(KR*A1,BJ11,BY11)
52.      T11=C1*(-BJ01*BY10+BJ10*BY01)
53.      T12=C1*(BJ10*BY11-BJ11*BY10)
54.      T21=C1*(BJ01*BY00-BJ00*BY01)
55.      T22=C1*(-BJ00*BY11+BJ11*BY00)
56.      GO TO 3
57. 2     CONTINUE
58.      T11=C3*CCOS(STK)
59.      T12=C3*CSIN(STK)
60.      T21=T12
61.      T22=T11
62. 3     CONTINUE
63. C-----COMPUTE DETERMINANT FOR TM CASE
64.      DD=H0*(-H1R*T11+HOR*T12/ETB)+H1*(-H1R*T21*ETB+HOR*T22)
65.      DO=C2/DD
66.      OUTPUT,DO
67.      SE=-20**ALOG10(CABS(DO))
68. C-----COMPUTE DETERMINANT FOR TE CASE
69.      DD=      H0*(-H1R*T11+ETB*HOR*T12)+H1*(-H1R*T21/ETB+HOR*T22)
70.      DO=C2/DD
71.      OUTPUT,DO
72.      SH=-20**ALOG10(CABS(DO))
73.      WRITE(108,100) FHZ,DABS,AK1,SH,SE
74.      FHZ=FHZ+DF
75. 1     CONTINUE
76.      STOP
77.      END

```

Sample output is given by:

RUN

A0 ■ .500000
A1 ■ .499000
EPSB ■ 1.00000
SIG ■ 10000.0
FO ■ 1.000000E 07
DF ■ 1.000000E 07
NF ■ 1

	FREQ.	ABS(KBA1)	KOA1	TESE	TMSE
DO	(3.921350E-04)	(8.023640E-04)			
DO	(5.863814E-04)	(4.950687E-03)			
	.1000000E 08	.4433989E 03	.1045103E 00	.4604617E 02	.6098236E 02
STOP 0					

APPENDIX C

CAD HOMOGENEOUS SHELL COUPLING ANALYSIS PROGRAM

An interactive computer program was written to determine the coupling of an exterior electromagnetic disturbance to a circuit situated inside a closed homogeneous thick shell. The low-frequency formulas of Section 5 are used for the interior penetration fields. The purpose of this appendix is to briefly describe the CAD program logic. This consists of descriptions of the following:

- ° User-specified input data for a given problem
- ° Computations performed
- ° CAD results

A typical problem is illustrated in Fig. C-1 where the interior circuit consists of a two-wire transmission line of length L and spacing h . The line is loaded at one end with an impedance Z_L . The excitation shown could result from a NEMP or NSL threat. The quantities of interest for computation are the open circuit voltage and short circuit current at the terminals shown in Fig. C-1. From this, the maximum power coupled to the circuit may be determined and thus various parametric design curves may be plotted to facilitate a CAD solution based on given burnout data for the load.

A block diagram of the computer program logic is shown in Fig. C-2. The various subroutines required are listed with capital letters inside blocks which identify the various program segments. Subroutine THREAT allows the user to define the threat as one of the following:

- NEMP - Nuclear electromagnetic pulse, plane wave excitation given by Equation (24) of Section 5.
Input H_o .
- NSL - Near-strike lightning, low-frequency line source excitation whose magnetic field is given by Equation (2) of Section 5. Input R.
- DSL - Direct-strike lightning, impressed longitudinal current density.

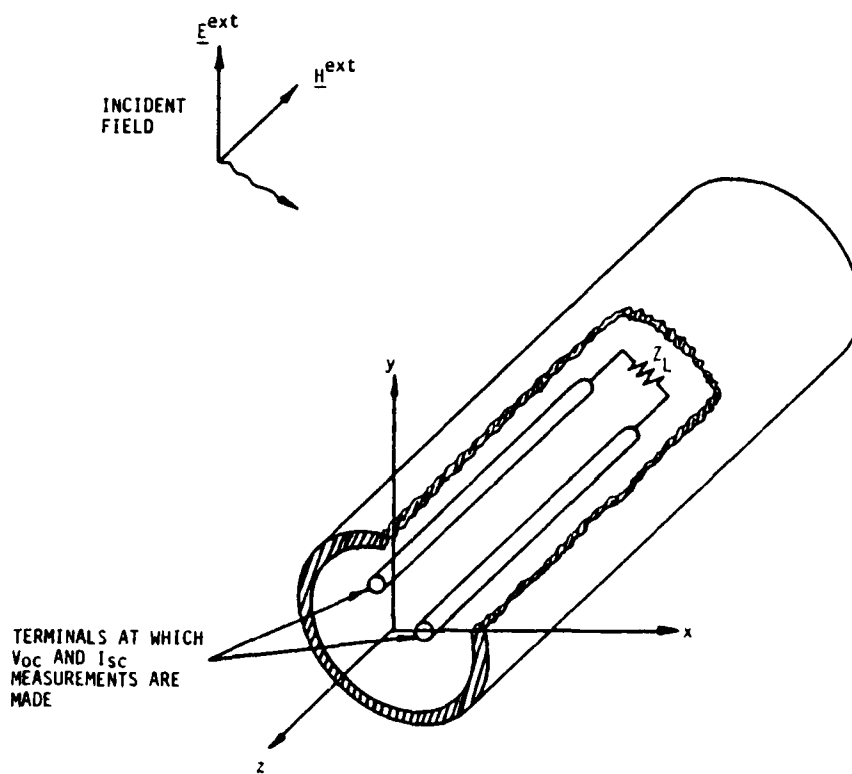
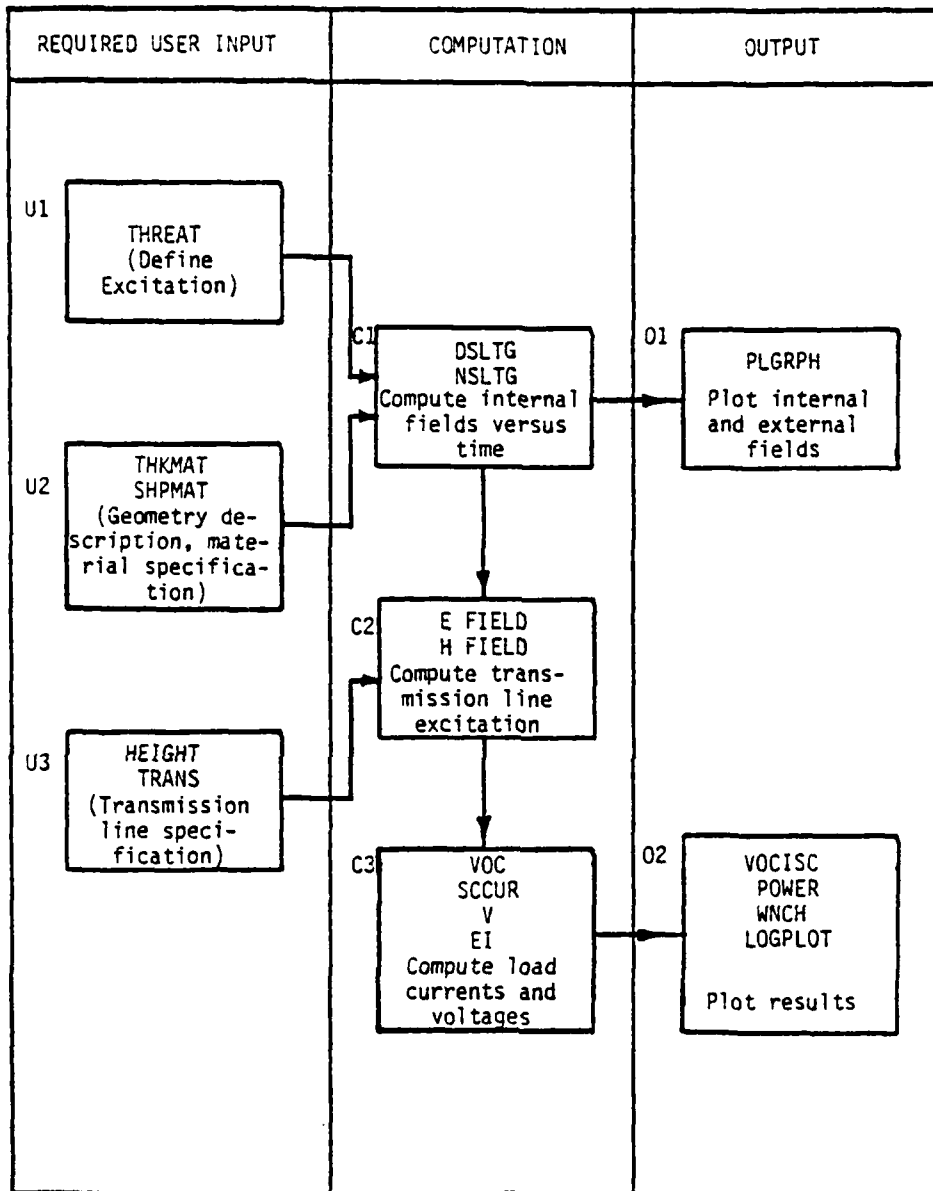


Figure C-1. Cutaway View of Infinitely Long Homogeneous Cylindrical Shell with Loaded Transmission Line Circuit Inside



Subroutines appear in CAPS.

Figure C-2. CAD Block Diagram

given by Equation (25) of Section 5. Once the threat is specified, subroutines THKMAT and SHPMAT are used to define the shell enclosure part of the problem. Data required here is

- σ = shell wall conductivity
- d = shell wall thickness (several units acceptable)
- VSR = volume to emface ratio of enclosure (meters)

Conductivities of various materials are tabulated in a data file.

The interior fields may now be computed for the empty homogeneous shell according to the formulas of Section 5. This is done in subroutines DSLTG and NSLTG as follows:

- NEMP excitation - Use NSLTG where internal field is given by Equation (18) with α and β defined following Equation (24)
- NSL excitation - Use NSLTG where internal field is given by Equation (18) with α and β defined following Equation (1)
- DSL excitation - Use DSLTG where internal field is given by Equation (36) with α and ϵ defined following Equation (1).

To complete the specification of the sample problem illustrated in Fig. C-1, the user must input data which defines the circuit under consideration. This is done in subroutines HEIGHT and TRANS. Data required here is:

- h = spacing of transmission line or effective area of standard cable (tabulated according to cable RG number)
- L = length of line in meters
- Z_0 = characteristic impedance of line
- Z_L = load impedance

Finally, the open circuit voltage and short circuit current at the transmission line terminals shown in Fig. C-1 may be computed. This is accomplished by the following subroutines:

VOC - Computes V_{oc} according to Equation (15) of Reference [4], p 6-6, in Section 5

SCCUR - Computes I_{sc} according to Equation (16) of Reference [4], p 6-6, in Section 5.

Once these computations have been made, various optional CAD curves for a given problem may be plotted. A sequence of typical plots for a problem is given by Figs. 6-5 through 6-11 of Section 6.

DATE
FILMED
-8